Annales Societatis Geologorum Poloniae (2019), vol. 89: 1–46. doi: https://doi.org/10.14241/asgp.2019.03

MIDDLE TO LATE JURASSIC CARBONATE-BIOSILICEOUS SEDIMENTATION AND PALAEOENVIRONMENT IN THE TETHYAN FATRICUM DOMAIN, KRÍŽNA NAPPE, TATRA MTS, WESTERN CARPATHIANS

Renata JACH[1*] & Daniela REHÁKOVÁ[2]

[1] Institute of Geological Sciences, Faculty of Geography and Geology, Jagiellonian University, Gronostajowa 3a, 30-387 Kraków, Poland; e-mail: renata.jach@uj.edu.pl
[2] Department of Geology and Palaeontology, Faculty of Natural Sciences, Comenius University, Ilkovičova 6, 842 15 Bratislava; Slovakia, e-mail: daniela.rehakova@uniba.sk
[*] corresponding author

Jach, R. & Reháková, D., 2019. Middle to Late Jurassic carbonate-biosiliceous sedimentation and palaeoenvironment in the Tethyan Fatricum Domain, Krížna Nappe, Tatra Mts, Western Carpathians. *Annales Societatis Geologorum Poloniae*, 89: 1–46.

Abstract: The Jurassic of the Alpine-Mediterranean Tethys was characterized by the formation of several interconnected basins, which underwent gradual deepening and oceanization. Sedimentation in each basin was influenced by a specific set of interrelated factors, such as tectonic activity, seawater circulation, climate, chemistry and trophic state of seawater as well as evolutionary changes of the marine biota. This paper deals with the Fatricum Domain (Central Carpathians, Poland and Slovakia), which in the Jurassic was a pull-apart basin on a thinned continental crust. The sedimentation history of this domain during the Bajocian–Tithonian and its governing factors have been revealed. Facies analysis of the Bajocian–Oxfordian deposits evidences considerable relief of the basin-floor topography. Deposits in the Western Tatra Mts represent sedimentation on a submarine intrabasinal high, whereas the coeval deposits of the eastern part of the Tatra Mts accumulated in a deeper basin. The basin succession began with Bajocian bioturbated "spotted" limestones and siliciclastic mudstones (Fleckenmergel facies). These were succeeded by uppermost Bajocian – middle Bathonian grey nodular limestones, affected by synsedimentary gravitational bulk creep. The coeval deposits of the intrabasinal high are represented by well-washed *Bositra*-crinoidal limestones with condensed horizons. Uniform radiolarite sedimentation commenced in the late Bathonian and persisted until the early late Kimmeridgian. The basal ribbon radiolarites (upper Bathonian – lower Oxfordian), which consist of alternating chert beds and shale partings, are a record of seawater eutrophication, a related crisis in carbonate production and the rise of the CCD, which collectively resulted in biosiliceous sedimentation. The overlying calcareous radiolarites (middle Oxfordian – lowermost upper Kimmeridgian) marked a gradual return to carbonate sedimentation. The return of conditions that were favourable for carbonate sedimentation took place in the late Kimmeridgian, when the red nodular limestones were deposited. They are partly replaced by basinal platy limestones (uppermost Kimmeridgian – Tithonian) in the Western Tatra Mts. This lateral variation in facies reflects a change in the sedimentary conditions governed by a bathymetric reversal of the seafloor configuration, attributed to a further stage in the pull-apart transcurrent tectonics of the Fatricum Domain.

Key words: Radiolarite, nodular limestone, Fleckenmergel facies, carbonate production crisis, calcite compensation depth, Tethys.

Manuscript received 7 February 2019, accepted 10 April 2019

INTRODUCTION

During Jurassic time, several interconnecting basins developed in the Alpine-Mediterranean Tethys, which resulted from the breakup and disintegration of the extensive shallow-water carbonate platforms and siliciclastic shelves that formerly had existed there (Fig. 1). The newly created basins were elongated and narrow; they were formed on continental crust that underwent stretching and thinning. The subsequent development of some of these basins led to the creation of oceanic crust. The basins were separated by shallow, intrabasinal highs bounded by normal faults

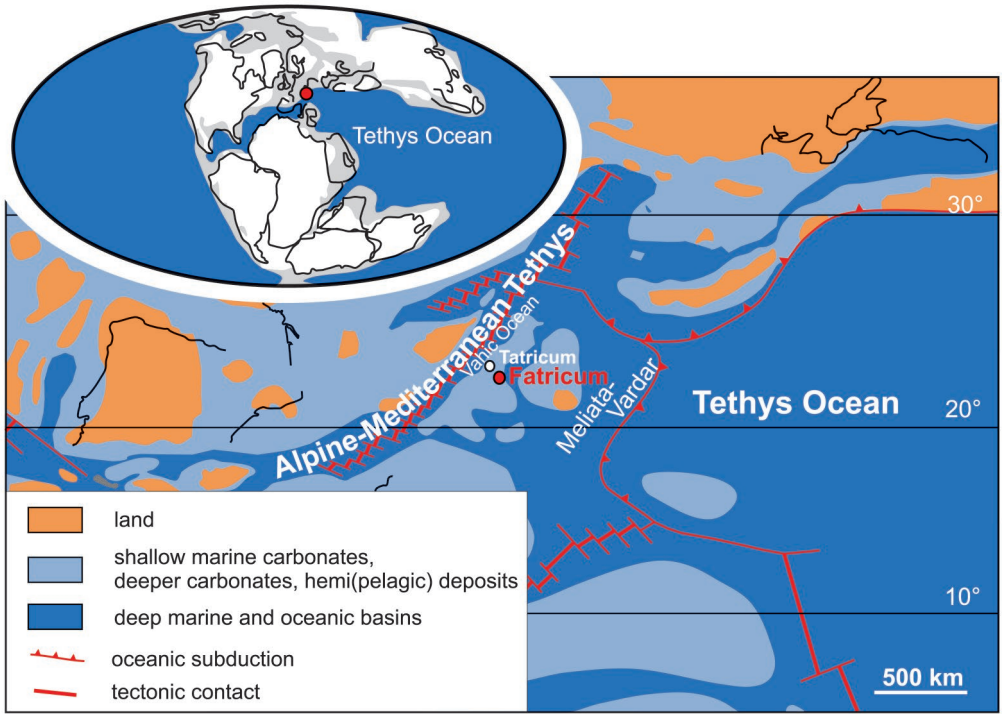

Fig. 1. General palaeogeographic position of the Fatricum Domain during the Callovian (after Thierry and Barrier, 2000; simplified). The location of the adjacent Tatricum (Ridge) also is indicated.

(e.g., Bernoulli and Jenkyns, 1974; Santantonio, 1994). They had the character of subaerially exposed lands, a shallow-water carbonate platform or submarine pelagic swells, called drowned or pelagic carbonate platforms. The processes of basin formation and its further development had various degrees of intensity in different sectors of the Alpine-Mediterranean Tethys. The spatial pattern of basins and intervening intrabasinal highs changed in place and time.

Specific sedimentary facies were laid down in basins and on the intervening intrabasinal highs (Bernoulli and Jenkyns, 1974; Santantonio, 1993). The facies formed a characteristic vertical succession. Crinoidal limestone, thin-shelled bivalve limestone and red nodular limestone were typical of the intrabasinal highs. The sedimentary record of such highs is punctuated by numerous discontinuities (stratigraphic gaps, omission surfaces) and includes strongly condensed horizons, commonly with pelagic microbialites. Conversely, carbonates exported from the intrabasinal highs, also redeposited by various gravity currents, and biosiliceous deposits, chiefly radiolarites or radiolarian limestones, predominated in the adjacent basins (Baumgartner, 1987). In the Late Jurassic, micritic pelagic carbonates were particularly widespread. They are composed of planktonic carbonate microfossils. Although the trends presented above are of general significance and can be traced in many parts of the Alpine-Mediterranean Tethys, each sector of this oceanic realm had its own site-specific development history. This was influenced by interrelated, local, regional and supraregional factors, such as the tectonic activity of a given area (Bertok and Martire, 2009; Picotti and Cobianchi, 2017), the major plate reorganization (e.g., Lewandowski *et al*., 2005; Muttoni *et al*., 2005, 2013), the circulation of seawater (Nieto *et al*., 2012; Vörös, 2012) and the eutrophication of seawater, which led to a crisis in carbonate production (Bartolini and Cecca, 1999; Morettini *et al*., 2002; Cecca *et al*., 2005; Baumgartner, 2013; De Wever *et al*., 2014) as well as the evolutionary changes of carbonate-secreting organisms that resulted in the prolific production of carbonates in the seawater column at the turn of the Jurassic and Cretaceous (Erba, 1989; Erba and Tremolada, 2004).

Middle and Late Jurassic sedimentation history and evolution of many sectors of the Alpine-Mediterranean Tethys have been studied broadly for a few decades. This has led to the formulation of several classic concepts on carbonate and biosiliceous sedimentation in a rifting and widening oceanic realm. The deposits that crop out in the Southern Alps, such as those formed on the Trento Plateau and the adjacent basins have been the subject of numerous thorough studies (e.g., Bernoulli and Jenkyns, 1974; Santantonio, 1993; Baumgartner, 1987; Martire, 1996). Jurassic deposits from other parts of the Alps, such as the Ligurian Alps, have been examined as well (Bertok *et al*., 2011). The studies of the particularly well-exposed Jurassic sections from the Apennines, Sicily and the Iberian Peninsula provide other significant interpretations (e.g., Santantonio, 1993; Di Stefano *et al*., 2002; Bertok and Martire, 2009; Coimbra *et al*., 2009; Navarro *et al*., 2009).

The Fatricum Domain was one of palaeogeographic domains of the northern passive margin of the Western Tethys (Fig. 1; e.g., Michalík *et al*., 1995; Thierry and Barrier, 2000; Plašienka, 2003). The Jurassic rocks that represent the larger part of the Fatricum Domain crop out in the Tatra Mts, in both Poland and Slovakia. The depositional history of these rocks was analysed in detail; however, the studies

focused particularly on the turn of the Triassic and Jurassic (Michalík *et al*., 2007, 2013), on the Lower Jurassic (e.g., Gradziński *et al*., 2004; Jach, 2005; Jach and Dudek, 2005; Iwańczuk *et al*., 2013) and on the uppermost Jurassic – lowermost Cretaceous (e.g., Grabowski and Pszczółkowski, 2006a, b; Grabowski *et al*., 2010, 2013). It has been documented that the basin underwent tectonic reorganization during the Triassic-Jurassic transition, which resulted from rifting processes (Plašienka, 2018). They were succeeded by further block tectonics in the Early Jurassic, leading to the formation of intrabasinal highs and adjacent basins. The subsequent Middle and Late Jurassic depositional history of the Tatra Mts part of the Fatricum Domain, has received decidedly less attention. This sharply contrasts with the far more completely reconstructed evolution of several Middle and Upper Jurassic basins of the Alpine-Mediterranean Tethys. The data and concepts on the facies development of the Fatricum Domain during Middle and Late Jurassic time, presented in the classic paper by Lefeld (1974; see also Lefeld, 1969), demand to be expanded and reinterpreted. Any new approach also must take into account the precise, integrated stratigraphy of the carbonate and biosiliceous deposits of this basin elaborated by Jach *et al*. (2014) and state-of-the-art knowledge of the processes, which acted in the Alpine-Mediterranean Tethys during the Jurassic and resulted in the origin of specific sedimentary facies in this oceanic realm.

The aim of this work is threefold: (1) to summarize the data on facies development of the Tatra Mts part of the Fatricum Domain during Middle and Late Jurassic time presented to date and interpretations of them, (2) to provide the results of current research on the facies and their depositional environments, and (3) to determine the factors controlling lateral facies variation and vertical facies trends as a consequence of local and regional processes. The purpose of this study is to decipher how the sedimentary systems of an evolving pull-apart basin reacted to various changing environmental factors. This has led to a more comprehensive view of the Jurassic history of the Carpathian sector of the Tethyan realm.

GEOLOGICAL SETTING

Middle–Upper Jurassic radiolarian-bearing limestones and cherts (hereafter called radiolarites) as well as accompanying limestones and marls were studied in the Krížna Nappe of the Tatra Mts, the northern part of the Central Western Carpathians, southern Poland and northern Slovakia. During the Late Cretaceous, the Krížna Nappe was thrust over the Tatra crystalline core and its autochthonous and allochthonous sedimentary cover (Fig. 2). The Krížna Nappe in the Tatra Mts is subdivided into several thrust sheets and slices (Bac-Moszaszwili *et al*., 1979; Nemčok *et al*., 1994).

The term Fatricum Domain is used to define a nappe system (Krížna Nappe *sensu lato*) of detached sedimentary sequences overlying the Tatric cover as well as their original basement (Plašienka, 2003). The sections studied represent one of these nappes belonging to the Fatricum Domain which was one of the domains of the passive continental margin of the Jurassic Tethys. It faced the Tatricum Domain (Ridge) to the north and the Cimmerian Wedge (*sensu* Michalík, 2007) to the south (in the present geographical coordinates; Csontos and Vörös, 2004; Schmid *et al*., 2008). The whole area separated two oceanic domains – the Meliata Ocean to the south and the Vahic Ocean to the north. The former ocean was in a phase of subduction, which presumably started in the Early Jurassic, and finally was closed by the latest Jurassic – earliest Cretaceous (Kozur, 1991; Plašienka, 2018; see also Missoni and Gawlick, 2011a, b).

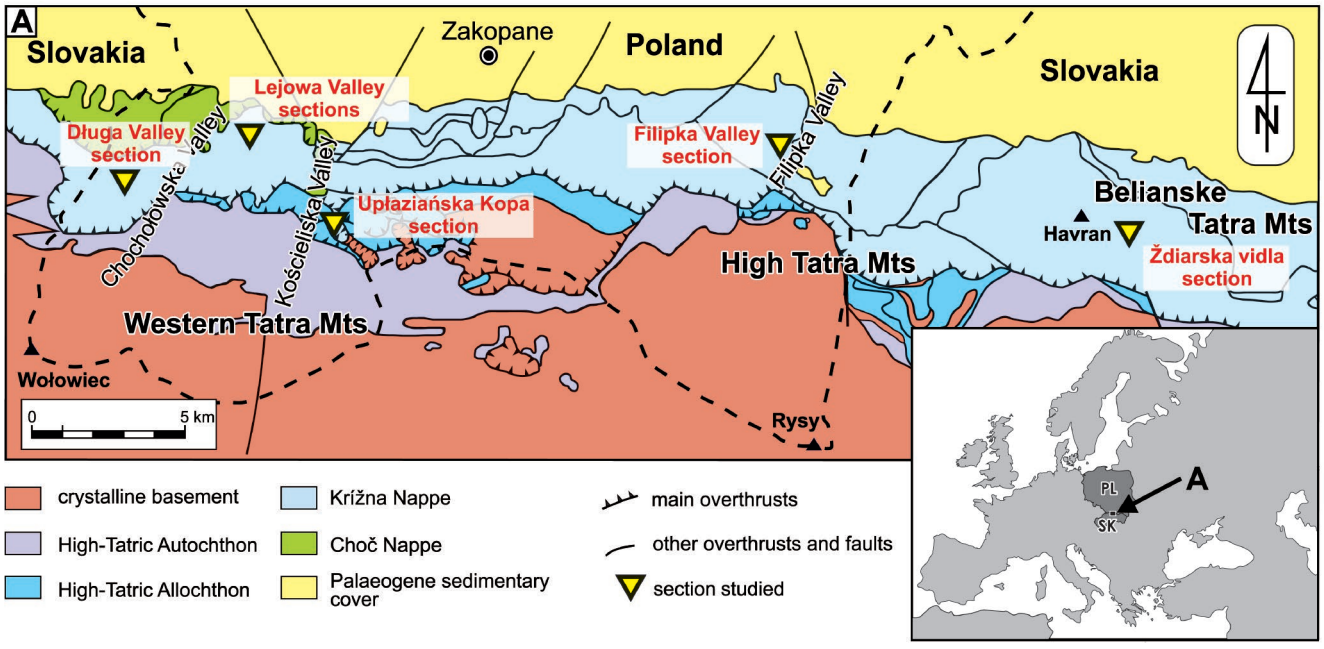

Fig. 2. Tectonic sketch map of the Tatra Mountains (after Bac-Moszaszwili *et al*., 1979; Nemčok *et al*., 1994, simplified) showing locations of the sections studied: Długa Valley, Lejowa Valley, Upłaziańska Kopa, Filipka Valley and Ždiarska vidla.

The rifting of the latter ocean started in the Middle Jurassic (Plašienka, 2018 and references therein).

During the Jurassic, the Fatricum Domain was an extensive, elongated, pull-apart basin, called the Zliechov Basin (Michalík, 2007; Michalík *et al.*, 2017), bordered by some elevated submarine zones represented, for example, by the Vysoká Unit (Koša, 1998; Grabowski *et al*., 2010). The basin resulted from rifting at the turn of the Triassic and Jurassic and was subsequently remodelled by synsedimentary tectonic activity in the latest Early Jurassic (Wieczorek, 2001; Gradziński *et al.*, 2004; Jach, 2005; Plašienka, 2012). The Fatricum Domain is considered to have been located on thinned and stretched continental crust during the Jurassic (e.g., Plašienka, 2003, 2012).

The Krížna Nappe in the Tatra Mts consists of a nearly continuous succession of Lower Triassic to Lower Cretaceous rocks. The Triassic rocks are in general laterally uniform. Conversely, the Lower Jurassic rocks are characterized by significant lateral variation in facies. This resulted from a marked rifting phase, which occurred in the Fatricum Domain at the turn of Triassic and Jurassic (Michalík, 2007; sea also Plašienka, 2003, 2018). It led to the formation of the extensional Zliechov Basin, the rocks of which later were incorporated into the Krížna Nappe. The subsequent rifting phase that took place in the latest Early Jurassic resulted in further diversification of the basin. A horst-and-graben topography was formed (Wieczorek, 2001; Gradziński *et al.*, 2004; Jach, 2005; Plašienka, 2012) and brought about distinct facies variation. The basins were filled with bioturbated "spotted" limestones and marls, known as the Fleckenmergel facies, whereas spiculites, crinoidal limestones and red nodular limestones with condensed horizons were laid down on the submarine elevations. Such inherited submarine topography still was present during the Middle Jurassic and controlled facies changes. More uniform radiolarite sedimentation started in the late Bathonian and persisted until the early late Kimmeridgian (Jach *et al*., 2014). Carbonate sedimentation returned in the late Kimmeridgian, when red nodular limestones were deposited ubiquitously.

Lefeld *et al.* (1985) established the formal lithostratigraphy of the Jurassic deposits of the Krížna Nappe in the Tatra Mts. The rock interval studied in this paper was subdivided into: the Sołtysia Marlstone Formation (spotted limestones), comprising the Łomy Limestone Member (spotted limestones with mudstones) and the Broniarski Limestone Member (cherty limestones); the Niedzica Limestone Formation (grey nodular limestones); the Sokolica Radiolarite Formation (ribbon radiolarites); the Czajakowa Radiolarite Formation (calcareous radiolarites); the Czorsztyn Limestone Formation (red nodular limestones); and the Pieniny Limestone Formation (platy limestones). This lithostratigraphic scheme was modified later. Polák *et al.* (1998) proposed the Ždiar Formation as a new unit, comprising the entire radiolarite succession, namely the Sokolica Radiolarite Formation and Czajakowa Radiolarite Formation (*sensu* Lefeld *et al*., 1985). Pszczółkowski (1996) distinguished two members within the Pieniny Limestone Formation. Subsequently, Grabowski and Pszczółkowski (2006b) adopted formal units, namely the Jasenina and Osnica formations, formerly distinguished in the Strážov Mts, that is in a different part of the Fatricum Domain (Michalík *et al*., 1990; see also Vašíček *et al*., 1994), as equivalents of the Pieniny Limestone Formation (*sensu* Lefeld *et al*., 1985). Birkenmajer (2012) significantly modified the earlier lithostratigraphic schemes of the Krížna Nappe in the eastern part of the Tatra Mts. In this paper, the formal lithostratigraphy by Lefeld *et al.* (1985) is used, with the modifications introduced by Grabowski and Pszczółkowski (2006b). However, the red nodular limestones are regarded as the Czorsztyn Limestone Formation (according to Lefeld *et al*., 1985), whereas the term Jasenina Formation is restricted to the overlying platy limestones. Careful lithostratigraphic revision in the Tatra Mts is required to clarify the stratigraphic problems summarized above, but this is beyond the scope of the present paper.

MATERIALS AND METHODS

Six lithologic sections (Table 1; Figs 3–9) were analyzed in detail, with reference to sedimentary structures, microfacies analysis and carbonate content. The integrated stratigraphy of these sections was established previously by Jach

Table 1

Locations of the sections studied

Section name	Code	Location	GPS coordinates at base of section	Tectonic unit*
Długa Valley	Dsp-Dsr	Western Tatra Mts, Poland	N49°15.599′; E19°48.014′	Bobrowiec Unit
Lejowa Valley	L		N49°15.913′; E19°50.883′	
	Lc		N49°15.897′; E19°50.979′	
Upłaziańska Kopa	Gd		N49°14.359′; E19°53.275′	Gładkie Upłaziańskie Thrust Slice
Filipka Valley	Fp Fz-Fk	High Tatra Mts, Poland	N49°15.952′; E20°4.325′ N49°16.137′; E20°4.348′	Belianske Tatra Unit
Ždiarska vidla	P	Belianske Tatra Mts, Slovakia	N49°14.588′; E20°12.636′	

* nomenclature after Bac-Moszaszwili *et al*. (1979) and Lefeld (1999), modified.

Fig. 3. General field view of the eastern slope of Ždiarska vidla in the Belianske Tatra Mountains (geology after Nemčok *et al*., 1994; modified).

et al. (2012, 2014). The supplementary detailed field studies in the Długa Valley revealed that the tectonic gap marked at ca. 30 m in the stratigraphic log of Jach *et al.* (2014, fig. 3) corresponds to ca. 4 m of the section. Although the sections studied belong to three different thrust-sheets (Table 1; Bac-Moszaszwili *et al*., 1979; Lefeld, 1999), they originally were located close to each other in the north-eastern part of the Fatricum Domain (see Michalík, 2007).

All six sections were studied bed-by-bed with detailed sampling; 1,217 rock samples were collected. The observations then were extended through microfacies analysis. Microfacies were studied in 286 thin sections under Carl Zeiss Axioskop and LEICA DM 2500P optical microscopes. Dunham's (1962) classification of microfacies was applied to the carbonate and siliceous sediments. The rock samples and the thin sections are stored at the Institute of Geological Sciences, the Jagiellonian University in Kraków.

The analyses of calcium carbonate content were carried out in 445 samples, including data presented by Jach *et al*. (2014). Analyses were performed with an Eijkelkamp calcimeter, which works in accordance with the Scheibler method.

The bulk-rock mineral composition was determined for 47 samples by X-ray powder diffraction (XRD) of randomly oriented preparations using a Philips X`PERT APD diffractometer, equipped with a CuKα lamp and graphite monochromator. The samples were analyzed from 2º to 65º 2Θ with 0.02º 2Θ/step and 1 s counting time. Selected thin sections were examined using a scanning electron microscope HITACHI S-4700, equipped with a NORAN Vantage analyzer.

Establishing a robust stratigraphic framework of bed-by-bed measured sections (Figs 4–9; Jach *et al*., 2014) allowed the estimation of the sedimentation rate for specific rock intervals. The five main synchronous horizons, dated precisely by chemo- or biostratigraphic methods, were identified in at least two key sections (Długa Valley and Ždiarska vidla) and were used for further calculations (see Fig. 19). They are as follows: (1) the early Bajocian positive $\delta^{13}C$ excursion, (2) the late Bathonian negative $\delta^{13}C$ shift, (3) the late Callovian positive $\delta^{13}C$ excursion, (4) the Middle Oxfordian positive $\delta^{13}C$ excursion, and (5) the first appearance datum (FAD) of *Colomisphaera pulla* (Borza), indicative of the earliest Tithonian. Additional synchronous horizons, namely: (6) late Bajocian negative $\delta^{13}C$ shift, (7) the FAD of *Stomiosphaera moluccana* Wanner, a marker of the late Kimmeridgian, (8) the FAD of *Parastomiosphaera malmica* (Borza), indicative of the early Tithonian, and (9) the FAD of *Longicollaria dobeni* (Borza), indicative of the early Tithonian, were used as supplementary markers. The age calibration of all these events according to Ogg *et al*. (2016) and Ogg (2019) is listed in Table 2. When a marker horizon was dated with precision to a bio- or magnetostratigraphic zone with a given time range, the middle of this range was used in calculations. The calculated sedimentation rate is affected by an error due to the following reasons: (1) the resolution of biostratigraphic data, (2) uncertainty as to the precise numerical age of marker synchronous horizons, and (3) the resolution of sampling, which varies from 0.05 m to more than 1 m.

SEDIMENTARY FACIES AND THEIR INTERPRETATION

Bositra-crinoidal limestones (Bajocian – middle Bathonian)

Description

In the Western Tatra Mts, Toarcian–?Aalenian red limestones (Kliny Limestones Member; Lefeld *et al*., 1985; Myczyński and Jach, 2009) are overlain by the *Bositra*-crinoidal limestones, which do not have a formal lithostratigraphic status. Formerly, they were assigned to the Aalenian – lower Bathonian (Jach, 2007), but later their age was constrained to Bajocian – middle Bathonian on the basis of integrated stratigraphy (Jach *et al*., 2014). The *Bositra*-crinoidal limestones are up to 15 m thick and generally are poorly exposed. The base of this facies is marked by an abrupt transition from the red nodular limestones. The contact abounds with glauconite grains and most probably represents an omission surface (Jach, 2007). This facies contains abundant thin-shelled bivalves that herein traditionally

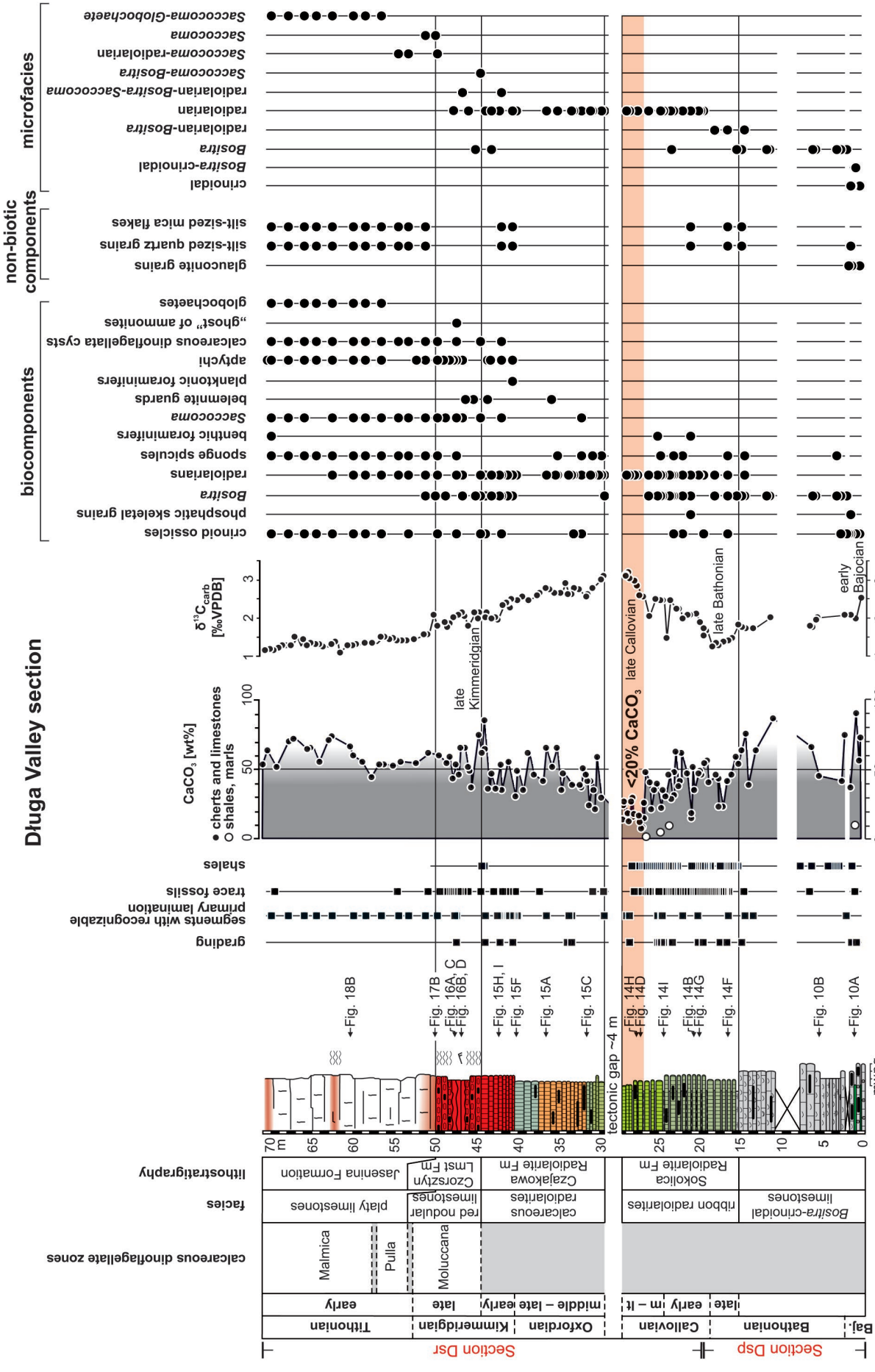

Fig. 4. Detailed log of the Długa Valley section in the Western Tatra Mountains. Lithology, stratigraphy, carbon-isotope curve, $CaCO_3$ content and microfacies analysis after Jach *et al.* (2014), modified and supplemented. Log colour reflects the natural rock hues. See Figure 9 for legend.

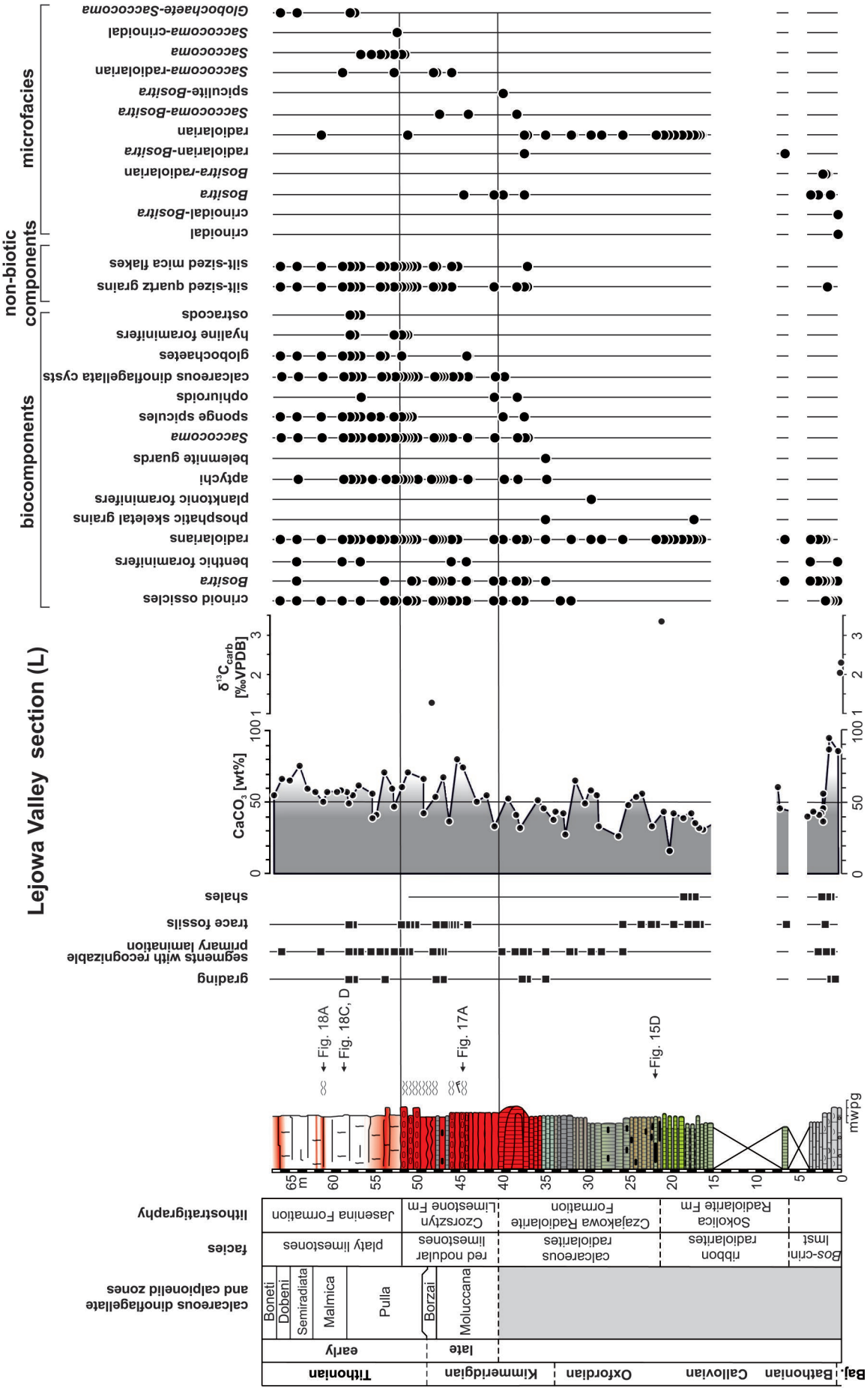

Fig. 5. Detailed log of the Lejowa Valley section (L) in the Western Tatra Mountains. Lithology, stratigraphy, carbon-isotope curve, $CaCO_3$ content and microfacies analysis after Jach *et al.* (2014), modified and supplemented. Log colour reflects the natural rock hues. See Figure 9 for legend.

Fig. 6. Detailed log of the Lejowa Valley section (Lc) in the Western Tatra Mountains. Lithology, stratigraphy, carbon-isotope curve, $CaCO_3$ content and microfacies analysis after Jach *et al.* (2014), modified and supplemented. Log colour reflects the natural rock hues. See Figure 9 for legend.

Fig. 7. Detailed log of the Uplaziańska Kopa section in the Western Tatra Mountains. Lithology, stratigraphy, carbon-isotope curve, $CaCO_3$ content and microfacies analysis after Jach *et al.* (2014), modified and supplemented. Log colour reflects the natural rock hues. See Figure 9 for legend.

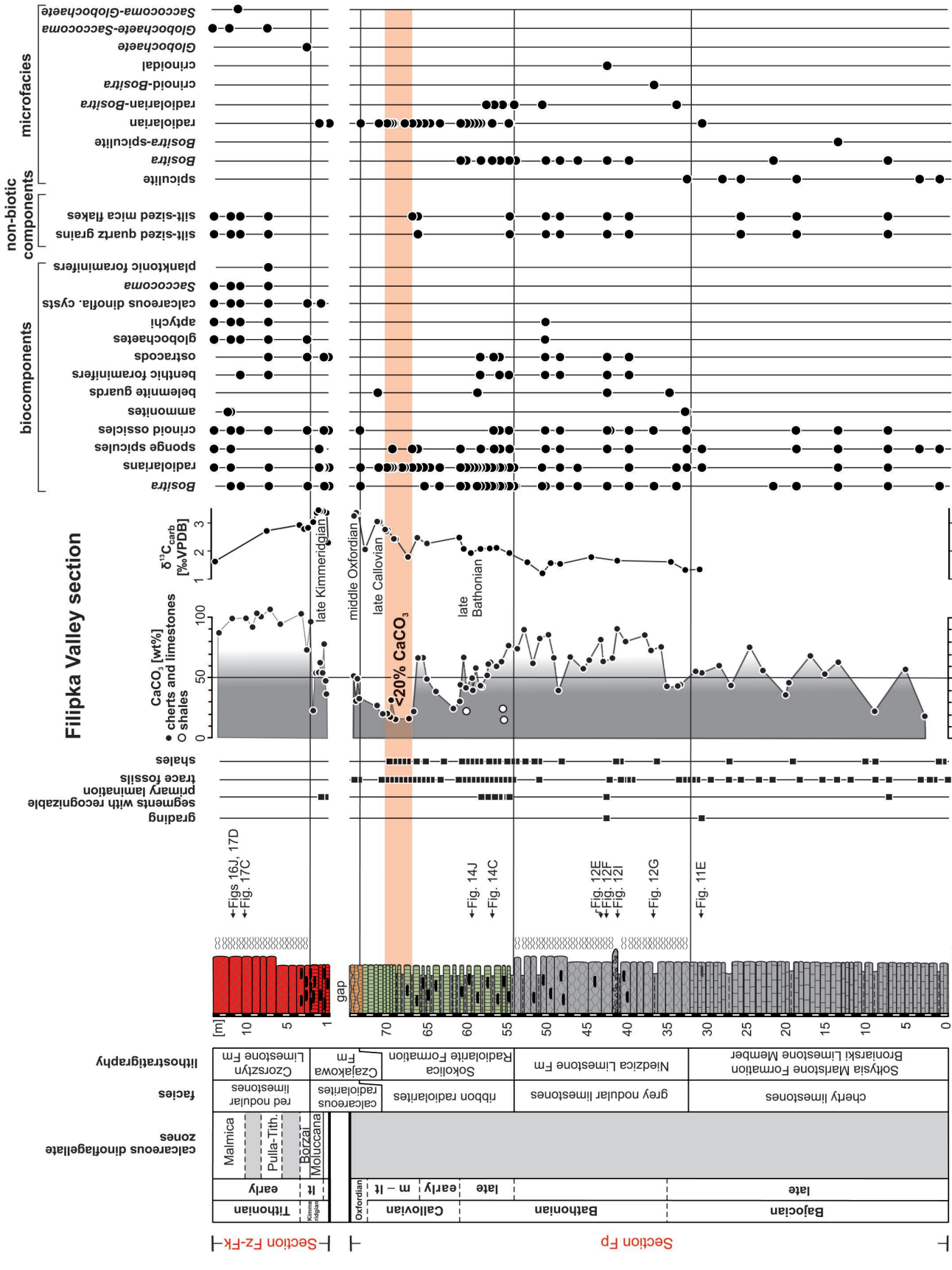

Fig. 8. Detailed log of the Filipka Valley section in the High Tatra Mts. Lithology, stratigraphy, carbon-isotope curve, $CaCO_3$ content and microfacies analysis after Jach *et al.* (2014), modified and supplemented. Log colour reflects the natural rock hues. See Figure 9 for legend.

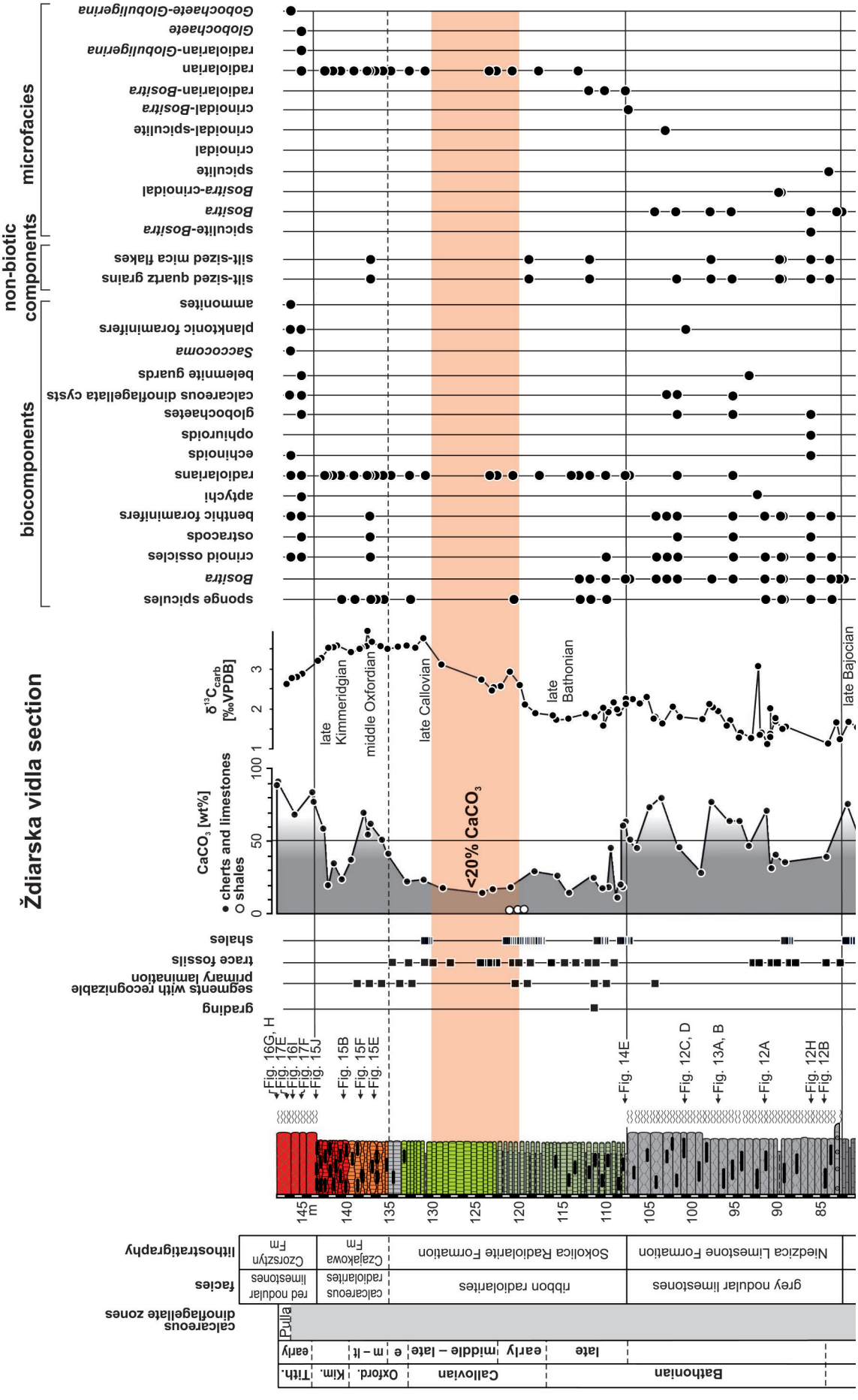
Ždiarska vidla section
non-biotic components
biocomponents
microfacies
sponge spicules
Bositra
crinoid ossicles
ostracods
benthic foraminifers
aptychi
radiolarians
echinoids
ophiuroids
globochaetes
calcareous dinoflagellata cysts
belemnite guards
Saccocoma
planktonic foraminifers
ammonites
silt-sized quartz grains
silt-sized mica flakes
spiculite-Bositra
Bositra
spiculite
crinoidal
crinoidal-spiculite
crinoidal-Bositra
radiolarian-Bositra
radiolarian
radiolarian-Globuligerina
Globochaete
Globochaete-Globuligerina
δ13Ccarb [‰VPDB]
CaCO3 [wt%]
• cherts and limestones
○ shales
<20% CaCO3
late Kimmeridgian
middle Oxfordian
late Callovian
late Bathonian
late Bajocian
grading
segments with recognizable primary lamination
trace fossils
shales
Fig. 16G, H
Fig. 17E
Fig. 16L
Fig. 17F
Fig. 15J
Fig. 15B
Fig. 15F
Fig. 15E
Fig. 14E
Fig. 12C, D
Fig. 13A, B
Fig. 12A
Fig. 12H
Fig. 12B
m
Bathonian
Callovian
Oxford.
Kim.
Tith.
late
early
middle – late
m – l
e
early
Pulla
calcareous dinoflagellate zones
grey nodular limestones
ribbon radiolarites
calcareous radiolarites
red nodular limestones
Niedzica Limestone Formation
Sokolica Radiolarite Formation
Czajakowa Fm
Czorsztyn Fm
facies
lithostratigraphy

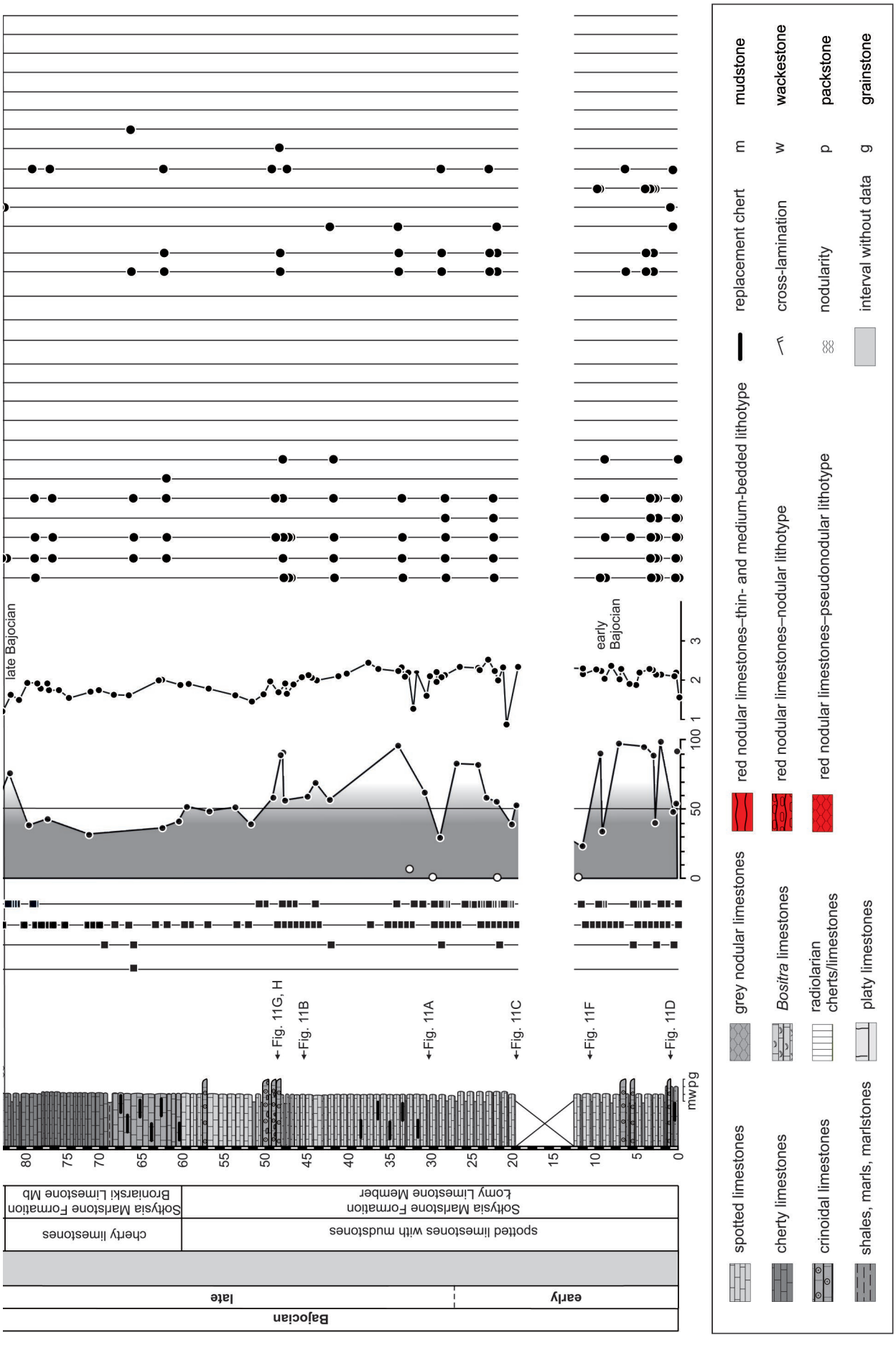

Fig. 9. Detailed log of the Ždiarska vidla section in the Belianske Tatra Mountains. Lithology, stratigraphy, carbon-isotope curve, $CaCO_3$ content and microfacies analysis after Jach *et al.* (2014), modified and supplemented. Log colour reflects the natural rock hues.

Table 2

Age calibration of synchronous horizons used in calculations of sedimentation rate; papers referred to are included in the reference list

Horizon	Bio- and magnetostratigraphic correlation	Age calibration (after Ogg *et al*., 2016; Ogg, 2019)	Age used in calculations
Main synchronous horizons			
early Bajocian positive $\delta^{13}C$ excursion	base of Humphriesianum Zone (O'Dogherty *et al*., 2006)	169.7 Ma	169.7 Ma
late Bathonian negative $\delta^{13}C$ shift	Orbis Zone (O'Dogherty *et al*., 2006)	166.41 to 166.24 Ma	166.33 Ma
late Callovian positive $\delta^{13}C$ excursion	uppermost part of Lamberti Zone (Wierzbowski, 2015)	≈ 163.2 Ma	163.2 Ma
middle Oxfordian positive $\delta^{13}C$ excursion	near the Plicatilis-Transversarium zones boundary (Bartolini, 1999; Wierzbowski, 2015; O'Dogherty *et al*., 2018)	≈ 159.88 Ma	159.88 Ma
FAD of *Colomisphaera pulla* (Borza) – base of Pulla Zone	Kimmeridgian-Tithonian boundary (Grabowski *et al*., 2010; Pszczółkowski *et al*., 2016)	152.06 Ma	152.06 Ma
Supplementary synchronous horizons			
late Bajocian negative $\delta^{13}C$ shift	within Parkinsonia Zone (O'Dogherty *et al*., 2006)	168.69 to 168.28 Ma	168.48 Ma
FAD of *Stomiosphaera moluccana* Wanner – base of Moluccana Zone	base of Acanthicum Zone (Reháková, 2000; Reháková *et al*., 2011)	154.47 Ma	154.47 Ma
FAD of *Parastomiosphaera malmica* (Borza) – base of the Malmica Zone	base of M21 Magnetozone (Michalík *et al*., 2009)	149.8 Ma	149.8 Ma
FAD of *Longicollaria dobeni* – base of Dobeni Subzone of Chitinoidella Zone	within M21n Magnetozone (Michalík *et al*., 2009; Grabowski *et al.*, 2010; Grabowski, 2011)	149.3 to 148.44 Ma	148.9 Ma

are regarded as *Bositra*, for the sake of simplicity. They can represent some other taxa (see Conti and Monari, 1992); however, the state of preservation makes their precise determination impossible.

The *Bositra*-crinoidal limestones are grey to greenish-grey in colour and well bedded; the bed thickness varies from 3 cm to 30 cm. Dark grey replacement chert lenses occur in the limestone beds. This facies includes crinoidal limestones and *Bositra* limestones.

The crinoidal limestones have sharp bedding planes and occasionally display normal grading. They occur in the lower parts of the Długa Valley and Lejowa Valley sections (Figs 4, 5), where they reach thicknesses of 1.7 m and 0.5 m, respectively. Their $CaCO_3$ content ranges from 56 to 90 wt%. Crinoidal grainstones and packstones constitute the predominant microfacies, with *Bositra*-crinoidal packstones occurring subordinately. The most abundant skeletal grains are crinoid ossicles; crushed *Bositra* shells are less common. Three sharp surfaces covered with centimetre-thick marls were identified within the crinoidal limestones in the Długa Valley section (see Jach, 2007). The marls contain glauconite grains, glauconitized crinoid debris, benthic foraminifera and phosphatic skeletal debris (Fig. 10A). They contain abundant siliciclastic grains, namely quartz and micas. This was confirmed by XRD analysis of the bulk sample, which indicates also calcite, chlorite and plagioclase.

Bositra shells abruptly start to predominate at 1.7 m of the Długa Valley section, leading to the formation of the 14 m-thick *Bositra* limestones. In the lowermost part, they are more marly. They contain from 39 to 89 wt% of $CaCO_3$. *Bositra* shells are the dominant components; they are accompanied by less common crinoidal ossicles and radiolarian tests. The latter are more common upward in the sections studied. *Bositra* grainstones and packstones are the dominant microfacies. Fabrics are shell-supported; the shells are disarticulated but only rarely broken, flattened and densely packed (Fig. 10B). As a result, during field inspection the rock appears to be regularly laminated. *Bositra* wackestones, mudstones and *Bositra*-radiolarian wackestones to packstones are subordinate.

Trace fossils are rare in the *Bositra*-crinoidal limestones; however, some parts of this facies are intensively bioturbated, for example, the *Bositra*-crinoidal packstones. In contrast to lower and upper parts of this facies, *Bositra* grainstones occurring in the central portion of this facies show almost no sign of bioturbation.

Interpretation

Crinoidal fragments are characterized by high primary porosity, which determines their hydrodynamic behaviour (Blyth Cain, 1968). As a result, they can be easily transported even by weak currents for relatively long distances. Thus, crinoidal fragments in the *Bositra*-crinoidal limestones probably represent bioclasts redeposited by bottom currents, whereas relatively well preserved *Bositra* shells are an autochthonous component.

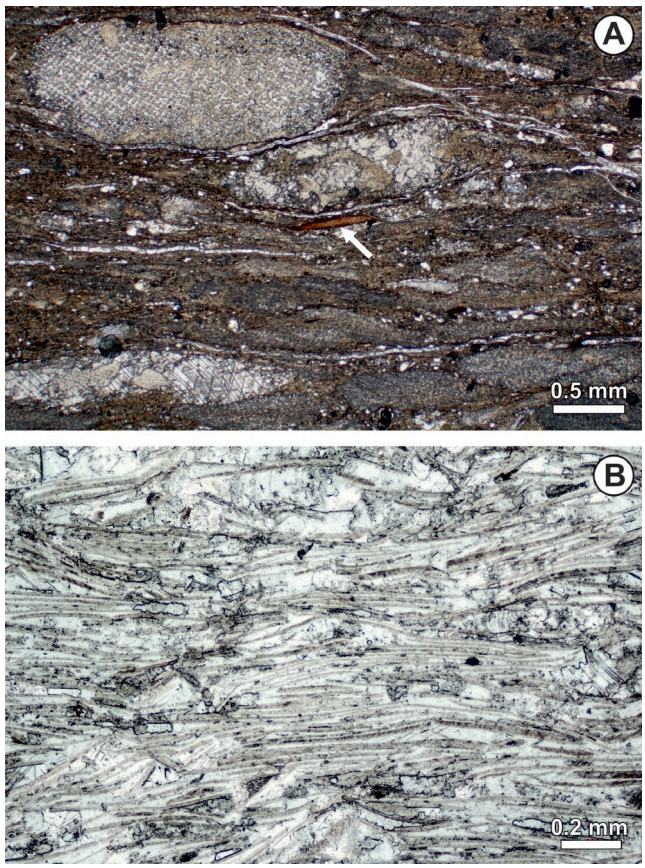

Fig. 10. *Bositra*-crinoidal limestones at the Długa Valley section (Fig. 4). **A.** Marls containing crinoidal ossicles partly filled with pale-green glauconite and rare phosphatic skeletal fragments (arrow). **B.** *Bositra* grainstone; thin section. For precise location of the samples see Appendix in the electronic version of the paper.

Accepting the above view, one can regard the graded crinoidal limestones as density flow deposits (see Jach, 2007). The *Bositra*-crinoidal packstones contain allochthonous and autochthonous material, presumably mixed by bioturbation (Monaco, 2016). The interbedded marls bear a resemblance to hiatal deposits, which reflect a very slow sedimentation rate or even minor breaks. They contain concentrations of glauconite grains and phosphatic skeletal debris, which are indicative of an omission surface (Christ *et al*., 2012; Brady and Bowie, 2017).

The overlying *Bositra* limestones represent a widespread facies in the Bathonian – Callovian of the Tethyan realm (e.g., Santantonio, 1993; Martire, 1996; Navarro *et al*., 2009, 2012; Vörös, 2012; O'Dogherty *et al*., 2018; Molina *et al*., 2018). The predominant clean-washed *Bositra* grainstones indicate a higher current regime, whereas the micrite-bearing *Bositra* packstones and wackestones evidence lower-energy conditions.

The high concentration of *Bositra* shells, which are the overwhelmingly dominant component, may result from the interplay of three type of factors, namely: (1) taphonomic, (2) ecological, and (3) dissolution (see Jach, 2007).

Bositra is considered to be a benthic organism, which preferred soft bottoms (e.g., Wignall, 1993; Röhl *et al*., 2001; Tomás *et al*., 2019). Thus, the concentration of well-washed but not fragmented *Bositra* shells indicates intense winnowing of the accompanying fine grained fraction by currents of a capacity that was too low to transport or crush *Bositra* shells (Jach, 2007).

It is commonly accepted that *Bositra* was an opportunistic, tolerant organism, which had fast generation times and thrived in stressed conditions (e.g., Caswell and Coe, 2013; Molina *et al*., 2018). Accepting this, the dominance of *Bositra* indicates some kind of environmental stress. Although *Bositra* was common in an oxygen-deficient environment (e.g., Röhl *et al*., 2001), this kind of stress must be excluded, since the deposits discussed were washed by currents and were bioturbated, which collectively indicates the presence of oxygen in the bottom seawater.

The complete lack of aragonite bioclasts in the *Bositra*-crinoidal limestones discussed might indicate the elimination of this mineral by dissolution in the seawater column or at the sea bottom (Jach, 2007). Although this possibility cannot be ruled out completely, the presence of ammonites in the coeval spotted limestones indicates that it is less probable.

Interestingly, the currents, which swept away the fine-grained components, did not cause the early cementation of *Bositra* shells. They underwent compaction and display a fitted fabric (*sensu* Clari and Martire, 1996).

Spotted limestones (Bajocian)

Description

This facies consists of spotted limestones, which occur in the Kopy Sołtysie of the High Tatra Mts (Filipka Valley section; Fig. 8) and in the Belianske Tatra Mts (Ždiarska vidla section; Fig. 9). They are included in the uppermost part of the Sołtysia Marlstone Formation (Lefeld *et al*., 1985) and are subdivided into two members, namely the lower Łomy Limestone Member and the upper Broniarski Limestone Member. They formerly were included to the uppermost part of the Janovky Formation (Gaździcki *et al*., 1979). The Bajocian age, based on ammonites (Myczyński, 2004; Iwańczuk *et al*., 2013), was fully supported by carbon-isotope chemostratigraphy (Jach *et al*., 2014).

The Łomy Limestone Member consists of highly bioturbated, medium grey, micritic limestones alternated with darker grey, siliciclastic mudstones (Fig. 11A). The measured thickness is 60 m in the Ždiarska vidla section. The limestones yielded rare ammonites and belemnites (Iwanow, 1973; Myczyński, 2004; Iwańczuk *et al*., 2013). Trace fossils are visible as variable, darker infillings in a totally bioturbated, light grey, micritic matrix. The siliciclastic mudstones are slightly bioturbated; lamination is commonly visible (Fig. 11C). Trace fossils are relatively common and moderately diverse (e.g., common *Chondrites*, *Planolites*, *Zoophycos*, *Teichichnus* and *Thalassinoides*; Fig. 11B; Wieczorek, 1995; Iwańczuk *et al*., 2013; Uchman and Jach, 2017). The limestone beds range in thickness from 3 to 60 cm; the average being about 20 cm, whereas individual siliciclastic mudstone beds vary from 1 to 90 cm, the average being about 10 cm. The limestone beds usually have sharp and well defined boundaries. Light grey

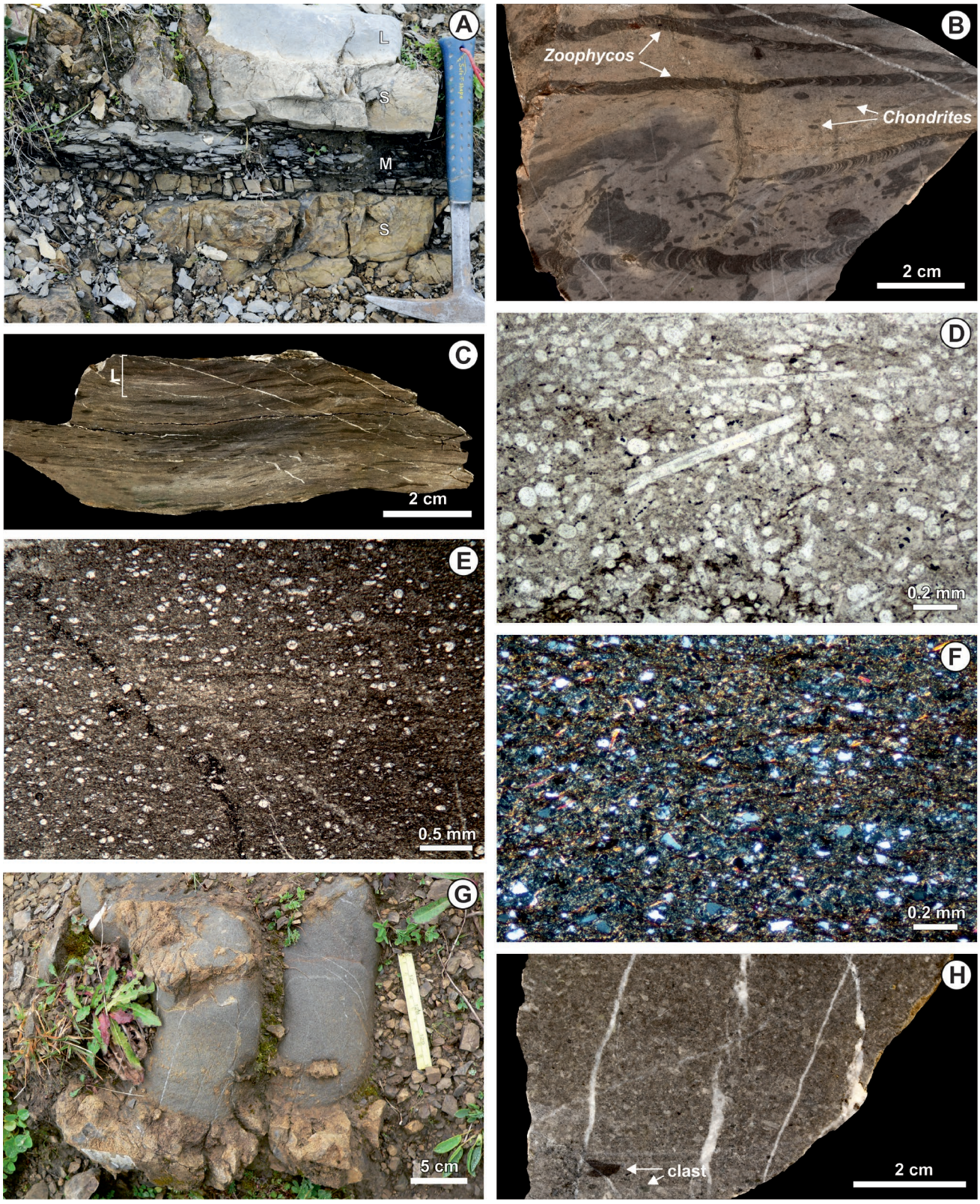

Fig. 11. Spotted limestones. **A.** Field photograph of light grey, bioturbated limestones (L) alternating with dark siliciclastic mudstones (M); irregular chert bands are distributed in base and top parts of the limestone beds (S); Ždiarska vidla section (Fig. 9), hammer for scale is 33 cm long. **B.** Vertical cross-section of the spotted limestone with trace fossils *Zoophycos* and *Chondrites*; Ždiarska vidla section (Fig. 9), polished slab. **C.** Partly bioturbated dark mudstone with preserved primary lamination in the uppermost part of sample (L); Ždiarska vidla section (Fig. 9), polished slab. **D.** Spiculite packstone; Ždiarska vidla section (Fig. 9), thin section. **E.** Radiolarian wackestone; Filipka Valley (Fig. 8), thin section. **F.** The principal constituents of siliciclastic mudstones are silt-size grains of quartz and mica flakes; Ždiarska vidla section (Fig. 9), thin section, cross-polarised light. **G.** Field photograph of a crinoidal turbidite; Ždiarska vidla section (Fig. 9). **H.** Crinoidal grainstone with small lithoclasts at the base; Ždiarska vidla section (Fig. 9), polished slab. For precise location of the samples see Appendix in the electronic version of the paper.

and brown, yellow weathering cherts commonly occur as irregular lenses and bands at their basal and top parts. The limestones contain relatively common sponge spicules, fragments of *Bositra* shells, crinoidal ossicles, radiolarian moulds and rare benthic foraminifera, ostracods (Fig. 11D, E). Locally, the limestones have a higher silty siliciclastic content (quartz, plagioclase, micas and chlorite), which was confirmed by XRD analysis. Texturally, the limestones are classified as wackestones and packstones, with spiculite-*Bositra*, spiculite, *Bositra*, crinoidal, and crinoidal-spiculite microfacies (Figs 8, 9). Thin-section observations and XRD analysis revealed that the siliciclastic mudstones are composed of fine-sand- to silt-sized quartz, micas, chlorites and plagioclase; calcareous microfossils are not present (Fig. 11F).

Seven discrete beds, composed mainly of crinoidal skeletal debris, 8–46 cm thick, occur within this facies in the Ždiarska vidla section (Fig. 11G). In addition to the predominant crinoidal material, rare foraminifera, sponge spicules, quartz grains and small clasts (up to 1 cm) of recrystallized unfossiliferous carbonates occur. Single beds show grading from grainstone to wackestone, with small lithoclasts at the base (Fig. 11H). The lower boundary of each of these beds is a sharp, erosive surface. No current structures were observed. Most probably, one of these beds were formally distinguished as the Łężny Encrinite Bed by Lefeld *et al*. (1985).

The limestones of the Łomy Limestone Member pass upward into cherty limestones of the Broniarski Limestone Member, which is about 25 m thick (Figs 8, 9). Dark, brownish-grey, cherty limestones are thin- to medium-bedded (average bed thickness about 15 cm) and rarely intercalated with marls. Trace fossils are less common in this unit. Macrofossils include rare and poorly preserved ammonites and rare aptychi.

These deposits reveal the spiculite, *Bositra*, crinoidal, *Bositra*-crinoidal, *Bositra*-spiculite, radiolarian and crinoidal-spiculite microfacies (wackestone to packstone; Figs 8, 9). Whole-rock X-ray diffraction of limestones revealed calcite, quartz, plagioclase, with minor micas and dolomite.

Generally, the $CaCO_3$ content in the limestone beds of the spotted limestones decreases upward, from 98 to 32 wt%, whereas the content in siliciclastic mudstones ranges from 0.3 to 6.2 wt%.

Interpretation

Spotted limestones and marls are a widespread Tethyan facies; they are called the Fleckenmergel-Fleckenkalk or the Allgäu facies (e.g., Jacobshagen, 1965; Gawlick *et al*., 2009 and references quoted therein). These deposits are interpreted as indicative of basinal, hemipelagic and oxygen-depleted condition (e.g., Wieczorek, 1995; Tyszka, 1994; Uchman and Myczyński, 2006; Šimo and Tomašových, 2013). Highly bioturbated alternating deposits, common in the Lower – Middle Jurassic of the Tethyan sections, originated in the intra-shelf basins. Generally, high sedimentation rates characterized the depocentres of such basins (Šimo and Tomašových, 2013). In the eastern part of the Tatra Mts, the spotted limestones, comprising 270 m of the upper Sinemurian – Bajocian, were deposited in a gradually deepening basin (Iwanow, 1973; Lefeld *et al*., 1985; Myczyński, 2004; Iwańczuk *et al*., 2013).

The dominance of micrite, depositional textures, microfauna association and absence of current structures indicate deposition of the spotted limestones in a low-energy hemipelagic environment (Eberli, 1988). Fluctuations in both trophic level and probably bottom seawater oxygenation, under which the spotted limestones and marls were deposited, exerted the primary controls on the tracemaker community and microbenthic assemblage (Wieczorek, 1995; see also Tyszka, 1994; Uchman and Myczyński, 2006; Šimo and Tomašových, 2013). Wieczorek (1995) recognized two phases of bioturbation associated with this oxygenation level. At first, a totally bioturbated matrix was produced during times of well-oxygenated bottom seawaters. During the second phase, fodinichnia-dominated trace fossils were produced under oxygen-deficient conditions. The deposition of limestones and siliciclastic mudstones took place in fluctuating oxygenation conditions. The oxygen-deficient conditions probably were related to the development of restricted seawater circulation and stratified seawater column conditions (e.g., Tyszka, 1994, 2001; Raucsik and Varga, 2008; Šimo and Tomašových, 2013). Rhythmic alternation of limestones and marls probably was controlled by periodic climatic changes, most probably during warm climate with monsoon-like, seasonally humid conditions (Raucsik *et al*., 2001).

The crinoidal limestone beds occurring within this facies are interpreted as calciturbidites (Mišík, 1959; see also Eberli, 1987, 1988; Matyszkiewicz, 1996) owing to: (1) the difference in composition and texture between them and the co-occurring spotted limestones, (2) the sharp erosive lower boundary, (3) the presence of grading, (4) the bi-modal distribution of components with lithoclasts occurring at their base. Turbidity currents carried crinoidal material derived from better-oxygenated, adjacent highs into the basinal area. During the lower Bajocian, crinoidal meadows occupied submarine elevations and their slopes, which were source areas for the crinoidal material shed as turbidites into the basin (Mišík, 1959; Iwańczuk *et al*., 2013).

Grey nodular limestones (uppermost Bajocian – middle Bathonian)

Description

The grey nodular limestones were distinguished formally as the Niedzica Limestone Formation by Lefeld *et al*. (1985), but their exact stratigraphic position remained unclear (Lefeld, 1974). Jach *et al.* (2014) revealed the location of these limestones directly below the Sokolica Radiolarites Formation (the ribbon radiolarites in this paper). The nodular limestones occur exclusively in the succession of the eastern part of the Tatra Mts, where they rest on the cherty limestones (Broniarski Limestone Member).

This facies succession, 22–25 m thick (Figs 8, 9), is organized in decimetre- to almost metre-thick beds. The limestones are grey and they become pale pink in colour only in the uppermost part of the Filipka Valley section. The most

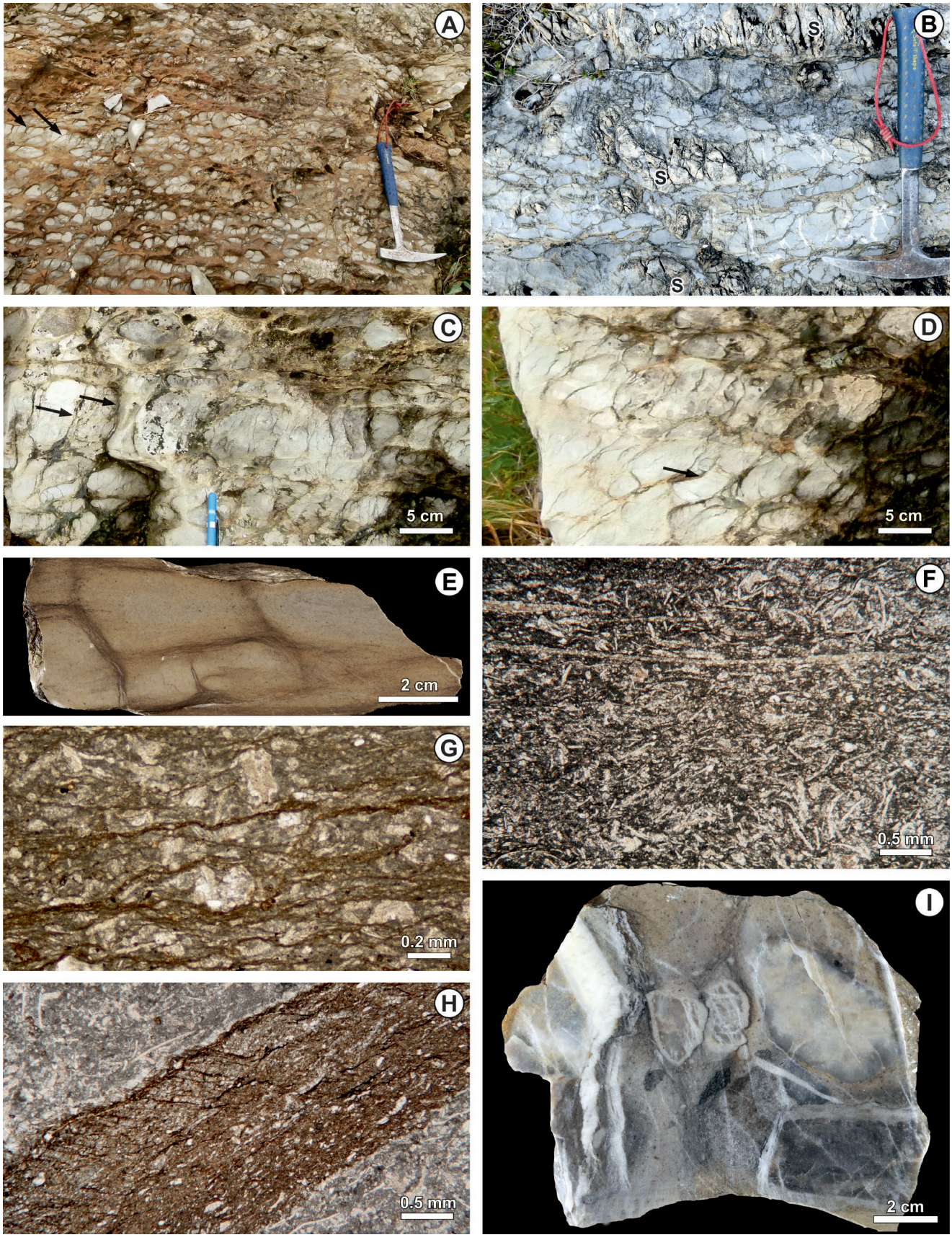

Fig. 12. Grey nodular limestones. **A.** Field photograph of the lithotype comprising nodules and abundant matrix; note the vertical and diagonal cracks in biggest nodules (black arrows); Ždiarska vidla section (Fig. 9), hammer for scale is 33 cm long. **B.** Field photograph of the lithotype comprising tightly packed nodules separated by a thin film of matrix; note the presence of cherts (S); Ždiarska vidla section (Fig. 9), hammer for scale is 33 cm long. **C.** Vertical and diagonal fractures (arrows) in a limestone bed, with steeply imbricated facoidal nodules in the lowest and uppermost parts (movement to the right); Ždiarska vidla section (Fig. 9). **D.** Steep imbrication of

distinctive feature of this facies is the presence of lenticular nodules that consist of grey limestone, enveloped in a darker, brownish grey siliciclastics-enriched matrix (Fig. 12A). Belemnite rostra are rare, whereas the internal moulds of ammonites are extremely scarce and poorly preserved. Cherts are common, distributed along bedding planes and forming variably shaped nodules or horizontally elongated lenses, up to 20 cm across (Fig. 12B). The limestone is totally bioturbated, but no determinable trace fossils have been recognized. The $CaCO_3$ content in this facies ranges from 29 to 82 wt%, averaging ca. 58 wt% (Figs 8, 9).

Two distinctly different limestone lithotypes are recognized in this facies, differing in the spatial pattern of nodules and the intervening matrix (Fig. 12A, B). They are regarded as two end-members, as they show gradational transitions with combined, intermediate characteristics. The first lithotype shows elongate, lenticular to ovoidal nodules, tightly enveloped in matrix (Fig. 12A). The nodule boundaries are often diffuse, with a gradual transition to the inter-nodular matrix (Fig. 13A). The matrix is volumetrically abundant, which makes the nodules look as if they were "floating" in the surrounding matrix (Fig. 12A). The majority of nodules are oriented horizontally, show little or no imbrication and are arranged in horizons parallel to the general bedding of the limestone (Fig. 12A). Vertical and diagonal fractures are common.

The second lithotype is much poorer in matrix and shows a jigsaw-puzzle texture of sharp-edged lenticular nodules (Fig. 12B), classified as a fitted fabric (*sensu* Bathurst, 1991). The nodules here are tightly packed and discrete, with only a thin film of matrix (Fig. 12H). The nodules are up to 12 cm across and their shapes are elongate, cuboidal, lozenge or irregular with a serrated outline (Fig. 12B, E). The limestone also shows vertical and diagonal fractures, commonly breaking the nodules (Fig. 12C, D). A common feature is the steep imbrication of nodules, locally subvertical (Fig. 12C, D).

The nodules include *Bositra*, *Bositra*-spiculite and *Bositra*-crinoidal, *Bositra*-radiolarian, spiculite, crinoidal wackestones and packstones (Fig. 12F). The bioclasts within nodules show a varying degree of fragmentation, but are mainly crushed and show little compaction. The XRD analysis documented calcite, quartz, micas, plagioclase and dolomite. The inter-nodular matrix contains crushed bioclasts that are distinctly more fragmented and compacted (Fig. 12H). There are abundant swarms of closely spaced, undulose dissolution seams, rich in non-calcareous clayey material (Fig. 12G), containing silt-sized quartz grains, mica flakes, plagioclase and apatite crystals. Microstylolites are locally present (Fig. 13).

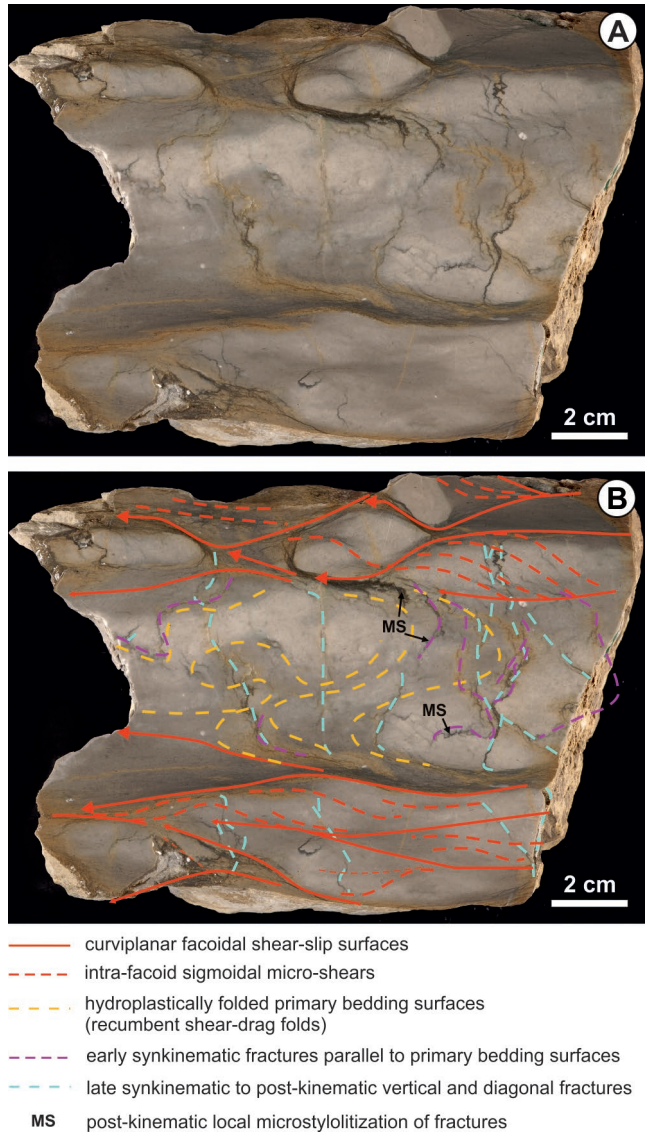

Fig. 13. Grey nodular limestones. **A, B.** Structural evidence of sediment creep deformation; Ždiarska vidla section (Fig. 9), polished slab. The lowermost and uppermost deposits show synsedimentary ductile shear deformation, followed by sparse subvertical brittle fracturing after their complete consolidation. The middle deposits were first deformed by shear drag folding and formed an outsized facoid; they were subsequently subjected to local synkinematic fracturing along their primary bedding surfaces due to the folding stresses, and finally underwent a brittle-state subvertical fracturing. The entire deformation process was gradual and occurred at a very slow rate, spanning the time from soft to rigid states of the sediments. General direction of creep movement to the left. For precise location of the sample see Appendix in the electronic version of the paper.

elongated facoidal nodules, with both plastic deformation (arrow) and later fracturing; Ždiarska vidla section (Fig. 9). **E.** Limestone bed sole showing cuboidal and lozenge nodules separated by thin matrix shear bands and post-kinematic subvertical fractures; Filipka Valley (Fig. 8), polished slab. **F.** Uncompacted *Bositra* packstone forming a nodule; Filipka Valley (Fig. 8), thin section. **G.** Compacted crinoidal *Bositra* packstone with undulose bifurcating dissolution seams forming matrix; Filipka Valley (Fig. 8), thin section. **H.** Sinistral shear band (matrix film) composed of compacted *Bositra* wackestone between two nodules composed of uncompacted *Bositra* wackestone; Ždiarska vidla section (Fig. 9), thin section. **I.** Bed sole view of clast-supported limestone conglomerate; note the calcite-coated and non-coated subangular clasts and calcite-filled fractures; Filipka Valley (Fig. 8), polished slab. For precise location of the samples see Appendix in the electronic version of the paper.

The basal part of the grey nodular limestone succession in the Filipka Valley section contains a remarkable conglomeratic bed, which is 70 cm thick (see log height 42 m in Fig. 8). This bed comprises a massive, non-graded, clast-supported limestone conglomerate (Fig. 12I), capped with a graded, crinoidal packstone. The conglomerate consists of a mixture of angular to subangular clasts (up to 2 cm across) of the *Bositra* limestones, spiculites, crinoidal limestones and recrystallized non-fossiliferous limestones with a sparse, fine-grained matrix containing a "hash" of broken *Bositra* shells and numerous crinoid fragments.

Interpretation

The grey nodular limestones are similar to the Jurassic nodular limestones of the Rosso Ammonitico type (cf. Martire, 1996). The main similarities include their primary microfacies characteristics and their distinct nodularity, with the under-compacted nodules enveloped by compacted matrix. This latter characteristic indicates that the nodules were formed mainly in a soft state of sediment early diagenesis, while the subsequent progressive fracturing indicates that the deformation proceeded continuously to the sediment brittle state of consolidation (cf. Clari and Martire, 1996). The nodules resulted from selective early cementation of carbonate deposits rich in microcrystalline calcite.

The nodular limestones in the present case are interpreted as a product of long-lasting, low-rate submarine sediment creep processes that spanned the time of sediment consolidation from the soft to the rigid state and involved a progression from plastic-ductile to brittle types of gravitational deformation (Fig. 13). The differences in deformation style, from bed to bed, are attributed to the sediment composition. In the first lithotype described above, richer in the clayey fraction, the synsedimentary ductile-shear facoidal deformation proceeded slowly until the sediment reached a brittle rheological state and fracturing commenced (Fig. 13). In the second lithotype, much poorer in clay, the incipient facoidal shear lenses – devoid of clayey lubricant – became directly subject to a synsedimentary fracture brecciation and an imbricate *in-situ* piling (Fig. 12D). Similar imbrication of nodules was reported from other mass-movement limestones (Bertok *et al.*, 2011). Likewise, a similar combination of plastic to brittle deformation was recognized elsewhere in the Rosso Ammonitico deposits, but was attributed mainly to slumping (e.g., Bernoulli and Jenkyns, 1970; Martire, 1996; Rais *et al*., 2007). The interpretation in the present study is consistent with the textbook opinions (e.g., Fossen, 2016) that not every synsedimentary recumbent shear-drag fold necessarily must indicate a slump and may instead be the product of a slow sediment creep process.

The vertical and diagonal fractures are similar to the extension gashes formed in lithified limestones (e.g., Bergerat *et al.*, 2011; Kullberg *et al.*, 2001; Matyszkiewicz and Kochman, 2016) and also the matrix-filled subvertical fractures support the notion of brittle-state late synsedimentary deformation. Analogous structures were reported from the Jurassic–Cretaceous submarine mass-movement deposits involving differently lithified marlstone-limestone couplets (Basillone, 2017). The submarine sediment creep would have been driven by gravity, but may have been instigated by a seismic shock (e.g., Field *et al.*, 1982; Neuweiler *et al*., 1999; Rychliński and Jaglarz, 2017). The basal conglomeratic bed in the Filipka Valley section, directly below the nodular limestone succession, is considered to be a debris-flow deposit capped by a crinoid-rich sandy calciturbidite. As an interpretative scenario, the slope space evacuation by these sediment gravity flows may have resulted in further slope instability (e.g., Eberli, 1987; Basillone *et al.*, 2016) and triggered the subsequent gravitational bulk creep of the carbonate slope deposits, resulting in the nodular limestone succession. Another interpretation is also possible. The conglomeratic bed might have originated from a seismic shock and the overlying calciturbidite may represent a tsunamite.

The cuboidal to lozenge-shaped nodules resemble those in the Cretaceous pelagic mass-movement limestones in the Apennines (Alvarez *et al*., 1985) and in the pseudonodular Jurassic limestones in the Ligurian Alps, interpreted as deformed by seismic shaking (Bertok *et al*., 2011). In both of these latter cases, the differential lithification of the primary carbonate deposits was invoked; this also may have been an important factor in the present case.

The grey nodular limestones in the present case apparently underwent a long-lasting, gradual deformation that evolved from their early soft diagenetic hydroplastic stage to the late brittle diagenetic stage (Fig. 13). The nodular limestone thickness is only slightly more than 20 m thick, fully compatible with the notion of a long-lasting process of slow, down-slope sediment creep. The process of sediment creep is very slow (ca. 1 mm/year) and best known from terrestrial hillslopes, particularly as so-called solifluction, but is known also as causing movement, shear deformation and folding in submarine pelagic deposits (Silva and Booth, 1984; Johns and Moore, 1988; Mitchell, 1996; Wynn and Stow, 2002; Ortner and Kilian, 2016).

This case-study interpretation of the Jurassic nodular limestones in the Tatra Mts does not necessarily mean that all the Rosso Ammonitico limestones in the Alpine-Mediterranean Tethyan province have a similar origin, especially since there are significant differences in the local sections. The most conspicuous difference is the grey, instead of red colouration of the nodular limestones in the present case. Red colouration of sediment traditionally has been associated with a high oxygen level in the depositional environment and the intense bioturbation of the grey limestones in the present case attests to an oxygen level in the near-bottom seawater and seafloor pore water that was sufficient for an infauna to flourish (cf. Bábek *et al*., 2018).

Mamet and Préat (2006) and Préat *et al*. (2006) pointed out the importance of benthic microbial communities to the red pigmentation of the Rosso Ammonitico limestones. Since such communities thrive in conditions of low sedimentation rate (e.g., Dromart *et al*., 1994; Vera and Martin-Algarra, 1994), it is reasonable to suppose that this environmental factor may have been important in the deposition of the grey nodular limestones in the present case. This interpretive notion is in line with the considerably higher sedimentation rate of the grey nodular limestones (1.25–1.47 cm/kyr) by comparison with that of the younger red nodular limestones in the same sections (0.1––0.22 cm/kyr) and that of many other Rosso Ammoniti-

co limestones in the Alpine-Mediterranean Tethys (see the next section "Remarks on sedimentation rates"). In short, the sedimentation rate in the present case was apparently too high to permit seafloor sediment reddening, while being the principal reason for down-slope gravitational sediment creep and synsedimentary deformation.

Ribbon radiolarites (upper Bathonian – lower Oxfordian)

Description

The base of the radiolarite succession consists of ribbon radiolarites (Sokolica Radiolarite Formation – Lefeld *et al*., 1985), which are composed of rhythmically alternating beds of centimetre- to decimetre-thick radiolarian-bearing cherts and siliceous millimetre- to centimetre-thick shale partings (Fig. 14A). These ribbon radiolarites formerly were subdivided into the lower, spotted radiolarites (upper Bathonian – lower Callovian) and the upper, green radiolarites (middle Callovian – lower Oxfordian; Jach *et al*., 2014); however, in this paper they are described and interpreted together for the sake of simplicity. Generally, the lowermost part of the ribbon radiolarites is poorly exposed, being covered by recent scree material on the slopes.

The contact of the ribbon radiolarites with the underlying deposits, meaning the *Bositra*-crinoidal limestones in the Western Tatra Mts and the grey nodular limestones in the eastern part of the Tatra Mts, is marked by 20 to 30 cm-thick *Bositra* marlstones with radiolarians (Figs 4, 8, 9, 14E). The content of $CaCO_3$ ranges between 52 and 63 wt%. According to the XRD analysis of bulk samples, the marlstones contain calcite, quartz, plagioclase and dolomite.

The chert beds of the ribbon radiolarites are grey, olive-grey, and greenish grey, while toward the top they are green, greenish grey, light olive and dark grey (Fig. 14B–D). Locally, chert beds contain darker grey, highly silicified zones (Filipka Valley and Ždiarska vidla sections). Above the late Callovian $\delta^{13}C$ positive excursion, the ribbon radiolarites become slightly reddish brown, with darker grey spots; however, they do not display a knobby character.

The occurrence of chert-shale couplets is the most characteristic feature of the ribbon radiolarites studied. Individual beds of chert are 3–22 cm thick, but mostly in the range of 6–10 cm, whereas the average thickness of intervening shale partings is 1.5 cm. The chert beds are bounded by sharp top and bottom bedding planes. In general, the bedding of the ribbon radiolarites is more regular toward the top of this facies and reveals upward thickening. Some chert beds display centimetre-thick partitioning more or less parallel to the bedding.

The chert beds are almost totally bioturbated and display common trace fossils visible on surfaces as variable spots against a lighter bioturbated background (Fig. 14B; Uchman and Jach, 2017; Jach *et al*., 2019). Primary sedimentary structures, such as indistinct horizontal lamination and grading are rare (Fig. 14C, F). Only some chert beds (for example at log height 16.5 m and 25 m in the Długa Valley section; Figs 4, 14F) display up to centimetre-thick intervals with symmetrical reverse-to-normal grading developed by an upward increase followed by a decrease in the amount of radiolarians (Fig. 14F). The intervening shales are usually structureless; only locally, a subtle horizontal lamination and scarce bioturbation are observed (Fig. 14I, J).

The chert beds are characterized by a wide range of carbonate content, fluctuating from 8 to 69 wt%, with a mean value of 31 wt%, whereas shale partings are carbonate-depleted (0.38–24 wt%; mean value 8.9 wt%). The $CaCO_3$ content of the cherts decreases upward in the ribbon radiolarites studied, reaching minimum values just below the late Callovian $\delta^{13}C$ positive excursion (Figs 4, 8, 9).

Texturally, chert beds range from mudstone to packstone (Fig. 14F–H). The ribbon radiolarites in all sections record an upward change from the *Bositra*-bearing microfacies (*Bositra*, radiolarian-*Bositra* and *Bositra*-radiolarian) to the pure radiolarian microfacies. Beside radiolarian tests and *Bositra* shells, bioclasts such as sponge spicules, crinoid ossicles, other echinoderm fragments, ostracods and benthic foraminifera occur. A distinct trend of decrease in calcitic bioclast content was observed upward in the ribbon radiolarites and they totally disappear just before the minimum content of $CaCO_3$ and the late Callovian $\delta^{13}C$ positive excursion. Generally, radiolarian tests are poorly preserved in the cherts, where they are usually filled with calcite, rarely with chalcedony or filled with both chalcedony and calcite.

Another characteristic feature of the ribbon radiolarites is a significant contribution of detrital material (clays and silt-sized clastics), as evidenced both by XRD analysis and observations of thin sections. The chert beds are slightly silt-rich (quartz grains and mica flakes) in microscopic view, with increasing content in lower portion of ribbon radiolarite facies. Some bulk samples of the middle portion of ribbon radiolarites contain micas, chlorite, plagioclase and rare K-feldspar in addition to the predominant quartz and calcite, which was confirmed by XRD analysis.

The shale partings are usually devoid of microfossils; only occasionally they contain some recrystallized calcitic fossil remains (Fig. 14I). Rare radiolarians are preserved as "ghost" or compressed relicts of tests filled with calcite and exceptionally with chlorite, which was confirmed by EDS. In some shales, *Bositra* shells, if they occur, are relatively well preserved and bear no signs of fragmentation or corrosion (Fig. 14J).

Interpretation

The upper Bathonian – lower Oxfordian ribbon radiolarites of the Fatricum Domain studied have many characteristics in common with the ribbon radiolarites described from other Tethyan areas (see McBride and Folk, 1979; Jenkyns and Winterer, 1982; Baumgartner, 1987, 2013) as well as with the Callovian ribbon radiolarites described from the central Pacific by Ogg *et al*. (1983, 1992). These examples are regarded as pelagic basinal deposits.

Most of primary sedimentary structures of the chert beds, if present at all in the radiolarites studied, seem to be indistinct, owing to bioturbation and diagenesis (Fig. 14B; Folk and McBride, 1978; McBride and Folk, 1979; Jach *et al*., 2019). The subtle lamination of centimetre scale, accentu-

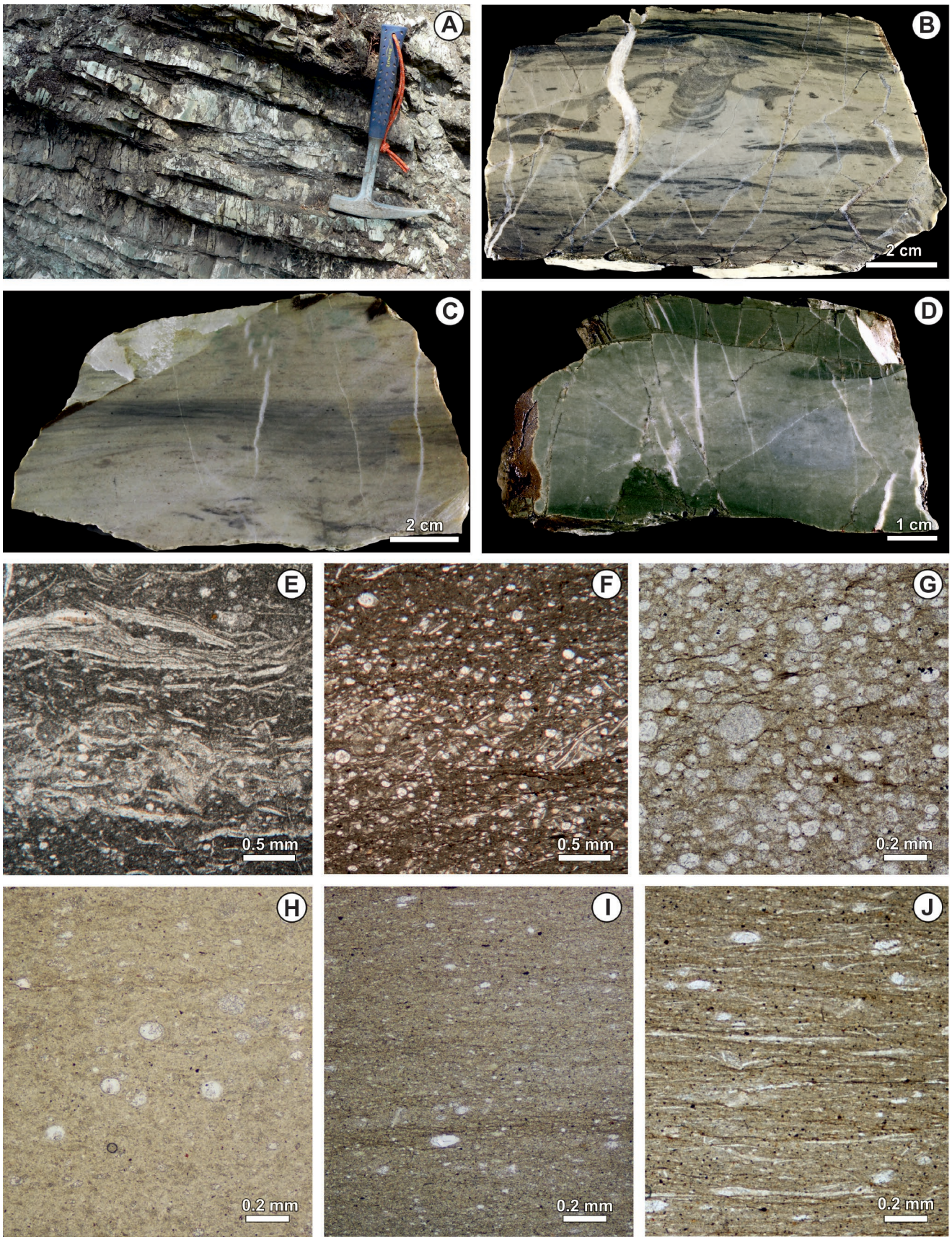

Fig. 14. Ribbon radiolarites. **A.** Field photograph of a ribbon radiolarites composed of rhythmically alternating beds of thick radiolarian-bearing cherts and thin shale partings; Długa Valley section (Fig. 4), hammer for scale is 33 cm long. **B.** Bioturbated grey radiolarian chert; Długa Valley section (Fig. 4), polished slab. **C.** Segment with preserved primary lamination within bioturbated radiolarian chert; Filipka Valley section (Fig. 8), polished slab. **D.** Highly siliceous green radiolarites; Długa Valley section (Fig. 4), polished slab. **E.** *Bositra* marlstones with radiolarians underlying radiolarites; Ždiarska vidla section (Fig. 9), thin section. **F.** Radiolarian-*Bositra* wackestone; note

ated by horizontal distribution of radiolarian tests, is the only structure which can be recognized exclusively in some chert beds. In such a case, the tests display symmetrical reverse-to-normal grading. Such structures were previously referred to the action of turbidity currents (Nisbet and Price, 1974; McBride and Folk, 1979; Kwiatkowski, 1981). However, they later were reinterpreted as an effect of sorting by bottom currents (e.g., Barrett, 1982). Bearing in mind the hydrodynamic behaviour of the radiolarian tests, which are characterized by a relatively low bulk density (Baumgartner, 1987, 2013), even feeble bottom currents could have been responsible for the winnowing, redistribution and sorting of them on the sea-bottom in a pelagic environment (see Gambacorta *et al*., 2014). The concentration of radiolarian tests in some horizons of a chert bed may be also regarded as an effect of productivity cycles, in response to the Milankovitch climatic oscillations (e.g., De Wever, 1987; Ogg *et al*., 1992; Baumgartner, 2013; De Wever *et al*., 2014; Ikeda *et al*., 2016). However, a record of such cycles is unlikely to have survived the activities of trace-makers or bottom-currents (Jach *et al*., 2019). Thus, it is preserved in an altered condition, in some cases to a significant extent.

The occurrence of rhythmically alternating chert-shale couplets is typical of the ribbon radiolarites studied. They have this feature in common with many other Jurassic radiolarites, especially those characterized by a low $CaCO_3$ content (e.g., McBridge and Folk, 1979; Jenkyns and Winterer, 1982; Ogg *et al*, 1983; Baumgartner, 2013). The regular alternation results from various proportions of biogenic silica and terrigenous clastic input. Three scenarios were invoked to explain such an alternation: (1) diagenetic redistribution of labile opaline silica, (2) variation in siliceous plankton productivity, and (3) periodic dilution by siliciclastic material of terrigenous origin. These processes and phenomena were addressed by McBride and Folk (1979) and later discussed in detail by Hori *et al*. (1993) and summarized by Hüneke and Henrich (2011).

The ribbon radiolarites studied do not provide unequivocal explanations for the origin of the chert-shale alternations. It is noticeable that the shale partings contain very rare and poorly preserved, calcified radiolarian tests and considerably more common *Bositra* shells. Therefore, the diagenetic remobilization of labile silica from the shale partings to the chert beds should be taken into account (Murray *et al*., 1992; De Wever *et al*., 1995). The low radiolarian/*Bositra* ratio should be regarded as a primary feature modified insignificantly by the diagenetic redistribution of silica (e.g., Hesse and Schacht, 2011) and, hence, the occurrence of chert-shale couplets is a primary feature of the rocks studied (see also discussion in McBride and Folk, 1979; Jenkyns and Winterer, 1982; Baumgartner, 2013; Ikeda *et al*., 2017). The lack of any structure indicative of current sorting, which might be expected in the shale partings if they were deposited by distal, low density turbidity currents, is significant. This indicates that the shale partings were laid down as hemipelagic background deposits. Only the scarce bioturbation structures in shales may reflect some kind of environmental stress, for example, an insufficient nutrient level (e.g., Wetzel and Uchman, 2018). Conversely, the alternating chert beds may have resulted from periodic radiolarian blooms in the seawater column, which led to the dilution of the constant background sedimentation and the fast accumulation of silica-rich beds on the sea floor (Mutch and Garrison, 1967; Hori *et al*., 1993; Baumgartner, 2013).

Calcareous radiolarites (middle Oxfordian – upper Kimmeridgian)

Description

The calcareous radiolarites (Czajakowa Radiolarite Formation – Lefeld *et al*., 1985) consist of bedded, wavy or knobby radiolarites, which are characterized by increased $CaCO_3$ content, the presence of rare thin or no shale intercalations and the occurrence of widespread secondary chert nodules. The calcareous radiolarites were previously subdivided into variegated and red radiolarites (Jach *et al*., 2014); however, in this paper they are described and interpreted together for the sake of simplicity. Owing to scree cover or tectonic gaps in the available exposures, the boundary between the basal ribbon radiolarites and the calcareous radiolarites has been documented only in the eastern part of the Tatra Mts. The change in lithology from the underlying basal ribbon radiolarites to carbonate radiolarites is located about 2 m below the Middle Oxfordian $\delta^{13}C$ positive excursion and is marked by increased $CaCO_3$ content (Filipka Valley and Ždiarska vidla sections; Figs 8, 9). The calcareous radiolarites show an average $CaCO_3$ content of about 42 wt%, ranging from 18 up to 70 wt%, hence this facies embraces both radiolarites and radiolarian limestones. The amount of $CaCO_3$ increases noticeably upward, then slightly decreases in the uppermost radiolarites; such a trend is recorded in the Długa Valley, Filipka Valley and Ždiarska vidla sections.

The calcareous radiolarites of the Western Tatra Mts differ in some details from those of the eastern part of the Tatra Mts. Hence, they are described separately. The calcareous radiolarites reach an approximate thickness of 15 m in the Western Tatra Mts. They show planar bedding, with no siliceous shale intercalations or with only very thin ones (Fig. 15A). Radiolarite beds are thin- to thick-bedded (from 4 to 40 cm thick). The calcareous radiolarites display a variety of colours; in the lower part, they are light olive, dusky red, pale green to yellowish grey, while toward the top they become pale red, pale olive, olive grey, red-green, moderate red and greyish red in colour (Fig. 15C, D). Replacement reddish, greyish and greyish-black chert nodules and lenses

---

the concentration of bioclasts in reverse-to-normally graded laminae; Długa Valley section (Fig. 4), thin section. **G.** Radiolarian packstone; Długa Valley section, (Fig. 4), thin section. **H.** Siliceous mudstone with radiolarians, shale parting; Długa Valley section (Fig. 4), thin section. **I.** Shale parting with rare compression-deformed bioclasts filled with calcite; Długa Valley section (Fig. 4), thin section. **J.** Laminated clayey mudstones with *Bositra* shells, shale parting; Filipka Valley section (Fig. 8), thin section. For precise location of the samples see Appendix in the electronic version of the paper.

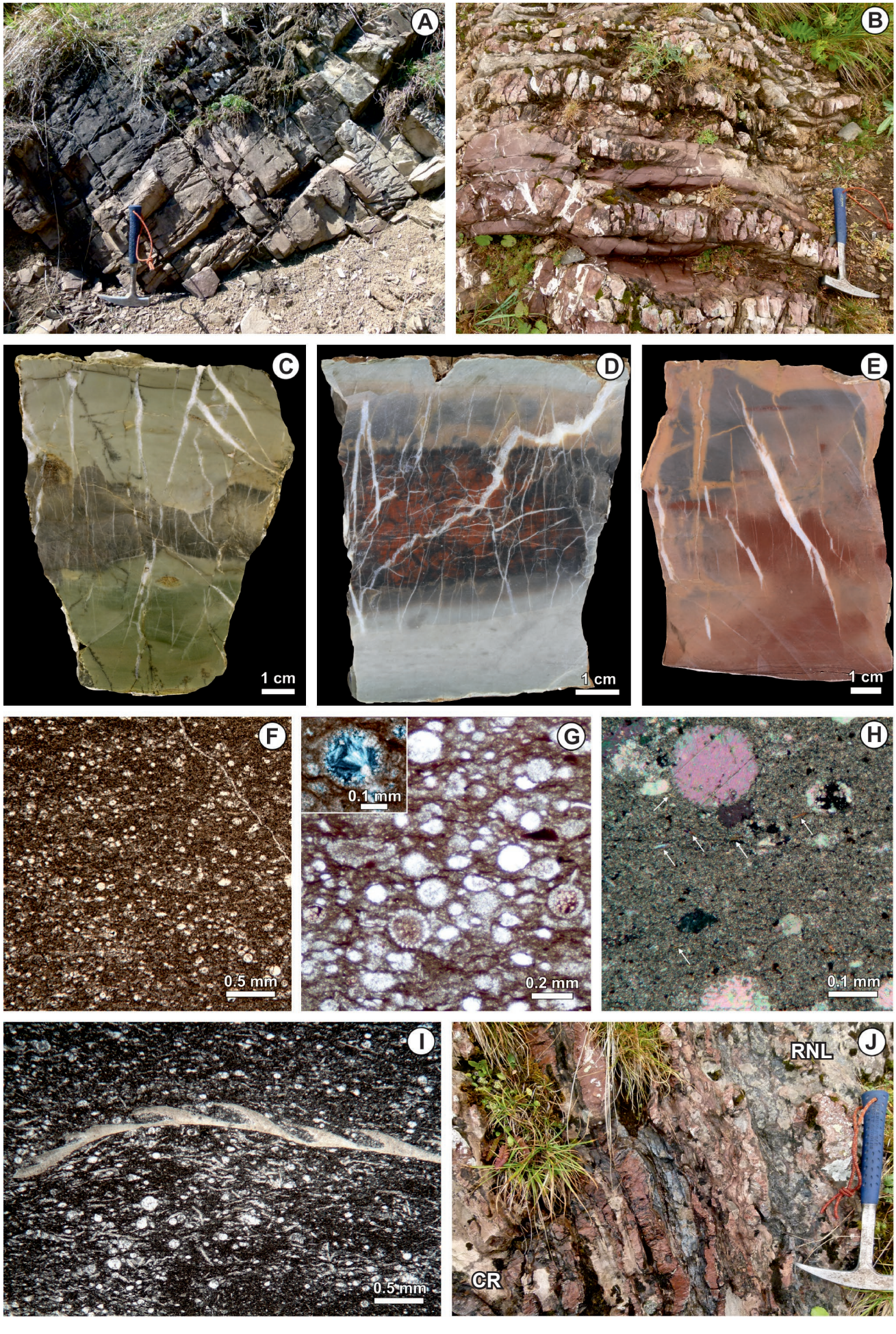
A
B
C
1 cm
D
1 cm
E
1 cm
F
0.5 mm
G
0.1 mm
0.2 mm
H
0.1 mm
I
0.5 mm
J
RNL
CR

are common. The calcareous radiolarites show an upward transition from radiolarian mudstone to packstone, which is accompanied by a marked increase in the abundance of bioclasts, such as crinoid ossicles, *Bositra* shells, *Saccocoma* sp., tests of planktonic *Globuligerina*, sponge spicules, aptychi, cysts of calcareous dinoflagellates, ophiuroids and ostracods (Fig. 15F–I). The facies represents a variety of the microfacies, such as radiolarian, and radiolarian-*Bositra*-*Saccocoma*, *Saccocoma*-*Bositra*, *Bositra*, spiculite-*Bositra* and *Bositra*-*Saccocoma* wackestones and packstones. The matrix is commonly slightly recrystallized and locally silicified. Radiolarian tests are filled with calcite, chalcedony or microcrystalline quartz (Fig. 15G). Aptychi and scarce belemnite rostra are found in the upper portion of calcareous radiolarites (Fig. 15I); they are concentrated mainly on the bedding planes (from the lowermost 40 m of Długa Valley section upwards).

Silt-sized quartz grains and mica flakes occur only in the upper part of the calcareous radiolarites (above 36 m in Długa Valley section; Fig. 15H). Most of the bulk samples contain quartz, calcite, accompanied only in the upper part of this facies by micas, chlorite and plagioclase, which were identified by XRD analysis.

Conversely, the calcareous radiolarites in the eastern part of the Tatra Mts reach a thickness of ca. 8.5 m. They are brick-red with dark grey spots and greyish to greyish-black (Fig. 15E). They display distinct bedding, which is wavy in the lower part and becomes knobby towards the top (Fig. 15B). Large replacement chert nodules and lenses, 5–6 cm in thickness, are very common; they are dark grey with numerous reddish spots. Laterally extensive, wavy chert lenses occur in the uppermost part of this facies (Fig. 15J).

The radiolarian wackestone microfacies predominates in the Filipka Valley and Ždiarska vidla sections; bioclasts other than radiolarians are extremely rare and are represented by *Bositra* shells, crinoid ossicles, sponge spicules, ostracods and aptychi. The calcareous matrix is slightly recrystallized, locally silicified.

The sedimentary structures of the calcareous radiolarites are similar in both parts of the Tatra Mts. Some beds show subtle horizontal lamination (laminae ca. 0.5 mm thick) and grading on a microscopic scale. The lamination is accentuated by indistinct concentrations of biodetritus or subtle colour changes. Although this facies is almost totally bioturbated, distinguishable trace fossils are rare; *Chondrites* and *Planolites* were recognized (Jach *et al*., 2012).

Interpretation

A change in lithology from basal ribbon radiolarites to overlying carbonate radiolarites is a common feature of many Tethyan sections (e.g., Bosselini and Winterer, 1975; McBride and Folk, 1979; Winterer and Bosselini, 1981; Jenkyns and Winterer, 1982; Baumgartner, 2013). The carbonate content abruptly increases, along with the colour changes from green to red. Two important characteristics of the calcareous radiolarites are noteworthy, namely a high carbonate content and a low content of siliciclastic admixtures, which differentiate the calcareous radiolarites from the underlying ribbon radiolarites.

The high carbonate content is manifested in two ways: a high abundance of carbonate bioclasts and a large amount of carbonate (micrite) matrix. Both these features may indicate more intensive production of calcium carbonate or increasing potential for its preservation in seawater, at the sea bottom or at shallow depths below the sediment-water interface. These factors are interrelated.

The calcareous radiolarites are poor in siliciclastic admixtures in comparison to the underlying ribbon radiolarites. This is revealed in the scarcity, or complete lack of siliciclastic grains dispersed in the radiolarite beds and the absence of shale partings. The latter feature means that periodic changes of environmental conditions, which led to the chert-shale alternations, did not affect the deposition of the calcareous radiolarites. The general scarcity of siliciclastic admixtures evidences diminishing supply or even a cut-off of the supply of terrigenous material into the basin. The broader, palaeoceanographic significance of the above features is discussed below in the section "Vertical facies changes and palaeoceanographic conditions".

Red nodular limestones (upper Kimmeridgian – lower Tithonian)

Description

The red nodular limestones represent the Ammonitico Rosso type of facies. The base of this facies is claimed to be diachronous within the Moluccana Zone of the late Kimmeridgian (Jach *et al*., 2014), whereas the upper boundary ranges from the latest Kimmeridgian through the earliest Tithonian (Semiradiata Zone) in the Western Tatra Mts to the late Tithonian in the High Tatra and Belianske Tatra Mts (Pszczółkowski, 1996; Grabowski and Pszczółkowski,

Fig. 15. Calcareous radiolarites. **A.** Field photograph of bedded calcareous radiolarites, without or with only very thin siliceous shale intercalations; Długa Valley section (Fig. 4), hammer for scale is 33 cm long. **B.** Field photograph of reddish calcareous radiolarites showing wavy to knobby bedding; Ždiarska vidla section (Fig. 9), hammer for scale is 33 cm long. **C.** Light olive-green calcareous radiolarite with irregular replacement chert; Długa Valley section (Fig. 4), polished slab. **D.** Light grey calcareous radiolarite with black-reddish chert; Lejowa Valley section (Fig. 5), polished slab. **E.** Brick-red calcareous radiolarites with dark grey spots; Ždiarska vidla section (Fig. 9), polished slab. **F.** Radiolarian wackestone-packstone; Ždiarska vidla section (Fig. 9), thin section. **G.** Radiolarian packstone with chalcedony-filled radiolarian tests; Upłaziańska Kopa section (Fig. 7), thin section. **H.** Radiolarian wackestone with calcified radiolarian tests; note the presence of silt-sized mica flakes (arrows); Długa Valley section (Fig. 4), thin section. **I.** Radiolarian-*Bositra* wackestone with aptychus; Długa Valley section (Fig. 4), thin section. **J.** Field photograph of a contact of the calcareous radiolarites (CR) with the red nodular limestones (RNL). The uppermost part of the calcareous radiolarites contains numerous thin wavy chert lenses; Ždiarska vidla section (Fig. 9), hammer for scale is 33 cm long. For precise location of the samples see Appendix in the electronic version of the paper.

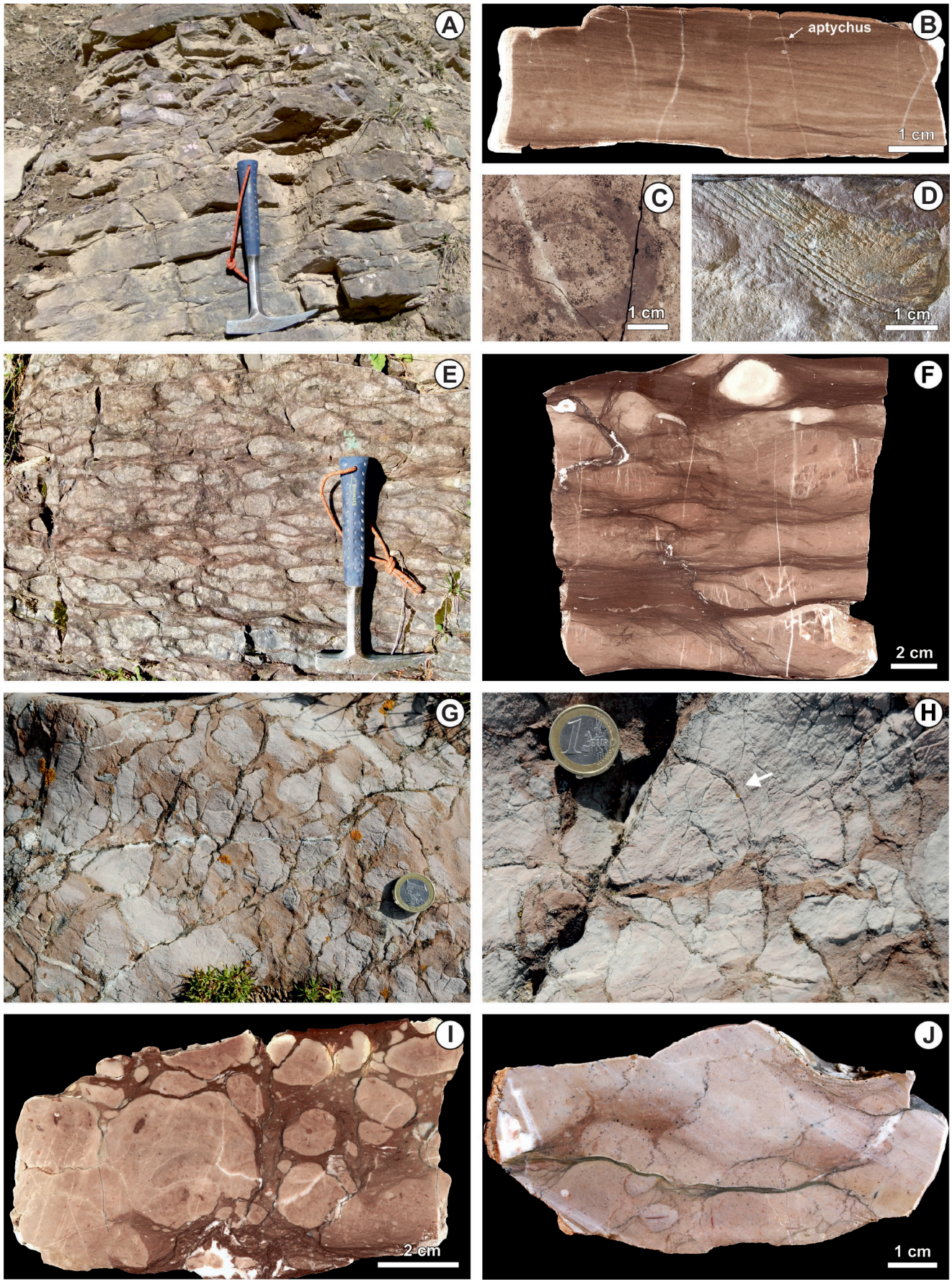

Fig. 16. Red nodular limestones. **A.** Field photograph of a thin- and medium-bedded lithotype at Długa Valley section (Fig. 4), hammer for scale is 33 cm long. **B.** thin- and medium-bedded limestones with highly compacted cross-lamination; Długa Valley section (Fig. 4), polished slab. **C.** Ammonite "ghost" visible at bedding plane; Długa Valley section (Fig. 4). **D.** Aptychus preserved at bedding plane;

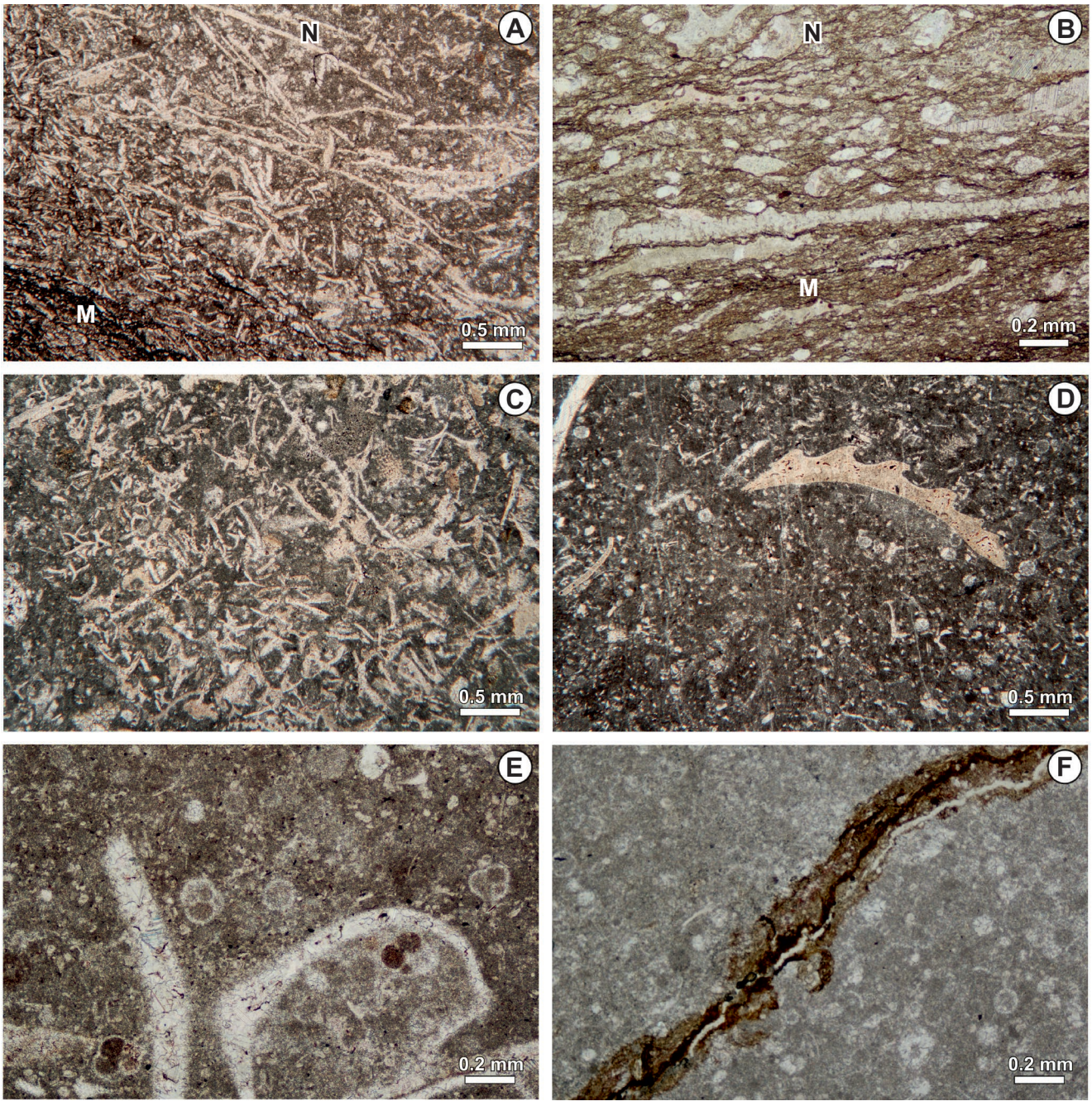

Fig. 17. Red nodular limestones; thin sections. **A.** *Bositra* packstone nodule (N) grading into the darker matrix (M); Lejowa Valley section L (Fig. 5). **B.** *Saccocoma* packstone nodule (N) grading into the darker matrix (M); Długa Valley section (Fig. 4). **C.** *Saccocoma-Globochaete* packstone; Filipka Valley (Fig. 8). **D.** *Globochaete-Saccocoma* wackestone with aptychus affected by microborings; Filipka Valley (Fig. 8). **E.** *Globochaete-Globuligerina* wackestone; Ždiarska vidla section (Fig. 9). **F.** Singular dissolution seams within pseudonodular limestone; Ždiarska vidla section (Fig. 9). For precise location of the samples see Appendix in the electronic version of the paper.

Długa Valley section (Fig. 4). **E.** Field photograph of the nodular lithotype at Lejowa Valley section Lc (Fig. 6), hammer for scale is 33 cm long. **F.** Calcareous nodules surrounded by clay-rich darker matrix, Lejowa Valley section Lc (Fig. 6), polished slab. **G.** Field photograph of a pseudonodular lithotype at Ždiarska vidla section (Fig. 9), coin for scale is 23.25 mm across. **H.** Pseudonodular limestone with ammonite mould; Ždiarska vidla section (Fig. 9), coin for scale is 23.25 mm across. **I.** Pseudonodular limestone; Ždiarska vidla section (Fig. 9), polished slab. **J.** Pseudonodular limestone; Filipka Valley (Fig. 8), polished slab. For precise location of the samples see Appendix in the electronic version of the paper.

2006a). This facies was assigned to the Czorsztyn Limestone Formation (Lefeld *et al*., 1985).

There is a substantial difference between the red nodular limestones of the Western Tatra Mts and eastern part of the Tatra Mts. In the former area, this facies attains a thickness of only 5.5 m and represents the nodular and subordinately the thin- and medium-bedded lithotypes (= facies *sensu* Martire, 1996). In the latter area, it reaches a thickness of ca. 14 m (Lefeld *et al*., 1985; see also Vašíček *et al*. 1994) and is composed of the pseudonodular lithotype (= facies *sensu* Martire, 1996).

The thin- and medium-bedded lithotype (1) occurs in the Długa Valley and Lejowa Valley sections (Figs 4, 5). This lithotype is characterized by planar to wavy bedding (Fig. 16A); alternations of beds of reddish limestones 5–8 cm thick with darker 1–2 cm-thick marls are visible. This lithotype is bioturbated. Highly compacted ripple cross-lamination was distinguished (Fig. 16B). Some chert nodules occur in the limestone beds. Well preserved aptychi were found on some bedding planes of this lithotype (Fig. 16D). Rare ammonite "ghosts" were noted at a bedding plane (Fig. 16C). This lithotype has an average $CaCO_3$ content of about 58 wt%. The limestones are *Saccocoma-Bositra*, *Bositra*, radiolarian, radiolarian-*Saccocoma-Bositra*, *Saccocoma*-radiolarian wackestones and packstones. In addition to the above bioclasts, the limestones contain fragments of foraminifera, calcified sponge spicules, aptychi, belemnite guards, crinoid ossicles, cysts of calcareous dinoflagellates and spores of *Globochaete alpina* as well as bivalve shales. The content of silt-sized clastics (mica flakes and quartz grains) increases upward in this facies. Microborings occur in some aptychi and *Saccocoma* fragments (Fig. 17D). Matrix and bioclasts locally are slightly silicified, especially at the turn of the Borzai–Pulla zones (uppermost Kimmeridgian – lower Tithonian).

The nodular lithotype (2) occurs in the Długa Valley, Lejowa Valley and Upłaziańska Kopa sections (Figs 4–7). A greenish grey radiolarite bed with a thickness of 40 cm occurs in this lithotype in the Lejowa Valley section. This lithotype is distinguished because of the occurrence of light-coloured micritic nodules, which are surrounded by a distinct dark reddish to brownish, clay-rich matrix with common swarms of dissolution seams (Fig. 16E, F). The nodules seem to "float" in an abundant clay-rich matrix. Distinct nodularity is clearly visible on weathered surfaces. The nodular lithotype has an average $CaCO_3$ content of ca. 60%. The nodules consist of the *Saccocoma-Bositra*, *Bositra* (Fig. 17A), radiolarian, radiolarian-spiculite, *Saccocoma* (Fig. 17B), *Saccocoma*-radiolarian, *Saccocoma* and *Saccocoma-Globochaete* microfacies (wackestone to packstone). This lithotype includes an assemblage of bioclasts similar to that of the thin-bedded lithotype. The bioclasts are more compacted in the matrix than in the nodules (Fig. 17B). The matrix contains a higher amount of silt-sized clastics (quartz grains, mica flakes). The XRD analysis revealed calcite, quartz, chlorite and plagioclase. Trace fossils, such as *Chondrites*, *Planolites* and less common *Zoophycos* and *Thalassinoides*, occur in the nodules (Jach *et al*., 2012).

The pseudonodular lithotype (3) occurs exclusively in the Filipka Valley and Ždiarska vidla sections (Figs 8, 9). The name reflects its massive appearance on a weathered surface, which results from the uniform weathering of nodules and matrix (Fig. 16G; Martire, 1996; Bertok and Martire, 2009). The rounded to subangular nodules exhibit various shapes, mainly irregular (Fig. 16I, J). They are surrounded by single dissolution seams or less often swarms of dissolution seams (Fig. 17F). The pseudonodular limestones are characterized by an insignificant non-carbonate admixture and have an average $CaCO_3$ content of about 85 wt%. The pseudonodular limestones are *Globochaete*, *Globochaete-Saccocoma*, *Saccocoma-Globochaete* and *Globochaete-Globuligerina* wackestones and packstones (Fig. 17C–E). The limestones comprise other pelagic components, such as calcified radiolarians, crinoid ossicles, ostracods, fragments of foraminifera, ammonites (mainly juvenile), calcified sponge spicules, aptychi, belemnite guards, cysts of calcareous dinoflagellates and bivalve shell fragments. Ammonite moulds are found only sporadically (Fig. 16H). Silt-sized quartz grains and mica flakes occur as well. This lithotype is totally bioturbated, but no determinable trace fossils have been found, nor have primary sedimentary structures been documented.

Interpretation

Red nodular limestones are one of the most typical Jurassic facies of the Alpine Mediterranean Tethys. Analogous limestones originated in other geological periods (e.g., Tucker, 1974; Channell *et al*., 2003; Bábek *et al*., 2018). Although different scenarios for their origin are still under discussion, it is generally accepted that they were formed under conditions of low sedimentation rate (e.g., Jenkyns, 1974; Tucker, 1974; Wieczorek, 1983; Martire, 1996). The data yielded in the sections studied fully confirm the above notion (see the section "Remarks on sedimentation rates" below). The uncompacted texture of the nodules proves that they underwent early diagenetic cementation, most probably at a very shallow depth below the sediment/water interface (e.g., Clari and Martire, 1996; Martire, 1996). It was a result of the interplay between physical, chemical and biological processes, such as current velocity, seawater pumping into the shallow subsurface, burrowing, aragonite dissolution and incipient early cementation (e.g., Jenkyns, 1974; Mullins *et al*., 1980; Clari and Martire, 1996; Bertok and Martire, 2009; Coimbra, *et al*., 2009; Reolid *et al*., 2015). During the subsequent stages of diagenesis, mechanical and chemical compaction took place and particularly affected the uncemented parts of the sediments (Clari and Martire, 1996; Łuczyński, 2001; Matyszkiewicz and Kochman, 2016), especially those with abundant clay components (Railsback, 1993).

Distinct variations between the three lithotypes of this facies can be explained by their different sedimentary and diagenetic environment. The thin- and medium-bedded lithotype (1) did not undergo early cementation, which is proved by the absence of nodules (see Martire, 1992, 1996). It also contains a significant amount of a non-carbonate fraction, which could impede early cementation (cf. Zankl, 1969; Möller and Kvingan, 1988). In contrast to the nodular lithotype, the thin-and medium-bedded lithotype is significantly less bioturbated, which may have resulted in the lack of early cementation. However, this lithotype must have

experienced some sorting by bottom currents, which is indicated by locally recognizable ripple-cross-lamination. The currents may have been related genetically to deep-water tides (Dykstra, 2012) or to contour currents (Eberli and Betzler, 2019). The carbonate mud probably flocculated with clay-particles, which enabled the formation of mud ripples (Schieber and Southard, 2009). Conversely, the nodular lithotype (2) originated from carbonates which were more bioturbated. The incipient nodules seem to have been dependent upon burrowing, since burrows caused increasing permeability of sediments, which facilitated the fluid migration indispensable for cement growth (Coimbra *et al.*, 2009). The pseudonodular lithotype (3) resulted from the selective cementation of carbonate deposits rich in microcrystalline calcite under the action of at least pulsatory currents (Martire, 1996; Bertok and Martire, 2009). The currents winnowed some fine-grained carbonates and clay particles from this depositional milieu.

Platy limestones (uppermost Kimmeridgian – lower Tithonian)

Description

The platy limestones studied belong to the lower part of the Jasenina Formation (*sensu* Michalík *et al*., 1990; see also Vašíček *et al*., 1994). In the Western Tatra Mts, the platy limestones range from the uppermost Kimmeridgian to the lowermost Berriasian, whereas in the eastern part of the Tatra Mts they are replaced in part laterally by red nodular limestones (see also Pszczółkowski, 1996; Michalík, 2007). This facies comprises light grey, grey-greenish, olive-grey or rarely reddish micritic marly limestones and marlstones with planar bedding (Fig. 18A, B; Jach *et al*., 2012, 2014). The bed thickness ranges from 2 to 10 cm. The limestones display wavy bedding and some nodular intercalations, mostly in the middle early Tithonian (Malmica Zone; Fig. 18A). Small irregular chert nodules (up to 2 cm) occur locally. The average $CaCO_3$ content is 58 wt%, ranging from 46 to 72 wt%.

Wackestones are the predominant microfacies; they are in particular *Saccocoma*, crinoidal-*Saccocoma*, *Saccocoma*-radiolarian and *Saccocoma*-*Globochaete* wackestones (Fig. 18C, D). In addition, the bioclasts include sponge spicules, *Bositra* shells, ostracods, foraminifers, crinoids, bivalves, the microproblematicum *Gemeridella minuta* Borza et Mišík, the cysts of calcareous dinoflagellates, for example, *Cadosina semiradiata semiradiata* (Wanner), chitinoidellids and numerous aptychi. Bioclasts are often partially silicified. Gąsiorowski (1959, 1962) described the common occurrence of *Laevaptychus* sp. in the lowermost part of this facies. The platy limestones have a significant

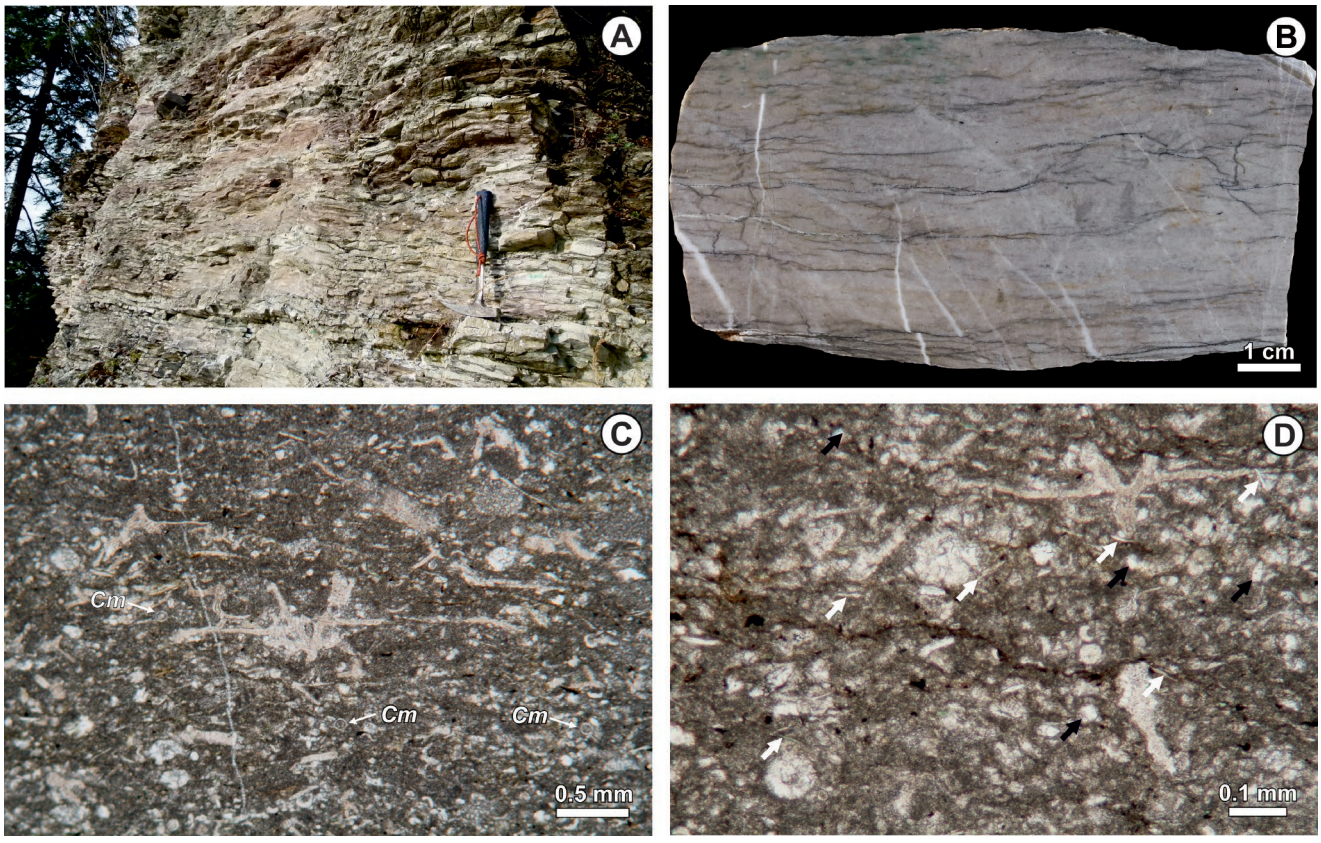

Fig. 18. Platy limestones. **A.** Field photograph of a platy limestones with horizons of pinkish and slightly nodular limestones; Lejowa Valley section (Fig. 5). **B.** Light grey pelitic limestones; Długa Valley section (Fig. 4), polished slab. **C.** *Saccocoma*-*Globochaete* wackestone containing common calcareous dinoflagellate cysts, mainly *Colomisphaera minutissima* (*Cm*); Lejowa Valley section (Fig. 5), thin section. **D.** *Saccocoma* limestone rich in silt-size quartz grains (black arrows) and mica flakes (white arrows); Lejowa Valley section (Fig. 5), thin section. For precise location of the samples see Appendix in the electronic version of the paper.

silt-sized clastic content (quartz and micas; Fig. 18D). XRD analysis revealed calcite, quartz, micas, chlorite and plagioclase. Pyrite is scattered in the matrix. The minute wackestone intraclasts, containing common cysts of *Colomisphaera pulla* and *Carpistomiosphaera tithonica* Nowak indicative of the Tithonica Zone (lower Tithonian), were found in the limestones of the Malmica Zone (lower Tithonian).

Some beds are indistinctly laminated, with concentrations of bioclasts in discrete laminae. The platy limestones are bioturbated; however, determinable trace fossils are rare. Only *Chondrites* was reported from the Lejowa Valley sections (Jach *et al*., 2012).

Interpretation

The platy limestones bear a strong resemblance to the basinal pelagic carbonates of the same age that are widespread in the Alpine-Mediterranean Tethys (e.g., Martire *et al*., 2006; Donatelli and Tramontana, 2014; Grabowski *et al*., 2017, see also reviews by Bernoulli and Jenkyns, 1974 and Wieczorek, 1988). Carbonate bioclasts of planktonic organisms are significant components of this facies, which clearly reflects the increasing role of calcareous plankton as carbonate producers in the Tithonian (e.g., Erba, 1989; Reháková, 2000; Bornemann *et al*., 2003). However, the abundant calcite micrite may be associated genetically to planktonic organisms or to export from shallow-water submarine highs (Pomar and Hallock, 2008 and references therein). The lamination indicates the periodic action of bottom currents, which could have sorted the bioclasts (Gambacorta *et al*., 2014), whereas the presence of intraclasts resulted from higher-energy episodes and additionally reflects the alternation of early cementation and erosion processes (Martire and Clari, 1994). The elevated content of siliciclastic material in this facies records efficient terrigenous input from the emerged land.

REMARKS ON SEDIMENTATION RATES

Description

An estimation of the Jurassic sedimentation rates in the eastern part of the Tatra Mts and Western Tatra Mts areas of the Fatricum Domain leads to a number of interesting observations (Fig. 19). A more or less steady sedimentation rate of 0.35–0.51 cm/kyr characterized early Bajocian to late Callovian deposition in the Długa Valley area of the Western Tatra Mts, when the *Bositra*-crinoidal limestones and the majority of the ribbon radiolarites were deposited (Table 3). The sedimentation rate of the coeval spotted limestones, grey nodular limestones and the lower part of the ribbon radiolarites in the Ždiarska vidla section was much higher, estimated at 3.22 cm/kyr.

The sedimentation rate of the main part of the ribbon radiolarites, deposited during the late Bathonian to late Callovian in the Ždiarska vidla section (eastern part of the Tatra Mts), is estimated at 0.5 cm/kyr, slightly higher than the coeval sedimentation rate of this facies in the Długa Valley area of the Western Tatra Mts, estimated at 0.35 cm/kyr. The uppermost part of the ribbon radiolarites and the lower part of the calcareous radiolarites (spanning the period from the late Callovian positive $\delta^{13}C$ excursion to the Kimmeridgian FAD of *S. moluccana*) in the Długa Valley area were deposited at an estimated sedimentation rate of 0.23 cm/kyr.

The Ždiarska vidla section in the eastern part of the Tatra Mts shows a gradual upward decrease in the sedimentation rate from the early Bajocian positive $\delta^{13}C$ excursion to the FAD of *C. pulla* (early Tithonian). The low sedimentation rate of 0.2 cm/kyr of the uppermost part of the ribbon radiolarites and the lowermost part of the calcareous radiolarites (spanning the time between the late Callovian positive $\delta^{13}C$ excursion and the middle Oxfordian positive $\delta^{13}C$ excursion) is noteworthy, decreasing to 0.1 cm/kyr in the upper part of the calcareous radiolarites and the lowermost part of the overlying calcareous nodular limestones, spanning the time between the middle Oxfordian positive $\delta^{13}C$ excursion and the FAD of *C. pulla*.

An opposite trend is discernible in the Długa Valley section, especially in the upper part, where – on the account of other marker horizons – the sedimentation rate increased upwards after the late Callovian positive $\delta^{13}C$ excursion (Fig. 19). The sedimentation rate of the upper part of the calcareous radiolarites, the red nodular limestones and the lowermost part of platy limestones (spanning time from the late Callovian positive $\delta^{13}C$ excursion and the FAD of *C. pulla*) was about 0.26 cm/kyr in the Długa Valley section that is roughly two times higher than in the Ždiarska vidla section. A trend similar to that in the Długa Valley section is observable in the Lejowa Valley section (Fig. 19).

The comparison of the local outcrop sections indicates that the Lejowa Valley section (labelled L, see also Jach *et al*., 2012) had a sedimentation rate similar to that of the Długa Valley section. The sedimentation rate in the second section in the Lejowa Valley (labelled Lc) was significantly lower. In contrast, the sedimentation rate in the Filipka Valley section was similar to that in the Ždiarska vidla section (Fig. 19).

Interpretation

Since the seminal paper by Bernoulli and Jenkyns (1974), it has been accepted widely that Jurassic carbonate sedimentation rate in the Mediterranean Tethys was much lower on the submarine intrabasinal highs than in the adjacent basinal troughs. More recent studies have shed further light on the issue of relative sedimentation rates (e.g., Baumgartner, 1990; Santantonio, 1993; Michalík *et al*., 1995; O'Dogherty *et al*., 2001; Muttoni *et al*., 2005; Grabowski and Pszczółkowski, 2006a; Chiari *et al*., 2007; Picotti and Cobianchi, 2017). The sedimentation rate is routinely based on sediment thickness and reported as so-called uncorrected (non-decompacted) values, which are not corrected for syn- and post-depositional physical and chemical compaction. Martire and Clari (1994) have calculated the real sedimentation rates for nodular limestone (Rosso Ammonitico Veronese, Middle–Upper Jurassic) and pelitic limestone (Biancone, Lower Cretaceous) and obtained higher rates of 3.5 to 1.4 times, respectively. Similarly, a decompaction factor for radiolarite chert is estimated at 5 and for the associated shale partings at 2 (De Wever *et al.,* 2001). This means that the uncorrected values of sedimentation rate are significantly lower than the real values (Matyszkiewicz, 1999). The compaction of sediment is strongly dependent upon sedimentary

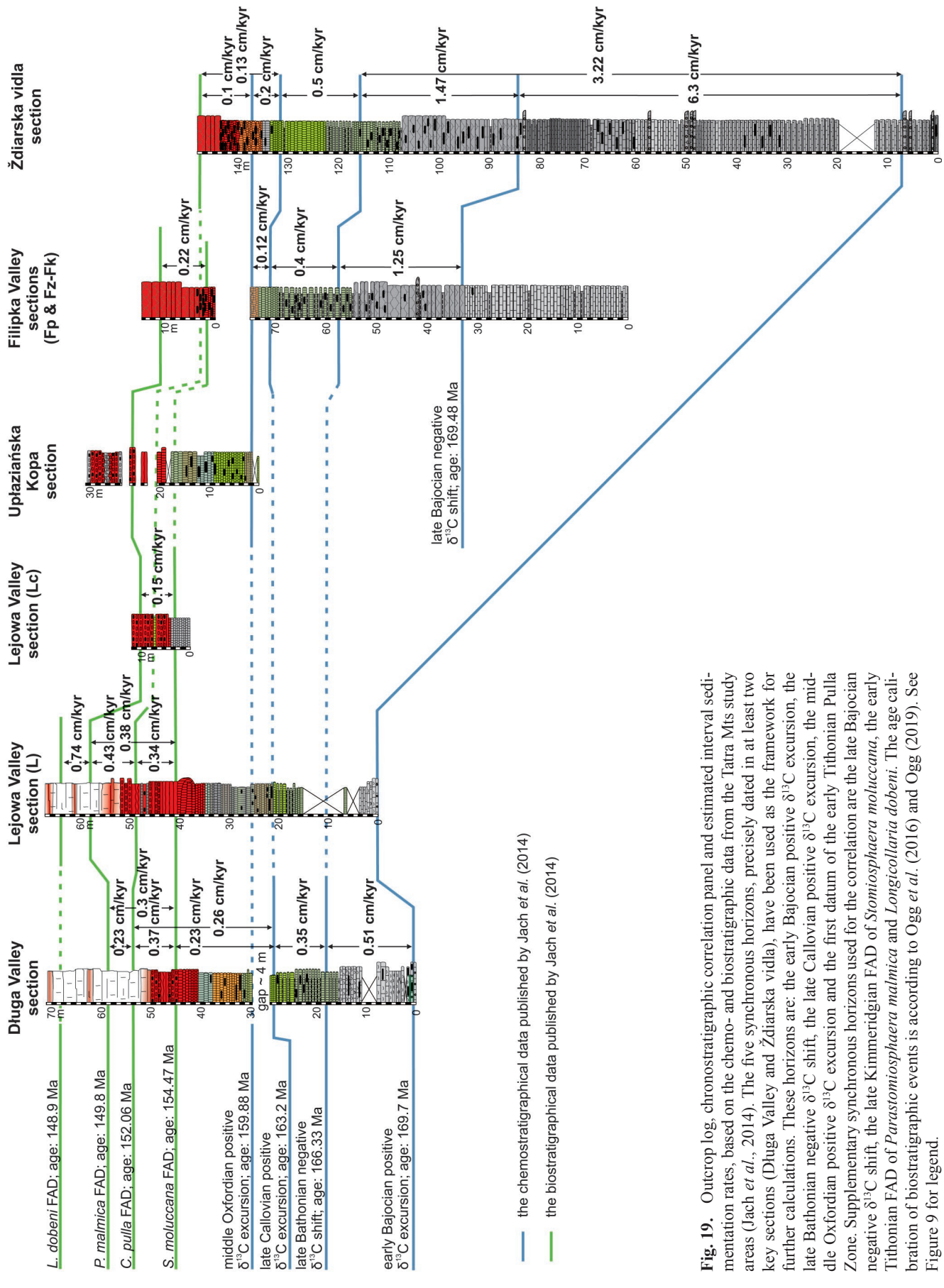

Fig. 19. Outcrop log, chronostratigraphic correlation panel and estimated interval sedimentation rates, based on the chemo- and biostratigraphic data from the Tatra Mts study areas (Jach *et al.*, 2014). The five synchronous horizons, precisely dated in at least two key sections (Długa Valley and Ždiarska vidla), have been used as the framework for further calculations. These horizons are: the early Bajocian positive $\delta^{13}C$ excursion, the late Bathonian negative $\delta^{13}C$ shift, the late Callovian positive $\delta^{13}C$ excursion, the middle Oxfordian positive $\delta^{13}C$ excursion and the first datum of the early Tithonian Pulla Zone. Supplementary synchronous horizons used for the correlation are the late Bajocian negative $\delta^{13}C$ shift, the late Kimmeridgian FAD of *Stomiosphaera moluccana*, the early Tithonian FAD of *Parastomiosphaera malmica* and *Longicollaria dobeni*. The age calibration of biostratigraphic events is according to Ogg *et al.* (2016) and Ogg (2019). See Figure 9 for legend.

Table 3

Estimation of sedimentation rate in the Długa Valley, Lejowa Valley, Filipka Valley and Ždiarska vidla sections (time scale after Ogg *et al.*, 2016; Ogg, 2019)

Marker horizon at the base	Marker horizon at the top	Interval [m]	Thickness [m]	Duration [My]	Sedimentation rate [cm/kyr]
Długa Valley section					
early Bajocian positive $\delta^{13}C$ excursion	late Bathonian negative $\delta^{13}C$ shift	0.54–17.69	17.15	3.37 (169.7–166.33)	**0.51**
late Bathonian negative $\delta^{13}C$ shift	late Callovian positive $\delta^{13}C$ excursion	17.69–28.66	10.97	3.13 (166.33–163.2)	**0.35**
late Callovian positive $\delta^{13}C$ excursion	FAD of *C. pulla*	28.66–53.66	29 (25 + 4)	11.14 (163.2–152.06)	**0.26**
late Callovian positive $\delta^{13}C$ excursion	FAD of *S. moluccana*	28.66–44.8	20.14 (16.14 + 4)	8.73 (163.2–154.47)	**0.23**
FAD of *S. moluccana*	FAD of *C. pulla*	44.8–53.66	8.86	2.41 (154.47–152.06)	**0.37**
FAD of *S. moluccana*	FAD of *P. malmica*	44.8–58.86	14.06	4.67 (154.47–149.8)	**0.3**
FAD of *C. pulla*	FAD of *P. malmica*	53.66–58.86	5.20	2.26 (152.06–149.8)	**0.23**
Lejowa Valley section (L)					
FAD of *S. moluccana*	FAD of *C. pulla*	40.5–48.68	8.18	2.41 (154.47–152.06)	**0.34**
FAD of *S. moluccana*	FAD of *P. malmica*	40.5–58.31	17.81	4.67 (154.47–149.8)	**0.38**
FAD of *C. pulla*	FAD of *P. malmica*	48.68–58.31	9.63	2.26 (152.06–149.8)	**0.43**
FAD of *P. malmica*	FAD of *L. dobeni*	58.31–65.01	6.70	0.9 (149.8–148.9)	**0.74**
Lejowa Valley section (Lc)					
FAD of *S. moluccana*	FAD of *P. malmica*	3.11–10.32	7.21	4.67 (154.47–149.8)	**0.15**
Filipka Valley section					
late Bajocian negative $\delta^{13}C$ shift	late Bathonian negative $\delta^{13}C$ shift	32.49–59.41	26.92	2.15 (168.48–166.33)	**1.25**
late Bathonian negative $\delta^{13}C$ shift	late Callovian positive $\delta^{13}C$ excursion	59.41–70.67	11.26	3.13 (166.33–163.2)	**0.4**
late Callovian positive $\delta^{13}C$ excursion	middle Oxfordian positive $\delta^{13}C$ excursion	70.67–74.78	4.11	3.32 (163.2–159.88)	**0.12**
FAD of *S. moluccana*	FAD of *P. malmica*	75.68–85.75	10.07	4.67 (154.47–149.8)	**0.22**
Ždiarska vidla section					
early Bajocian positive $\delta^{13}C$ excursion	late Bajocian negative $\delta^{13}C$ shift	7.3–84.04	76.74	1.22 (169.7–168.48)	**6.3**
early Bajocian positive $\delta^{13}C$ excursion	late Bathonian negative $\delta^{13}C$ shift	7.3–115.67	108.37	3.37 (169.7–166.33)	**3.22**
late Bajocian negative $\delta^{13}C$ shift	late Bathonian negative $\delta^{13}C$ shift	84.04–115.67	31.63	2.15 (168.48–166.33)	**1.47**
late Bathonian negative $\delta^{13}C$ shift	late Callovian positive $\delta^{13}C$ excursion	115.67–131.17	15.50	3.13 (166.33–163.2)	**0.5**
late Callovian positive $\delta^{13}C$ excursion	middle Oxfordian positive $\delta^{13}C$ excursion	131.17–137.77	6.60	3.32 (163.2–159.88)	**0.2**
late Callovian positive $\delta^{13}C$ excursion	FAD of *C. pulla*	131.17–145.94	14.77	11.14 (163.2–152.06)	**0.13**
middle Oxfordian positive $\delta^{13}C$ excursion	FAD of *C. pulla*	137.77–145.94	8.17	7.82 (159.88–152.06)	**0.1**

facies, which means that great caution must be exercised, when comparing the non-decompacted sedimentation rates of different facies.

The sedimentation rate between the early Bajocian positive $\delta^{13}C$ excursion and the late Bajocian negative $\delta^{13}C$ shift in the Ždiarska vidla section (Fig. 19) is estimated at 6.3 cm/kyr and falls within the broad range that was typical for Jurassic deposits accumulating in basinal settings. For comparison, Picotti and Cobianchi (2017) have estimated the sedimentation rates in the Belluno Basin, Southern Alps, as ranging from 0.3 cm/kyr for the Igne Formation representing Toarcian–early Bajocian starved-basin conditions, to 30 cm/kyr for the Vajont Limestone Formation, representing Bajocian–Bathonian well-supplied-basin conditions. Santantonio (1993) has estimated the sedimentation rate of basinal carbonate deposits in the Umbria–Marche Apennines as being at least 15 mm/kyr. A similar rate was estimated by Baumgartner (1990) for the Bajocian basinal carbonates in the same basin and by Muttoni *et al*. (2005, fig. 2) for the Lower to Middle Jurassic carbonates of the Lombardian Basin. The sedimentation rate estimated for the Bajocian–Bathonian carbonate deposits in the basinal areas of the Tatra Mts thus matches well the estimates for similar Jurassic deposits elsewhere in the Mediterranean.

The sedimentation rate of the early Bajocian–Bathonian *Bositra*-crinoidal limestone in the Długa Valley section is estimated at 0.51 cm/kyr, which compares well with the sedimentation rate suggested for many other pelagic carbonate platforms, such as the value of 0.32 cm/kyr estimated by Martire and Clari (1994) for the facies Ammonitico Rosso Veronese, a classic example of Jurassic pelagic carbonate platform deposits. This estimate is, however, an order of magnitude higher than the rate of 0.5 mm/kyr, calculated by Santantonio (1993) for pelagic carbonate platform deposits in the Umbria–Marche Apennines.

The sedimentation rate of the upper Bathonian – Callovian ribbon radiolarites in the outcrop sections in the Długa Valley, Filipka Valley and the Ždiarska vidla (Fig. 19) appears to be fairly uniform, varying between 0.35 and 0.5 cm/kyr. This rate is comparable to that estimated for many analogous carbonate-free radiolarites in many Jurassic Tethyan sections. Classic examples come from the Lombardian Basin, where the green, carbonate-free radiolarites (ribbon radiolarites) of the Breggia Gorge section were deposited at a rate of 0.32 cm/kyr according to recalculated data given by Baumgartner (2013), a rate of 0.2–0.3 cm/kyr according to Muttoni *et al.* (2005) or a wide range in rate of 0.6–3 cm/kyr according to Chiari *et al.* (2007). Similarly, the sedimentation rate of black, carbonate-free Bathonian radiolarites in the Betic Cordillera is estimated at between 0.1–0.2 and 1 cm/kyr (O'Dogherty *et al*., 2001).

Since the Długa Valley and other sections in the Western Tatra Mts represent deposits on an intrabasinal high in the Middle Jurassic, while the Ždiarska vidla and Filipka Valley sections represent basinal deposits, the ribbon radiolarites must have levelled the pre-existing topography of the basin floor.

All the studied sections indicate that the sedimentation rate of the calcareous radiolarites was lower than that of the green radiolarites. A similar relationship was observed in the Lombardian Basin, where the sedimentation rate of the calcareous radiolarian cherty limestone and the Rosso ad Aptici units, which are lithological equivalents to the Tatra calcareous radiolarites, is estimated at 0.15–0.2 and 0.13––0.6 cm/kyr (Chiari *et al*., 2007). Although Baumgartner (2013) estimated that the sedimentation rate of knobby radiolarites in the Breggia section (Lombardy Basin), an equivalent of the calcareous radiolarites described in the present account, was higher than that of the underlying ribbon radiolarites (0.78 cm/kyr and 0.32 cm/kyr, respectively), the overlying limestones with chert bands (Rosso ad Aptici) were deposited at a rate of 0.12 cm/kyr. Similarly, the more calcareous upper part of the Calcari Diasprigni carbonate-biosiliceous unit in the Umbria-Marche Apennines is characterized by a sedimentation rate lower than that of its lower, more siliceous part (Baumgartner, 1990). The estimates collectively indicate that the decrease in sedimentation rate from carbonate-free to carbonate-rich Jurassic radiolarites could be a more general trend, implying a decline in radiolarian productivity, which is discussed further in the text (section "Carbonate-biosiliceous-carbonate succession as a record of seawater column eutrophication and carbonate production/preservation crisis").

The upward increase of sedimentation rate is clearly recognizable in the Lejowa Valley section (L) (Fig. 19), where its value in the interval between the FAD of *P. malmica* and the FAD of *L. dobeni* reached 0.74 cm/kyr. This estimate is higher than the data of Grabowski and Pszczółkowski (2006a), who approximated the sedimentation rate of 0.54 cm/kyr (magnetozone M20n; the value was recalculated according to the time scale of Ogg *et al*., 2016) for the younger Tithonian deposits of Jasenina Formation. The value of the sedimentation rate from the Lejowa Valley section corresponds to an average sedimentation rate of 0.71 cm/kyr between the FADs of *P. malmica* and *L. dobeni* in the deposits of the Jasenina Formation in the Strážovce section (Michalík *et al*., 1995). A similar increase of sedimentation rate was reported from the well-studied Italian basins, such as the Umbria–Marche Apennines (Baumgartner, 1990), the Ligurian Basin (Muttoni *et al*., 2005) and the Trento Plateau (Martire and Clari, 1994). This a general increase of sedimentation rate in the latest Jurassic resulted apparently from a recovery of carbonate productivity. Therefore, the decreasing trend in sedimentation rate for the coeval deposits of the Ždiarska vidla section (Fig. 19) is puzzling. Although the section studied ends approximately at the FAD of *Colomisphaera pulla* (Jach *et al*., 2014), the biostratigraphic data of Pszczółkowski (1996) indicate an extremely low sedimentation rate in this section until the Tithonian. According to Pszczółkowski (1996), the thickness of the red nodular limestones, which represent the Chitinoidella Zone in this section, is only 0.3 m, whereas the thin-bedded limestones and marly shales of the same zone reach a thickness of 7 m in the Długa Valley section (his Pośrednie section). This puzzling issue is discussed further in this paper (the section "The Late Jurassic tectono-geomorphic restructuring of basin floor").

DISCUSSION

Vertical facies changes and palaeoceanographic conditions

The stratigraphic arrangement of facies in Tethyan basins was controlled by several interrelated factors, such as the gradual break-up of Pangea that created the individual basins and controlled their subsidence at the rifting stage and the subsequent thermal subsidence, combined with eustatic and climatic changes that collectively affected the chemistry of the ocean water and its trophic state (e.g., Reis *et al*., 2007; Vörös, 2012; Baumgartner, 2013). Another important factor to be taken into consideration is the evolutionary changes affecting carbonate-precipitating organisms. This section is an interpretive discussion of the influence of these factors in the present case.

Carbonate-biosiliceous-carbonate succession as a record of eutrophication and carbonate production/ preservation crisis

The stratigraphic trend of the sedimentary succession from carbonate to biosiliceous and back to carbonate facies (C-BS-C) in the Fatricum Domain was interpreted traditionally as the record of a gradual oceanization of the basin, with the radiolarites within a general carbonate succession considered to indicate the greatest depositional depth of a particular basin (Lefeld, 1974, 1981). A similar opinion was held by numerous authors on the many occurrences of Jurassic radiolarites in the Alpine-Mediterranean Tethys (e.g., Bosselini and Winterer, 1975; Barrett, 1982; Winterer and Bosselini, 1981). However, the study by Baumgartner (1987) indicated that the concentration of radiolarians in several Jurassic basins of the Alpine-Mediterranean Tethys was controlled mainly by their lateral transport from intrabasinal topographic highs. The concentration of radiolarian tests in the basin then would have had taphonomic causes and would have depended on eutrophic conditions in the seawater column.

The present study strongly supports this notion and indicates that the Jurassic C-BS-C succession in the present case originated owing to changes in the trophic conditions of the basin. A large body of literature, based on recent examples, contends that radiolarians are a good indicator of eutrophic conditions in the upper part of the seawater column (e.g., De Wever *et al*., 2001; Boltovskoy *et al*., 2010), as also has been demonstrated by palaeoenvironmental studies (e.g., Mutti and Hallock, 2003; Baumgartner, 2013; De Wever *et al*., 2014; Bąk and Bąk, 2018). Analyses of fossil *Bositra* taphocenoses have led to the conclusion that this bivalve group was well adapted to stress conditions, particularly to an increased nutrient level (e.g., Bartolini and Cecca, 1999; Santantonio, 1993). The intimate association of *Bositra* and radiolarians in the present case therefore can be explained as an indicator of eutrophication. It is worth noting that *Bositra* in the present case forms the dominant bioclasts in the *Bositra*-crinoidal limestones and in the grey nodular limestones directly underlying the ribbon radiolarites, while being almost the sole carbonate component in the latter. However, more extensive palaeontological and geochemical research may be needed to prove the present microfacies-based interpretation.

Some further support for the present hypothetical interpretation is lent by the palaeogeographic evolution of the basin. According to the Baumgartner's (1987) concept, radiolarite deposition in a basin should occur in seafloor lows, bordered by intrabasinal highs with condensed carbonates, from which radiolarians would be swept into these depressions. The basinal Fatricum Domain in the present case indeed was bordered by the Tatric Ridge (Tatricum), where the Middle–Upper Jurassic consists of ferruginous limestones, stromatolites and nodular limestones (Szulczewski, 1963, 1965; Lefeld, *et al*., 1985; Łuczyński, 2001, 2002) indicative of a radiolarite-free elevation with a low carbonate accumulation rate. Although the lack of exact biostratigraphic dating hampers precise correlation of the Tatricum carbonates with the Fatricum sections studied (Łuczyński, 2002), the latest integration of biostratigraphic and carbon isotope data from the Kimmeridgian–Berriasian succession of the Tatric Ridge indicates condensation of its Callovian to Oxfordian deposits (Pszczółkowski *et al*., 2016). These condensed deposits would then be coeval with the radiolarites deposited in the Fatricum basinal environment.

The formation of biosiliceous deposits in the Fatricum Domain corresponds to the widespread crisis in the production and preservation potential of carbonates in the whole Alpine-Mediterranean Tethys and its shelves (e.g., Santantonio, 1993; Bartolini *et al,* 1999; Morettini *et al*., 2002; Rais *et al*., 2007; Donnadieu *et al*., 2011; Jadoul, 2018). The crisis included neritic settings and reefs (Lainfelder *et al*., 2002; Ramajo and Aurell, 2008) and involved a fall of biodiversity (Bartolini and Cecca, 1999), an inhibition of biocalcification (Erba and Tremolada, 2004) and a drastic drop in the calcium carbonate content of pelagic sediments (Ogg *et al*., 1983). The causes of this carbonate crisis are disputed still, with the eutrophication of the seawater column considered as one of the most important factors (Bartolini and Cecca, 1999; Cecca *et al*., 2001; Morettini *et al*., 2002).

Notably, the crisis was manifested not only in the decreased production of calcium carbonate, but also by a reduction of its preservation potential (Santantonio, 1993). The lack of aragonite components (e.g., ammonites or their "ghosts") and the presence of calcite components (e.g., aptychi, *Bositra* shells), as noticed earlier by Lefeld (1974), is confirmed fully by careful inspection in the present study. This observation implies that the seawaters at that time were sufficiently corrosive to dissolve aragonite, which in turn indicates deposition of these facies below the aragonite compensation depth (ACD). Conversely, nearly the entire sedimentary succession apparently was deposited above the calcium compensation depth (CCD). Since the $CaCO_3$ content of 20 wt% is an arbitrarily defined limit for deposits formed below the CCD (e.g., Bostock *et al*., 2011), only the middle – upper Callovian part of the ribbon radiolarites (Figs 4, 8, 9, 20) potentially would have been deposited below the CCD.

If the reasoning above is correct, it can be hypothesized that the crisis caused a rise in both the CCD and ACD and that the Fatricum basin-floor depositional environment was below the ACD between the middle Bathonian and late Kimmeridgian and below the CCD in the middle to late Callovian. The rise of the CCD and ACD may have resulted

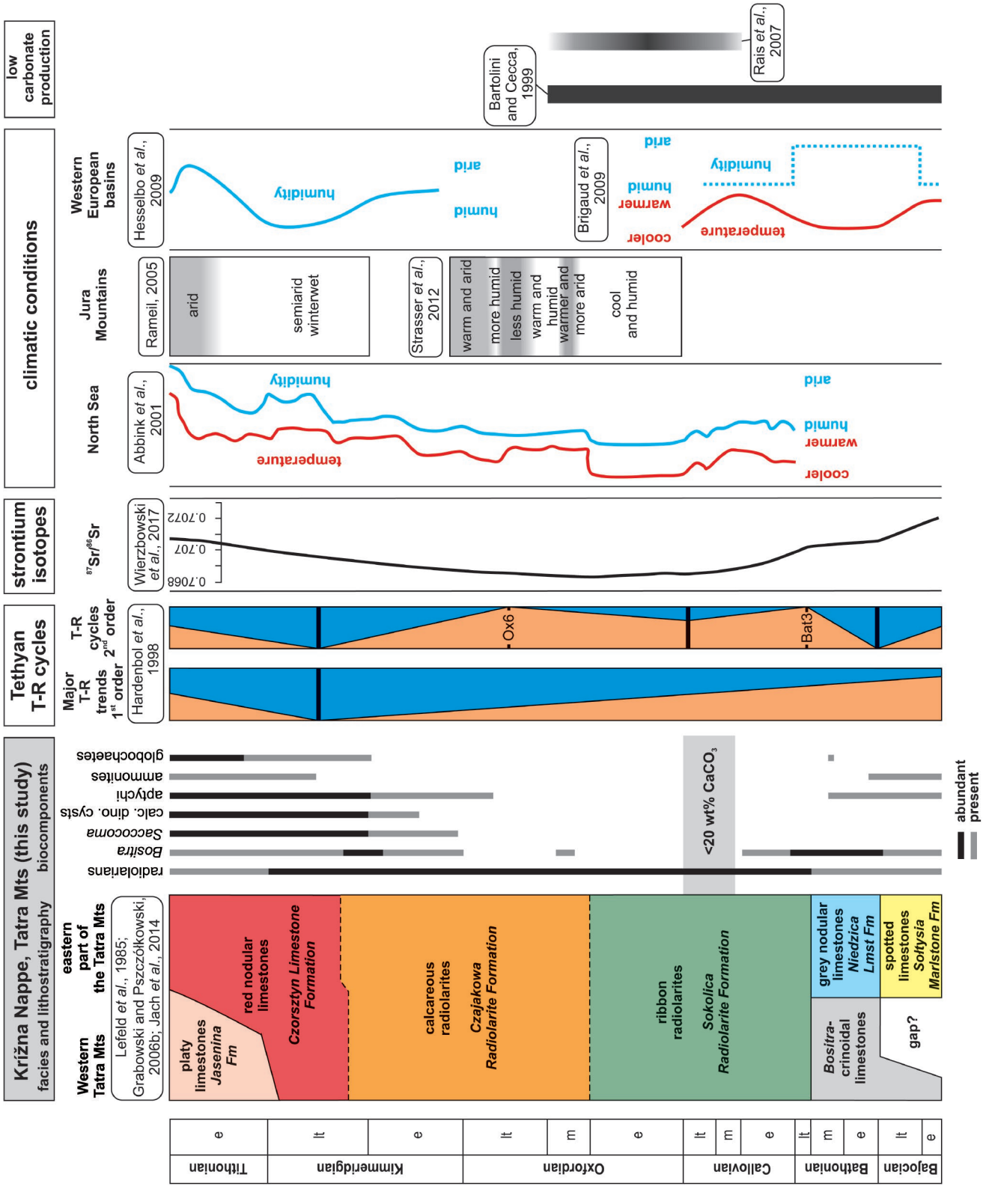

Fig. 20. Facies and range of selected biocomponents in the Tatra Mts sections studied, compared to general sea-level curve and $^{87}Sr/^{86}Sr$ curve, palaeoclimatic data and carbonate productivity for the Bajocian – early Tithonian.

from the lower flux of carbonate components as an effect of the reduced carbonate productivity caused by eutrophication and/or of the acidification of oceanic water during the Callovian and early Oxfordian (Ramajo and Aurell, 2008; Vörös, 2012).

Surprisingly, the crisis coincided with a low ratio of the $^{87}Sr/^{86}Sr$ isotopic signature of Jurassic seawater (Fig. 20; Wierzbowski *et al*., 2017), which marked an increased supply of volcanic or hydrothermal strontium. Such coincidences of a low $^{87}Sr/^{86}Sr$ ratio and radiolarian blooms in the geological past were noted earlier by Racki and Cordey (2000), who attributed the blooms to an increase in silica supply by volcanic and hydrothermal activity. However, the calculations of silica budget indicate that the vast majority of silica supplied to the global ocean is derived from continental fluvial run-off (e.g., Tréguer *et al*., 1995; Dürr *et al*., 2011). The temporal coincidence may thus have another cause-and-effect relationship. Volcanic and hydrothermal activity may have affected ocean chemistry through an increased supply of CO_2, which then led to seawater acidification and, in consequence, triggered the carbonate production/preservation crisis (Vörös, 2012). These processes also could have influenced the climate. High atmospheric CO_2, regarded as a proxy of the greenhouse periods, promoted elevated humidity, rainfall, intensified continental run-off and greater productivity, potentially responsible for the decrease in seawater pH and rise in the CCD (e.g., Larson and Erba, 1999).

In the light of the preceding discussion, the onset and demise of biosiliceous sedimentation in the Fatricum Domain apparently spanned the period between the deterioration and resumption of carbonate productivity. Apart from the signs of eutrophication, indicated by the deposition of the *Bositra*-crinoidal and grey nodular limestones below the ribbon radiolarites, the onset of biosiliceous sedimentation was rapid. The solitary layer of *Bositra*- and radiolaria-rich marlstone, 30 cm thick and directly underlying the radiolarites (Fig. 14E), was a turnover horizon of the environmental switch from carbonate to biosiliceous sedimentation. This transitional layer recorded a sudden slow-down in carbonate production, while biosiliceous production was still about to increase. Notably, this transitional marlstone unit occurs in all the outcrop sections studied in the present case (Figs 4, 8, 9). Similar horizons of marlstones underlying radiolarites were reported from other Tethyan basins, such as the Austro-Alpine region (Vecsei *et al.*, 1989) and the Umbria-Marche Apennines (Baumgartner, 1990). This means that the rapid onset of biosiliceous production may be regarded as a widespread regional phenomenon. Conversely, the resumption of carbonate production was a gradual change, marked by the deposition of the calcareous radiolarites in the present case (Fig. 20). This gradual return of carbonate sedimentation spanned the middle Oxfordian to late Kimmeridgian, when carbonate production was increasing slowly, while biosiliceous production declined (see Hüneke and Henrich, 2011). The thickness of the calcareous radiolarites, relative to the corresponding time span, indicates a low sedimentation rate and "starved-basin" conditions, typically oligotrophic with very low nutrient concentrations and lower primary productivity than in the previous interval.

Eustatic and climatic influence

Recognition of 3rd-order eustatic cycles in the deep neritic to bathyal sedimentary succession studied is difficult without more precise biostratigraphic dating, but the general increase in water depth of Fatricum from the Middle to Late Jurassic corresponds well with a net eustatic sea-level rise of about 50 m (Hardenbol *et al*., 1998; Snedden and Liu, 2010). The eustatic deepening in the Fatricum Domain probably was enhanced by thermal sagging and pull-apart tectonic subsidence (Fig. 21), which would mean a combination of eustatic and tectonic forcing.

The deposition of well-washed grainstones in the upper part of the *Bositra*-crinoidal limestone unit corresponds to the late Bathonian 2nd-order eustatic sea-level fall of ca. 50 m (Bat3; Hardenbol *et al*., 1998), whereas the subsequent deposition of the carbonate-poor ribbon radiolarites coincides with the late Bathonian and Callovian sea-level rise (Hardenbol *et al*., 1998; Snedden and Liu, 2010). The sea-level fall probably would have intensified the winnowing effect of bottom currents (Martire, 1992). The return of pure carbonate sedimentation – the red nodular limestones – corresponded to the Kimmeridgian sea-level highstand (Hardenbol *et al*., 1998; Snedden and Liu, 2010).

The Middle to Late Jurassic witnessed several 3rd- and lower order eustatic cycles (Hardenbol *et al*., 1998; Snedden and Liu, 2010). It is therefore quite likely that the regular chert-shale alternations in the ribbon radiolarites and the mudstone-limestone alternations in the spotted limestones represent lower-order (Milankovitch range) cycles (e.g., see De Wever, 1987; Ikeda *et al*., 2016). However, since the time span of these lithofacies alternations is unknown; the present authors decline to venture into any further possible speculations on this issue. Likewise, it can only be speculated as to how the eustatic changes possibly might have affected the bathymetric position of the ACD and CCD through climate and, consequently, productivity fluctuations.

Palaeoclimate seems to have been a factor that exerted a significant control on the sedimentation of the deposits studied and in particular on the sedimentation of the green and calcareous radiolarites. The onset of biosiliceous sedimentation, dated as late Bathonian (Jach *et al*., 2014), was coeval with increasing humidification of the climate, inferred from the kaolinite to illite + illite-smectite mixed layer clay mineral ratio in the Paris Basin (Brigaud *et al*., 2009). Pellenard *et al*. (2014), on the basis of $\delta^{18}O$ of bivalve shells and belemnite rostra, indicated intense freshwater input into the Paris Basin at that time, which additionally points to relatively humid conditions. Although deterioration of the climate commenced at the turn of the middle and late Callovian and the temperatures decreased (e.g., Dromart *et al*., 2003a, b; Wierzbowski *et al*., 2013), the humid conditions persisted till the end of the early Oxfordian. This is demonstrated by pollen spectra (Abbink *et al*., 2001), clay mineral assemblage (Strasser *et al*., 2012; Pellenard *et al*., 2014) and palaeochemotaxonomic data (Hautevelle *et al*., 2006). The above climatic conditions recorded in the peri-Tethyan basins of the North West Europe correspond well to the elevated content of siliciclastic admixtures in the ribbon radiolarites studied.

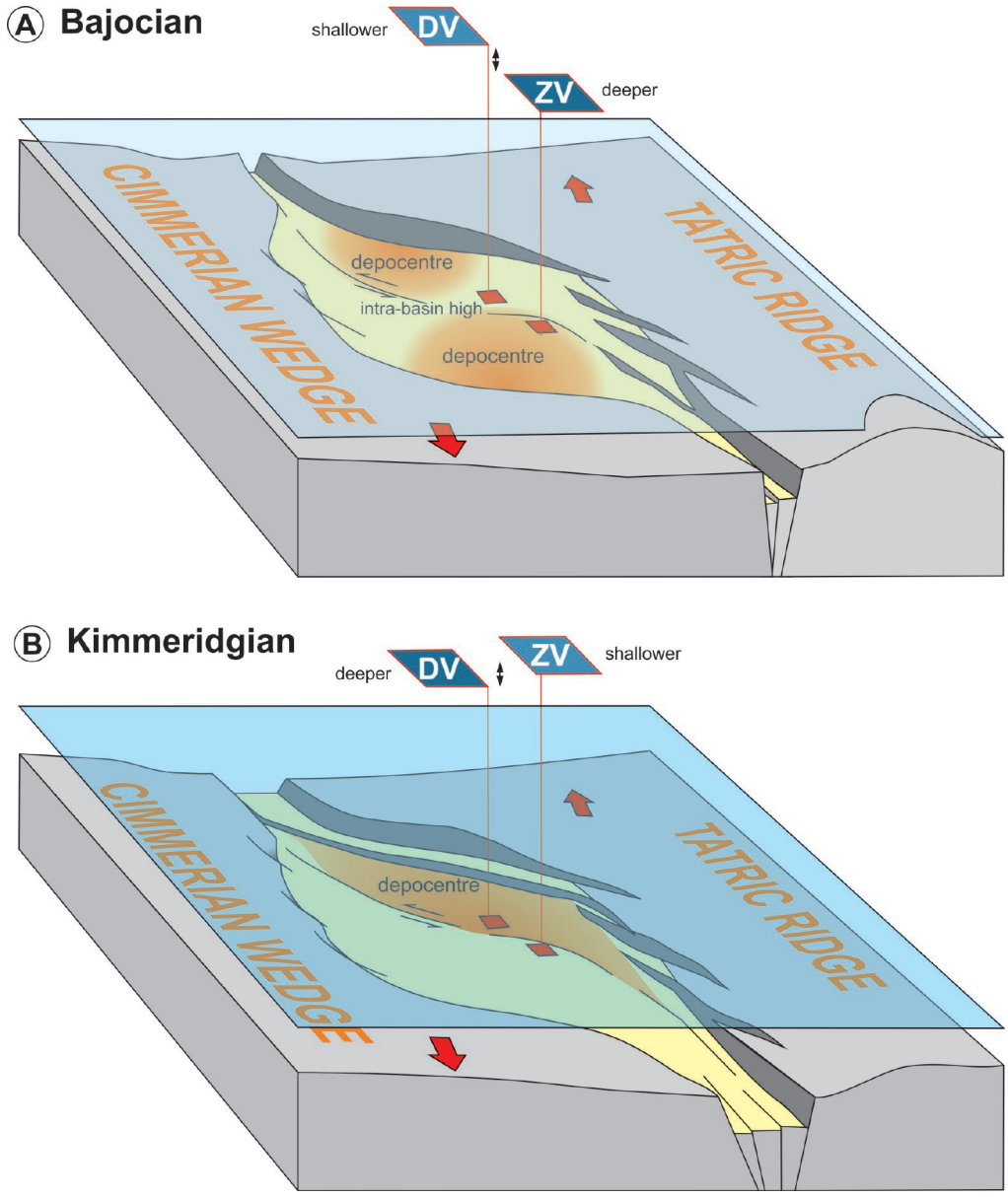

Fig. 21. Schematic tectonic model (not to scale, inspired by Michalík, 2007 and Wu *et al*., 2009) for palaeobathymetric differences and changes in the study area between Długa Valley (DV) and Ždiarska vidla (ZV). The Zliechov Basin formed as a transtensional pull-apart seaway at the Fatric interface between the Cimmerian accretionary crustal wedge to the south and the Tatric Ridge to the north.

The switch from the ribbon to calcareous radiolarites sedimentation dated to the turn of the early and middle Oxfordian synchronized well with the climate aridization and warming recorded in the peri-Tethyan basins (Abbink *et al*., 2001; Hautevelle *et al*., 2006; Pellenard *et al*., 2014) and the increase in seawater temperature in the Tethys and the peri-Tethyan basins (Price and Rogov, 2009; Wierzbowski, 2004, 2015; Arabas, 2016). Arid climatic conditions are reflected in the scarcity or complete lack of siliciclastic admixtures of continental origin in the calcareous radiolarites studied. An arid climate is also in line with more oligotrophic seawater due to reduced continental runoff. The further aridization and warming of climate seems to favour the reestablishment of carbonate production.

Therefore, biosiliceous sedimentation of the radiolarites studied appears to have been influenced by climatic conditions; it especially was favoured during the humid climate intervals. Interestingly, this notion fits both scenarios explaining the origin of the Jurassic Tethyan radiolarites (Baumgartner, 2013; De Wever *et al*., 2014). Baumgartner (2013) drew attention to riverine input of dissolved organic matter into the sea as the cause of the high fertility of surface seawater, whereas De Wever *et al*. (2014) associated the trophic state of seawater to monsoonal upwelling, which must have caused increasing precipitation on the lands and increasing riverine run-off of siliciclastics.

A subsequent Late Jurassic warming, with gradually increasing aridity, is recorded in various palaeogeograph-

ical areas (Abbink *et al*., 2001; Rameil, 2005; Brigaud *et al*., 2009; Jenkyns *et al*., 2012; Wierzbowski, 2015; Arabas, 2016). In the latest Kimmeridgian and early Tithonian, the climate shifted from monsoonal relatively humid to more arid conditions with semiarid winter-wet seasons (Rameil, 2005; Bover-Arnal and Strasser, 2013). In the late early Tithonian, it was followed by aridization (Hesselbo *et al*., 2009). It is suggested that the Acme Zone of *Cadosina semiradiata semiradiata* (Semiradiata Zone, early Tithonian) indicates warmer surface seawater (Michalík *et al*., 2009), which corresponds well with the arid phase of the 'Hudlestoni event' recognized in NW Europe (Rameil, 2005; Hesselbo *et al*., 2009). These cysts were found in the Lejowa Valley (L) and Upłaziańska Kopa sections.

It is worth noting that changes in climate and sedimentation during the Middle–Late Jurassic were interpreted as being due to a fast, equatorward movement of some Western Tethyan domains (Lewandowski *et al*., 2005; Muttoni *et al*., 2005). Interestingly, low palaeolatitudes of ca. 22° N (± 5°) were recorded for the Callovian–Kimmeridgian of the Pieniny Klippen Belt (Márton *et al*., 2016). This southward shift and return to the north recorded in Western Tethyan region also may have been responsible for the recorded facies change (C-BS-C). The radiolarian-bearing deposits may have originated, when the Fatricum Domain moved to sub-equatorial latitudes, whereas a gradual return of favourable environmental conditions for carbonate sedimentation took place, when it returned to higher latitudes (Muttoni *et al*., 2005, 2013).

Basin palaeobathymetry

The Jurassic basins of the Alpine-Mediterranean Tethys traditionally were considered to have been of deep-water type, on the account of radiolarites as a marker of deposition below the CCD (Garrison and Fischer, 1969; Bosselini and Winterer, 1975; Winterer and Bosselini, 1981). A similar view on the Fatricum radiolarites was held by Lefeld (1974) – especially for the carbonate-poor ribbon radiolarites (his green radiolarites) – with reference to the depth distribution of siliceous and carbonate pelagic sediments in modern oceans (e.g., Berger, 1970) as an analogue. This reasoning laid the ground for the long-held wider opinion that the ribbon radiolarites of the Tatra Mts may have been deposited at a water depth of ca. 3000 m (Lefeld, 1974, p. 313).

However, this view is highly questionable. First, the use of modern oceans as an analogue for the Jurassic may be mistaken, as the CCD and ACD in the Middle to Late Jurassic were much shallower than today and had deepened to perhaps ca. 3,000 m only at the end of the Jurassic (McBride and Folk, 1979; Winterer and Bosellini, 1981; Barrett, 1982; Aiello and Hagstrum, 2001). Second, it has been argued compellingly by Baumgartner (1987) that there is no direct dependence of the depth of basin water on the deposition of radiolarites. For example, it has been shown that the Jurassic radiolarites in some basins are intercalated with and overlain by relatively shallow-marine deposits, such as limestones with hummocky cross-stratification or with pennular corals indicating the photic zone (Santantonio, 1993; Santantonio *et al*., 1996; Molina *et al*., 1999). The analysis of inclusions also demonstrated that the crinoidal limestones of intrabasinal highs in some basins were deposited in shallow settings at a depth range of 23 to 112 m (Mallarino *et al*., 2002). Third, it has been widely demonstrated that the CCD depth may change significantly within a basin (e.g., Bostock *et al*., 2011) and can change independently in isolated or semi-isolated, adjacent basins (e.g., Lee *et al*., 2000).

The Jurassic basins in the Alpine-Mediterranean Tethyan realm obviously were not identical and differed considerably in tectonic development and bathymetric history, but their radiolarite deposits are comparable and seem to confirm Baumgartner's (1987) notion that there is little or no direct link between the deposition of radiolarites and basin bathymetry. This notion puts into question the previous palaeobathymetric suggestions for the Fatricum Domain basins, based on the present-day bathymetry of the oceanic CCD and ACD.

The palaeobathymetric meaning of the CCD and ACD must be treated with great caution, as their depth positions are by no means steady and varied considerably in geological time, as evidenced for the Cenozoic by the ocean drilling programs (e.g., Rea and Lyle, 2005; Pälike *et al*., 2012). The depth of CCD and ACD was strongly dependent on such interrelated factors as: (1) the supply of $CaCO_3$ to the basin; (2) the influx of terrigenous non-carbonate sediment, which would cause the dilution of $CaCO_3$ in the bottom sediments; (3) the influx of siliceous or biosiliceous skeletal material; (4) the influx of organic matter, which then would undergo decomposition on an oxygenated seafloor and boost acidification of the sediment pore water, thereby instigating an effective dissolution of $CaCO_3$; (5) the possible episodic influx of volcanic ashfall tephra; and (6) the net sedimentation rate, which would determine the exposure time of $CaCO_3$ particles to the chemical or mechanical influence of seawater (cf. Bostock *et al*., 2011; Pälike *et al*., 2012; Cobianchi *et al.,* 2015).

Unfortunately, there is little unequivocal palaeobathymetric evidence that the present study can offer. Most of the sediments apparently were deposited well below the storm wave base, with the exception of the early Toarcian crinoidal limestones, in which hummocky cross-stratification was recognized (Jach, 2005). Any further palaeobathymetric inferences necessarily must be hypothetical and based on some indirect or new lines of evidence.

It remains unclear what the actual palaeobathymetry of the Middle to Late Jurassic CCD and ACD levels was. The hypothetical water depth suggested by Bernoulli and Jenkyns (2009, fig. 33) for various Tethyan pelagic facies on the basis of a hypothetical depth of the CCD and ACD must be considered with much caution (see Baumgartner, 2013). Accordingly, the ribbon radiolarites and the red nodular limestones would have been deposited at water depths of ca. 2.5 km and ca. 2 km, respectively. From considerations of the perturbations of the seawater trophic level in the Alpine-Mediterranean Tethys and the depth fluctuations of the CCD discussed earlier, it is highly probable that the actual depositional depth was much shallower, although the sediment delivered to the basin interior was mainly pelagic, with minor hemipelagic fluxes.

The Middle Jurassic sedimentation in Fatricum Domain: passive burial of post-rift topography or active tectonics?

On the account of the Jurassic plate-tectonic development in the Central Carpathians and the entire Alpine-Mediterranean Tethys, it is reasonable to believe that syndepositional tectonic activity occurred in the study area. It was located in the eastern-central part of the Fatricum Domain and evolved from a late Triassic intracontinental rift into a Jurassic pull-apart seaway at the Fatricum interface between the Cimmerian accretionary wedge to the south and the Tatric Ridge to the north (Michalík, 1994, 2007; Michalík *et al.,* 2017). Many other post-Triassic Tethyan rift basins, such as in the Sicilian Trapanese Domain (Bertok and Martire, 2009) and in the Provençal and Dauphinois domains of the Western Alps (Bertok *et al*., 2011; Barale *et al*., 2017), remained tectonically active long after their rifting stages. The regional notion of Jurassic syndepositional, transcurrent tectonics (Fig. 21) may explain the observed intrabasinal palaeobathymetric differences and their reversals revealed by the present study (cf. Gradziński *et al*., 2004; Jach, 2007; Michalík, 2007; Iwańczuk *et al*., 2013; Michalík *et al.,* 2017).

The present facies analysis of the Middle Jurassic deposits in the part of the Fatricum Domain studied indicates considerable relief of the basin-floor topography. Deposits in the Western Tatra Mts (the Długa Valley, Lejowa Valley and Upłaziańska Kopa sections; Fig. 19) had accumulated on a submarine intrabasinal high, as evidenced by: (1) their relatively minor thickness and hence low accumulation rate; (2) the occurrence of the well-washed grainstone-packstone facies of the *Bositra*-crinoidal limestones with signs of stratigraphic condensation; and (3) the scarcity of any resedimented deposits (cf. Santantonio, 1993). The coeval deposits in the eastern part of the Tatra Mts (the Filipka Valley and Ždiarska vidla sections), in contrast, represent a deeper-marine basinal environment, as evidenced by: (1) their greater thickness and hence much higher sedimentation rate; (2) the predominance of pelagic wackestone-mudstone facies with no signs of condensation; and (3) the occurrence of resedimented deposits, such as crinoidal turbidites, lithoclastic debrites and slump deposits (see also Mišík, 1959; Iwańczuk *et al.*, 2013). The relative palaeobathymetric difference between the two areas of the Fatricum Domain can be attributed to the development of an intrabasinal high separating the two depocentres (Fig. 21A; cf. Wu *et al*., 2009).

A more detailed comparison of the thickness and facies of the intarbasinal high and adjacent basins may shed some light of their palaeotopographic relationship. The late Pliensbachian – Toarcian deposits in the Western Tatra Mts have a thickness of ca. 70 m, comprising about 40 m of spiculites, crinoidal limestones, manganese limestones, red nodular limestones and marls (Jach, 2002, 2005; Gradziński *et al*., 2004; Jach and Dudek, 2005) and about 30 m of *Bositra*-crinoidal limestones and overlying ribbon radiolarites (Figs 4, 5). The coeval deposits in the eastern part of the Tatra Mts are ca. 280 m thick, comprising pelagic limestones, marls and grey nodular limestones overlain by ribbon radiolarites (Iwańczuk *et al.*, 2013, fig. 7; Jach *et al*., 2014, fig. 8). On the basis of the cumulative thickness of the deposits, the palaeobathymetric difference can be estimated at ca. 210 m. On the one hand, this can be regarded as a minimum palaeobathymetric estimate, because the compaction of pelagic wackestone-mudstone carbonates may have been more than 50% greater than that of the shallower-water grainstone-packstone carbonates (Clari and Martire, 1996). On the other hand, the present conservative estimate may still be reasonable, since experimental studies have shown that most of the compaction occurs under an early sediment overburden load of ca. 2 m (Kochman and Matyszkiewicz, 2013). It must be stressed that the above calculation assumes uniform subsidence of the intrabasinal high and adjacent basin-floor, which probably was not the case. Conversely, the coeval deposits of these areas indicate their active differential subsidence. The presence of resedimented deposits in the basin may suggest its active tectonic subsidence combined with the effect of sediment compaction.

It is worth noting that the resedimented deposits in the eastern part of the Tatra Mts are not limited to any particular stratigraphic episode, but are scattered as discrete isolated beds in the basinal succession and constitute a component of subordinate thickness (2 vol.%). This evidence indicates that sediment gravity flows were rare events unrelated to the basinal environment and may have thus been triggered by seismo-tectonic activity (see discussion by Jo *et al*., 2015). However, this suggestion is hypothetical and requires much caution, because not all calciturbidites are necessarily seismites – as shown, for example, by studies of the Neogene to Quaternary slope deposits of the Bahamian carbonate platform. Calciturbidites may be genetically related to sea-level fluctuations and platform accommodation deficit, carbonate platform productivity and/or non-uniform sediment cementation (e.g., Betzler *et al*., 1999; Reijmer *et al*., 2015).

Tectonic significance also may be attached to the grey nodular limestones, which occur exclusively in the eastern part of the Tatra Mts. They originated through early – middle Bathonian down-slope creep of selectively cemented, fine-grained carbonates, following submarine slumping, perhaps triggered by seismo-tectonic activity (Figs 8, 9, 12, 13). The notion of seismically triggered slope instability is hypothetical but seems compatible with the occurrence of a debris-flow deposit at the base of this nodular limestone facies (Figs 8, 12I), as the debris flow would have destabilized the submarine slope and initiated sediment gravitational creep (see review by Drzewiecki and Simó, 2002).

The high-relief seafloor topography of the eastern part of the Tatra Mts and Western Tatra Mts was eventually levelled off by Oxfordian time, when differential subsidence temporarily declined and the sedimentary facies of calcareous radiolarites covered both study areas.

The Late Jurassic tectono-geomorphic restructuring of basin floor

The Late Jurassic witnessed a major change in the sedimentary environment of the Fatricum Domain, with an apparent bathymetric reversal between the eastern part of

the Tatra Mts and the Western Tatra Mts (Fig. 21B). The late Kimmeridgian to Tithonian red nodular limestones (Czorsztyn Limestone Formation) in the eastern part of the Tatra Mts are at least partly coeval with platy limestones of the Jasenina Formation in the Western Tatra Mts (Pszczółkowski, 1996, fig. 11; Michalík, 2007, fig. 7). The westward regional pinch-out of the red nodular limestones was documented earlier by Lefeld (1974) and confirmed by Jach *et al*. (2014). Moreover, there is a strong contrast in the lithotypes of the red nodular limestones between the eastern part of the Tatra Mts and the Western Tatra Mts. The pseudonodular, carbonate-rich lithotype (average $CaCO_3$ content of 85 wt%) occurs in the former area (Figs 8, 9). Conversely, the nodular and thin- and medium-bedded lithotypes, rich in non-carbonate matter (average $CaCO_3$ content of 60 wt%), are typical of the latter area (Figs 4, 5). The Jurassic red nodular pelagic limestones, known as the Ammonitico Rosso facies, are generally associated with Tethyan submarine elevations (e.g., Aubouin, 1964; Jenkyns, 1974; Borza and Michalík, 1987; Martire, 1996), whereas the red marly limestones characterize deeper-water basinal areas (Aubouin, 1964; Martire, 1996; Michalík, 2007). This lateral change in the limestone facies over a short distance indicates a marked bathymetric reversal of the topographic configuration of the seafloor in the Fatricum Domain. The change is attributed to a more advanced stage in the pull-apart transcurrent tectonics of the Fatricum Domain – with a new depocentre formed on the other side of the axial master strike-slip fault bend of the basin (Fig. 21B; cf. Wu *et al.*, 2009). During the Late Jurassic and Early Cretaceous, marls and limestones of the Jasenina and Osnica formations were deposited in this depocentre (cf. Michalík, 2007; Michalík *et al.,* 2017).

The Late Jurassic relative palaeobathymetric difference between the eastern part of the Tatra Mts and Western Tatra Mts is difficult to estimate (Fig. 21B). However, the lack of gravity flow deposits as well as other redeposited facies in the basin indicate an insignificant drowning of the basin. The only indication of redeposition is the presence of intraclasts of the early Tithonian Tithonica Zone in the early Tithonian Malmica Zone marly limestones in the Długa Valley section. The marked facies contrast between neighbouring sections located over a very short distance noted in the Lejowa Valley (Jach *et al*., 2012) may be interpreted as a record of a synsedimentary fault activity during the early Tithonian. A similar spatial facies relationship was typical of the flanks of pelagic carbonate platforms; however, it can be recognized fully only in well-exposed sections (e.g., Di Stefano *et al*., 2002; Martire and Pavia, 2004).

The Middle–Late Jurassic development in the Fatricum Domain commenced with the ultimate subduction of the Meliata-Vardar oceanic realm, possibly with local obduction (see the Meliata Ocean of Plašienka, 2018), which led to transcurrent lateral-escape plate tectonics. A similar plate-tectonic development with lateral changes in subsidence was described, for example, from the Belluno Basin and the Friuli-Adriatic Platform by Picotti and Cobianchi (2017). Changes in subsidence in this area are interpreted as an expression of the far-field compression, associated with the closure of the Vardar Ocean on the opposite side of the Adria Plate.

CONCLUSIONS

1. A detailed facies analysis of the Middle Jurassic deposits in the part of the Fatricum Domain studied indicates considerable relief of the submarine basin-floor topography. Deposits in the Western Tatra Mts accumulated on a submarine intrabasinal high, whereas the coeval deposits of the eastern part of the Tatra Mts represent a deeper basinal environment.
2. The basin was filled with bioturbated "spotted" limestones (Fleckenmergel facies; Bajocian) and grey nodular limestones (uppermost Bajocian – middle Bathonian), which resulted from subsequent gravitational bulk creep of the carbonate slope deposits and were affected by synsedimentary deformation. Coeval deposits of the intrabasinal high consist of *Bositra*-crinoidal limestones with omission surfaces.
3. The deposition of the ribbon radiolarites in the late Bathonian – middle Oxfordian was a record of a rise of the CCD. It coincided with a widespread crisis in carbonate production in the Tethyan realm, caused by interrelated environmental factors, such as eutrophication and acidification of seawater, humidification of the climate and probably elevated CO_2 input associated with volcanic activity.
4. The overlying middle Oxfordian – upper Kimmeridgian calcareous radiolarites marked the gradual waning of biosiliceous sedimentation and reestablishment of carbonate production in "starved basin" conditions, when carbonate production was slowly increasing and biosiliceous production declined. The switch from biosiliceous to carbonate sedimentation coincided with warming and increasing aridity of climate.
5. The high-relief seafloor topography of the eastern part of the Tatra Mts and the Western Tatra Mts was levelled during sedimentation of the upper Bathonian – lower Oxfordian ribbon radiolarites.
6. Sedimentation of the red nodular limestones during the late Kimmeridgian – early Tithonian in the eastern part of the Tatra Mts. was characteristic for the submarine elevation. These limestones are partly coeval with platy limestones deposited in the basin.
7. The Late Jurassic displays apparent bathymetric reversal between the eastern part of the Tatra Mts and the Western Tatra Mts. The latter area became a basin, whereas the former was a submarine elevation. The reversal is attributed to a more advanced stage in the pull-apart transcurrent tectonics of the Fatricum Domain. Thus, the Fatricum Domain was tectonically active long after its rifting stage.

Acknowledgments

The work was financed by the Grant No. N307 016537 to Renata Jach. Daniela Reháková was supported by the Grant Agency of the Slovak Republic (projects APVV-14-0118 and VEGA 2/0034/16). The authorities of the Polish Tatra National Park (TPN, Zakopane) and the Slovak Tatra National Park (TANAP, Tatranská Lomnica) provided permission for the fieldwork, for which the authors are very grateful. Michał Gradziński, Mariusz Mucha and Alfred Uchman gave excellent assistance in the field. Katarzyna Maj-Szeliga provided XRD analysis, Waldemar Obcowski helped with the figures,

Anna Łatkiewicz operated the SEM. The paper greatly benefited from the discussion with Wojciech Nemec, reviews by Roman Aubrecht, Špela Goričan and an anonymous reviewer as well as from the editorial work of Alfred Uchman and Frank Simpson. The authors are deeply indebted to all these individuals and institutions.

REFERENCES

Abbink, O., Targarona, J., Brinkhuis, H. & Visscher, H., 2001. Late Jurassic to earliest Cretaceous palaeoclimatic evolution of the southern North Sea. *Global and Planetary Change*, 30: 231–256.

Aiello, I. W. & Hagstrum, J. T., 2001. Paleomagnetism and paleogeography of Jurassic radiolarian cherts from the northern Apennines of Italy. *Geological Society of America Bulletin*, 113: 469–481.

Alvarez, W., Colacicchi, R. & Montanari, A., 1985. Synsedimentary slides and bedding formation in Apennine pelagic limestones. *Journal of Sedimentary Petrology*, 55: 720–734.

Arabas, A., 2016. Middle–Upper Jurassic stable isotope records and seawater temperature variations: New palaeoclimate data from marine carbonate and belemnite rostra (Pieniny Klippen Belt, Carpathians). *Palaeogeography, Palaeoclimatology, Palaeoecology*, 446: 284–294.

Aubouin, J., 1964. Réflexions sur le facies "Ammonitico Rosso". *Bulletin de la Société Géologique de France, Série* 7, 6: 475–501.

Bábek, O., Faměra, M., Hladil, J., Kapusta, J., Weinerová, H., Šimiček, D., Slavík, L. & Ďurišová, J., 2018. Origin of red pelagic carbonates as an interplay of global climate and local basin factors: Insight from the Lower Devonian of the Prague Basin, Czech Republic. *Sedimentary Geology*, 364: 71–78.

Bac-Moszaszwili, M., Burchart, J., Głazek, J., Iwanow, A., Jaroszewski, W., Kotański, Z., Lefeld, J., Mastella, L., Ozimkowski, W., Roniewicz, P., Skupiński, A. & Westwalewicz-Mogilska, E., 1979. *Geological Map of the Polish Tatra Mountains 1:30 000.* Wydawnictwa Geologiczne, Warszawa.

Bąk, M. & Bąk, K., 2018. Palaeoceanographic regime during the Oxfordian–Kimmeridgian in the Western Tethys recorded by radiolarian assemblages in the siliceous sediments of the Pieniny Klippen Belt, Carpathians. *Geological Journal*, 1–14.

Barale, L., Bertok, C., D'Atri, A., Martire, L. & Pavia, G., 2017. Stratigraphy, sedimentology and syndepositional tectonics of the Jurassic–Cretaceous successions at the transition between Provençal and Dauphinois domains (Maritime Alps, NW Italy). *Rivista Italiana di Paleontologia e Startigrafia*, 123: 355–378.

Barrett, T. J., 1982. Stratigraphy and sedimentology of Jurassic bedded chert overlying ophiolites in the North Apennines, Italy. *Sedimentology*, 29: 353–373.

Bartolini, A., Baumgartner, P. O. & Guex, J., 1999. Middle and Late Jurassic radiolarian palaeoecology versus carbon-isotope stratigraphy. *Palaeogeography, Palaeoclimatology, Palaeoecology*, 145: 43–60.

Bartolini, A. & Cecca, F., 1999. 20 My hiatus in the Jurassic of Umbria-Marche Apennines (Italy): carbonate crisis due to eutrophication. *Comptes Rendus de l'Académie des Sciences. Série 2, Sciences de la Terre et des Planètes*, 329: 587–595.

Basilone, L., 2017. Seismogenic rotational slumps and translational glides in pelagic deep-water carbonates. Upper Tithonian–Berriasian of Southern Tethyan margin (W Sicily, Italy). *Sedimentary Geology*, 356: 1–14.

Basilone, L., Sulli, A. & Morticelli, M. G., 2016. The relationship between soft-sediment deformation structures and synsedimentary extensional tectonics in Upper Triassic deep-water carbonate succession (Southern Tethyan rifted continental margin – Central Sicily). *Sedimentary Geology*, 344: 310–322.

Bathurst, R. G. C., 1991. Pressure-dissolution and limestone bedding: the influence of stratified cementation. In: Einsele, G., Ricken, W. & Seilacher, A. (eds), *Cycles and Events of Stratigraphy*. Springer, Berlin, pp. 450–463.

Baumgartner, P. O., 1987. Age and genesis of Tethyan Jurassic radiolarites. *Eclogae Geologicae Helvetiae*, 80: 831–879.

Baumgartner, P. O., 1990. Genesis of Jurassic Tethyan radiolarites – the example of Monte Nerone (Umbria-Marche Apennines). In: Pallini, G., Cecca, F., Cresta, S. & Santantonio, M. (eds), *Atti 2. Convegno, Fossili Evoluzione Ambiente*. Editore Comitato Centenario Raffaele Piccinini, Pergola, pp. 19–32.

Baumgartner, P. O., 2013. Mesozoic radiolarites – Accumulation as a function of sea surface fertility on Tethyan margins and in ocean basins. *Sedimentology*, 60: 292–318.

Berger, W. H., 1970. Biogenous deep-sea sediments: fractionation by deep-sea circulation. *Geological Society of America Bulletin*, 81: 1385–1402.

Bergerat, F., Collin, P.-Y., Ganzhorn, A.-C., Baudin, F., Galbrun, B., Roguet, I. & Schnyder, J., 2011. Instability structures, synsedimentary faults and turbidites, witnesses of a Liassic seismotectonic activity in the Dauphiné Zone (French Alps); A case in the Lower Pliensbachian at Saint-Michel-en-Beaumont. *Journal of Geodynamics*, 51: 344–357.

Bernoulli, D. & Jenkyns, H. C., 1970. A Jurassic basin: The Glasenbach Gorge, Salzburg, Austria. *Verhandlungen der Geologischen Bundesanstalt*, 4: 504–531.

Bernoulli, D. & Jenkyns, H. C., 1974. Alpine, Mediterranean and Central Atlantic Mesozoic facies in relation to the early evolution of the Tethys. In: Dott, R. H. & Sharer, R. H. (eds), *Modern and Ancient Geosynclinal Sedimentation. Society of Economic Paleontologists and Mineralogists, Special Publication*, 19: 129–160.

Bernoulli, D. & Jenkyns, H. C., 2009. Ancient oceans and continental margins of the Alpine-Mediterranean Tethys: deciphering clues from Mesozoic pelagic sediments and ophiolites. *Sedimentology*, 56: 149–190.

Bertok, C. & Martire, L., 2009. Sedimentation, fracturing and sliding on a pelagic plateau margin: the Middle Jurassic to Lower Cretaceous succession of Rocca Busambra (Western Sicily, Italy). *Sedimentology*, 56: 1016–1040.

Bertok, C., Martire, L., Perotti, E., d'Atri, A. & Piana, F., 2011. Middle–Late Jurassic syndepositional tectonics recorded in the Ligurian Briançonnais succession (Marguareis–Mongioie area, Ligurian Alps, NW Italy). *Swiss Journal of Geosciences*, 104: 237–255.

Betzler, C., Reijmer, J. J. G., Bernet, K., Eberli, G. P. & Anselmetti, F., 1999. Sedimentary patterns and geometries of the Bahamian outer carbonate ramp (Miocene–Lower Pliocene, Great Bahama Bank). *Sedimentology*, 46: 1127–1143.

Birkenmajer, K., 2012. Geology of the Lower Subtatric Nappe, Kopy Sołtysie area, Eastern Tatra Mts (West Carpathians, Poland). *Studia Geologica Polonica*, 135: 55–116.

Blyth Cain, J. D., 1968. Aspects of the depositional environment and palaeoecology of the crinoidal limestones. *Scottish Journal of Geology*, 4: 191–208.

Boltovskoy, D., Kling, S. A., Takahashi, K. & Biorglund, K. R., 2010. World atlas of distribution of recent Polycyctina (Radiolaria). *Palaeontologica Electronica*, 13, 18A: 1–230.

Bornemann, A., Aschwer, U. & Mutterlose, J., 2003. The impact of calcareous nannofossils on the pelagic carbonate accumulation across the Jurassic–Cretaceous boundary. *Palaeogeography, Palaeoclimatology, Palaeoecology*, 199: 187–228.

Borza, K. & Michalík, J., 1987. On stratigraphy and lithology of Czorsztyn Limestone Formation in the Central West Carpathians (Jurassic, Malm). *Geologický Zbornik – Geologica Carpathica*, 38: 259–284.

Bosselini, A. & Winterer, E. L., 1975. Pelagic limestone and radiolarite of the Tethyan Mesozoic: A genetic model. *Geology*, 3: 279–282.

Bostock, H. C., Hayward, B. W., Neil, H. L., Currie, K. I. & Dunbar, G. B., 2011. Deep-water carbonate concentrations in the southwest Pacific. *Dep-Sea Research I*, 58: 72–85.

Bover-Arnal, T. & Strasser, A., 2013. Relative sea-level change, climate and sequence boundaries insights from the Kimmeridgian to Berriasian platform carbonates of Mount Saleve (E France). *International Journal of Earth Sciences*, 102: 493–515.

Brady, M. & Bowie, C., 2017. Discontinuity surfaces and microfacies in a storm dominated shallow epeiric sea, Devonian Cedar Valley Group, Iowa. *The Depositional Record*, 3: 136–160.

Brigaud, B., Durlet, C., Deconinck, J.-F., Vincent, B., Pucéat, E., Thierry, J. & Trouiller, A., 2009. Facies and climate/environmental changes recorded on a carbonate ramp: a sedimentological and geochemical approach on Middle Jurassic carbonates (Paris Basin, France). *Sedimentary Geology*, 222: 181–206.

Caswell, B. A. & Coe, A. L., 2013. Primary productivity controls on opportunistic bivalves during Early Jurassic oceanic deoxygenation. *Geology*, 41: 1163–1166.

Cecca, F., Garin, M. B., Marchand, D., Lathuiliere, B. & Bartolini, A., 2005. Paleoclimatic control of biogeographic and sedimentary events in Tethyan and peri-Tethyan areas during the Oxfordian (Late Jurassic). *Palaeogeography, Palaeoclimatology, Palaeoecology*, 222: 10–32.

Cecca, F., Savary, B., Bartolini, A., Remane, J. & Cordey, F., 2001. The Middle Jurassic – Lower Cretaceous Rosso Ammonitico succession of Monte Inici (Trapanese domain, western Sicily): sedimentology, biostratigraphy and isotope stratigraphy. *Bulletin de la Société Géologique de France*, 172: 647–659.

Channell, J. E. T., Kozur, W. H., Sievers, T., Aubrecht, R. & Sykora, M., 2003. Carnian–Norian biomagnetostratigraphy at Silická Brezová (Slovakia): correlation to other Tethyan sections and to the Newark Basin. *Palaeogeography, Palaeoclimatology, Palaeoecology*, 191: 65–109.

Chiari, M., Cobianchi, M. & Picotti, V., 2007. Integrated stratigraphy (radiolarians and calcareous nannofossils) of the Middle to Upper Jurassic Alpine radiolarites (Lombardian Basin, Italy): Constraints to their genetic interpretation. *Palaeogeography, Palaeoclimatology, Palaeoecology*, 249: 233–270.

Christ, N., Immenhauser, A., Amour, F., Mutti, M., Tomas, S., Agar, S. M., Alway, R. & Kabiri, L., 2012. Characterization and interpretation of discontinuity surfaces in a Jurassic ramp setting (High Atlas, Morocco). *Sedimentology*, 59: 249–290.

Clari, P. A. & Martire, L., 1996. Interplay of cementation, mechanical compaction, and chemical compaction in nodular limestones of Rosso Ammonitico Veronese (Middle-Upper Jurassic, northeastern Italy). *Journal of Sedimentary Petrology*, 66: 447–458.

Cobianchi, M., Mancin, N., Lupi, C., Bordiga, M. & Bostock, H. C., 2015. Effects of oceanic circulation and ash-fall on calcite dissolution in bathyal sediments from the SW Pacific Ocean over the last 550 ka. *Palaeogeography, Palaeoclimatology, Palaeoecology*, 429: 72–82.

Coimbra, R., Immenhauser, A. & Olóriz, F., 2009. Matrix micrite $\delta^{13}C$ and $\delta^{18}O$ reveals synsedimentary marine lithification in Upper Jurassic Ammonitico Rosso limestones (Betic Cordillera, SE Spain). *Sedimentary Geology*, 219: 332–348.

Conti, M. A. & Monari, S., 1992. Thin-shelled bivalves from the Jurassic Rosso Ammonitico and Calcari a Posidonia Formations of the Umbrian-Marchean Apennine (Central Italy). *Palaeopelagos*, 2: 193–213.

Csontos, L. & Vörös, A., 2004. Mesozoic plate tectonic reconstruction of the Carpathian region. *Palaeogeography, Palaeoclimatology, Palaeoecology*, 210: 1–56.

De Wever, P., 1987. Radiolarites rubanées et variations de l'orbite terrestre. *Bulletin de la Société Géologique de France*, *Série* 8, 3: 957–960.

De Wever, P., Baudin, F., Azema, J. & Fourcade, E., 1995. Radiolarians and Tethyan radiolarites from primary production to their paleogeography. In: Nairn, A. E. M., Ricou, L.-E., Vrielynck, B. & Dercourt, J. (eds), *The Ocean Basins and Margins. Volume 8: The Tethys Ocean*. Plenum Press, New York, pp. 267–318.

De Wever, P., Dumitrica, P., Caulet, J. P., Nigrini, C. & Caridroit, M., 2001. *Radiolarians in the Sedimentary Record*. Gordon and Breach Science Publications, London, 533 pp.

De Wever, P., O'Dogherty, L. & Goričan, Š., 2014. Monsoon as a cause of radiolarite in the Tethyan realm. *Comptes Rendus Geoscience*, 346: 287–297.

Di Stefano, P., Galácz, A., Mallarino, G., Mindszenty, A. & Vörös, A., 2002. Birth and early evolution of a Jurassic escarpment: Monte Kumeta, Western Sicily. *Facies*, 46: 47–50.

Donatelli, U. & Tramontana, M., 2014. Platform-to-basin facies transition and tectono-sedimentary processes in the Jurassic deposits of the Furlo area (Umbria-Marche Apennines, Italy). *Facies*, 60: 514–560.

Donnadieu, Y., Dromart, G., Goddéris, Y., Pucéat, E., Brigaud, B., Dera, G., Dumas, C. & Oliver, N., 2011. A mechanism for brief glacial episodes in the Mesozoic greenhouse. *Paleoceanography*, 26: PA3212.

Dromart, G, Gaillard, C. & Jansa, L. F., 1994. Deep-marine microbial structures in the Upper Jurassic of Western Tethys. In: Bertrand-Sarfati, J. & Monty, C. (eds), *Phanerozoic Stromatolites II*. Kluwer, Dordrecht, pp. 295–318.

Dromart, G., Garcia, J.-P., Gaumet, F., Picard, S., Rousseau, M., Atrops, F., Lécuyer, C., Sheppard, S.M.F., 2003a. Perturbation of the carbon cycle at the Middle/Late Jurassic transition: geological and geochemical evidence. *American Journal of Science*, 303: 667–707.

Dromart, G., Garcia, J.-P., Picard, S., Atrops, F., C. Lécuyer, C. & Sheppard, S. M. F., 2003b. Ice age at the Middle–Late Jurassic transition? *Earth and Planetary Science Letters*, 213: 205–220.

Drzewiecki, P. A. & Simó, A. A., 2002. Depositional processes, triggering mechanisms and sediment composition of carbonate gravity flow deposits: examples from the late Cretaceous of the south-central; Pyrenees, Spain. *Sedimentary Geology*, 146: 155–189.

Dunham, R. J., 1962. Classification of carbonate rocks according to depositional texture. In: Ham, W. E. (ed.), *Classification of Carbonate Rocks. A Symposium. American Association of Petroleum Geologists, Memoire*, 1: 108–121.

Dürr, H., Meybeck, M., Hartmann, J., Laruelle, G. & Roubeix, V., 2011. Global spatial distribution of natural riverine silica inputs to the coastal zone. *Biogeoscience*, 8: 597–620.

Dykstra, M., 2012. Deep-water tidal sedimentology. In: Davis, R. A. Jr & Dalrymple, R. W. (eds), *Principles of Tidal Sedimentology*. Springer, Berlin, pp. 371–395.

Eberli, G. P., 1987. Carbonate turbidite sequences in rift basins of the Jurassic Tethys Ocean (eastern Alps, Switzerland). *Sedimentology*, 34: 363–388.

Eberli, G. P., 1988. The evolution of the southern continental margin of the Jurassic Tethys Ocean as recorded in the Allgäu Formation of the Austroalpine Nappes of Graubnden (Switzerland). *Eclogae Geologicae Helvetiae*, 81: 175–214.

Eberli, G. P. & Betzler, C., 2019. Characteristics of modern contourite drift. *Sedimentology*, in press, doi.org/10.1111/sed.12584.

Erba, E., 1989. Upper Jurassic to Lower Cretaceous *Nannoconus* distribution in some sections from northern and central Italy. *Memorie di Scienze Geologiche*, 41: 255–261.

Erba, E. & Tremolada, F., 2004. Nannofossil carbonate fluxes during the Early Cretaceous: Phytoplankton response to nutrification episodes, atmospheric CO_2, and anoxia. *Paleoceanography*, 19: 1–18.

Field, M. E., Gardner, J. V., Jennings, A. E. & Edwards, B. D., 1982. Earthquake-induced sediment failures on a 0.25 slope, Klamath River delta, California. *Geology*, 10: 542–546.

Folk, R. L & McBride, E. F., 1978. Radiolarites and their relation to subjacent "oceanic crust" in Liguria, Italy. *Journal of Sedimentary Petrology*, 48: 1069–1102.

Fossen, H., 2016. *Structural Geology*. Cambridge University Press, New York, 550 pp.

Gambacorta, G., Bersezio, R. & Erba, E., 2014. Sedimentation in the Tethyan pelagic realm during the Cenomanian: Monotonous settling or active redistribution? *Palaeogeography, Palaeoclimatology, Palaeoecology*, 409: 301–319.

Garrison, R. E. & Fischer, A. G., 1969. Deep-water limestones and radiolarites of the Alpine Jurassic. In: Friedman, G. M. (ed.), Depositional environments in carbonate rocks. *Society of Economic Paleontologists and Mineralogists, Special Publications*, 14: 20–56.

Gąsiorowski, S. M., 1959. On the age of radiolarites in the Sub-Tatric series in the Tatra Mts. *Acta Geologica Polonica*, 9: 221–230. [In Polish, with English summary.]

Gąsiorowski, S. M., 1962. Aptychi from the Dogger, Malm and Neocomian in the Western Carpathians and their stratigraphical value. *Studia Geologica Polonica*, 10: 1–151.

Gawlick, H.-J., Missoni, S., Schagintweit, F., Suzuki, H., Frisch, W., Krystyn, L., Blau, J. & Lein, R., 2009. Jurassic tectonostratigraphy of Austroalpine domain. *Journal of Alpine Geology*, 50: 1–152.

Gaździcki, A., Michalík, J., Planderová, E. & Sýkora, M., 1979. An Upper Triassic-Lower Jurassic sequence in the Krížna nappe (West Tatra Mountains, West Carpathians, Czechoslovakia). *Západne Karpaty, Geológia*, 5: 119–148.

Grabowski, J., 2011. Magnetostratigraphy of the Jurassic/Cretaceous boundary interval in the Western Tethys and its correlations with other regions: a review. *Volumina Jurassica*, 9: 105–128.

Grabowski, J., Haas, J. & Stoykova, K., 2017. Environmental changes around the Jurassic/Cretaceous transition: New nannofossil, chemostratigraphic and stable isotope data from the Lókút section (Transdanubian Range, Hungary). *Sedimentary Geology*, 360: 54–72.

Grabowski, J., Michalík, J., Pszczółkowski, A. & Lintnerová, O., 2010. Magneto- and izotope stratigraphy around the Jurassic/Cretaceous boundary in the Vysoká Unit (Malé Karpaty Mountains, Slovakia): correlations and tectonic implications. *Geologica Carpathica*, 61: 309–326.

Grabowski, J. & Pszczółkowski, A., 2006a. Magneto- and biostratigraphy of the Tithonian–Berriasian pelagic sediments in the Tatra Mountains (central Western Carpathians, Poland): sedimentary and rock magnetic changes at the Jurassic/Cretaceous boundary. *Cretaceous Research*, 27: 398–417.

Grabowski, J. & Pszczółkowski, A., 2006b. The Upper Tithonian and Berriasian in the Lower Sub-Tatric Nappe of the Western Tatra Mts in the light of litho-, bio- and magnetostratigraphic data (southern Poland). *Przegląd Geologiczny*, 54: 870 – 877. [In Polish, with English summary.]

Grabowski, J., Schnyder, J., Sobień, K., Koptiková, L., Krzemiński, L., Pszczółkowski, A., Hejnar, J. & Schnabl, P., 2013. Magnetic susceptibility and spectral gamma logs in the Tithonian – Berriasian pelagic carbonates in the Tatra Mts (Western Carpathians, Poland): palaeoenvironmental changes at the Jurassic/Cretaceous boundary. *Cretaceous Research*, 43: 1–17.

Gradziński, M., Tyszka, J., Uchman, A. & Jach, R., 2004. Large microbial-foraminiferal oncoids from condensed Lower–Middle Jurassic deposits: A case study from the Tatra Mountains, Poland. *Palaeogeography, Palaeoclimatology, Palaeoecology*, 213: 133–151.

Hardenbol, J., Thierry, J., Farley, M. B., Jacquin, T., de Graciansky, P.-C. & Vail, P. R., 1998. Mesozoic and Cenozoic sequence chronostratigraphic framework of European basins. In: de Graciansky, P.-C., Hardenbol, J., Jacquin, T., Vail, P. R. (eds), Mesozoic and Cenozoic Sequence Chronostratigraphic Framework of European Basins. *Society of Economic Paleontologists and Mineralogists, Special Publication*, 60: 763–781.

Hautevelle, Y., Michels, R., Malatere, F. & Trouiller, A., 2006. Vascular plant biomarkers as proxies for palaeoflora and palaeoclimatic changes at the Dogger/Malm transition of the Paris Basin (France). *Organic Geochemistry*, 37: 610–625.

Hesse, R. & Schacht, U., 2011. Early diagenesis of deep-sea sediments. In: Hüneke, H. & Mulder, T. (eds), *Deep-Sea Sediments*. Elsevier, Amsterdam, pp. 557– 714.

Hesselbo, S. P., Deconinck, J-F., Huggett, J. M. & Morgans-Bell, H. S., 2009. Late Jurassic palaeoclimatic change from clay mineralogy and gamma-ray spectrometry of the Kimmeridge Clay, Dorset, UK. *Journal of the Geological Society*, 166: 1123–1133.

Hori, R. S., Cho, C.-F. & Umeda, H., 1993. Origin of cyclicity in Triassic-Jurassic radiolarian bedded cherts of the Mino accretionary complex from Japan. *Island Arc*, 3: 170–18.

Hüneke, H., & Henrich, R., 2011. Pelagic sedimentation in modern and ancient oceans. In: Hüneke, H. & Mulder, T. (eds), Deep-Sea Sediments. *Developments in Sedimentology,* 63: 215–351.

Ikeda, M., Bôle, M. & Baumgartner, P. O., 2016. Orbital-scale changes in redox condition and biogenic silica/detrital fluxes of the Middle Jurassic Radiolarite in Tethys (Sogno, Lombardy, N-Italy): Possible link with glaciation? *Palaeogeography, Palaeoclimatology, Palaeoecology*, 457: 247–257.

Ikeda, M., Tade, R. & Ozaki, K., 2017. Astronomical pacing of the global silica cycle recorded in Mesozoic bedded cherts. *Nature Communication*, 8: 15532. doi: 10.1038/ncomms15532.

Iwańczuk, J., Iwanow, A. & Wierzbowski, A., 2013. Lower Jurassic to lower Middle Jurassic succession at Kopy Sołtysie and Płaczliwa Skała in the eastern Tatra Mts (Western Carpathians) of Poland and Slovakia: stratigraphy, facies and ammonites. *Volumina Jurassica*, 11: 19–58.

Iwanow, A., 1973. New data on geology of the Lower Subtatric Succession in the eastern part of the Tatra Mts. *Bulletin of the Polish Academy of Sciences*, *Earth Sciences*, 21: 65–74.

Jach, R., 2002. Lower Jurassic spiculite series from the Krížna Unit in the Tatra Mts, Western Carpathians, Poland. *Annales Societatis Geologorum Poloniae*, 72: 131–144.

Jach, R., 2005. Storm-dominated deposition of the Lower Jurassic crinoidal limestones in the Krížna Unit, Western Tatra Mountains, Poland. *Facies*, 50: 561–572.

Jach, R., 2007. *Bositra* limestones – a step towards radiolarites: case study from the Tatra Mountains. *Annales Societatis Geologorum Poloniae*, 77: 161–170.

Jach, R., Djerić, N., Goričan, Š. & Reháková, D., 2014. Integrated stratigraphy of the Middle Upper Jurassic of the Krížna Nappe, Tatra Mountains. *Annales Societatis Geologorum Poloniae*, 84: 1–33.

Jach, R. & Dudek, T., 2005. Orign of a Toarcian manganese carbonate/silicate deposits from the Krížna Unit, Tatra Mountains, Poland. *Chemical Geology*, 224: 136–152.

Jach, R., Goričan, Š., Reháková, D., Uchman, A. & Iwańczuk, J., 2019. Comment on "Decadal to millennial variations in water parameters in pelagic marine environments of the Western Tethys (Carpathian realm) during Middle–Late Jurassic – Evidence from the radiolarian record" by M. Bąk, K. Bąk and M. Michalik. *Global and Planetary Change*, in press, https://doi.org/10.1016/j.gloplacha.2018.10.009.

Jach, R., Reháková, D. & Uchman, A., 2012. Biostratigraphy and palaeoenvironment of the Kimmeridgian–Lower Tithonian pelagic sediments of the Krížna Nappe, Lejowa Valley, Tatra Mts., southern Poland. *Geological Quarterly*, 56: 773–788.

Jacobshagen, V., 1965. Die Allgäu-Schichten (Jura-Fleckenmergel) zwischen Wettersteingebirge und Rhein. *Jahrbuch der Geologischen Bundesanstalt*, 108: 1–114.

Jadoul, F., 2018. Stratigraphic-paleogeographic evolution of Eastern Sardinia Jurassic passive margin carbonates: synthesis and future developments. *Journal of Mediterranean Earth Sciences* 10: 147–154.

Jenkyns, H. C., 1974. Origin of red nodular limestones (Ammonitico Rosso, Knollenkalke) in the Mediterranean Jurassic: a diagenetic model. In: Hsü, K. J. & Jenkyns, H. C. (eds), *Pelagic Sediments: On Land and Under the Sea*. *International Associations of Sedimentologists*, *Special Publications*, 1: 249–271.

Jenkyns, H. C., Schouten-Huibers, S. & Sinninghe Damsté, J. S., 2012. Warm Middle Jurassic–Early Cretaceous high-latitude sea-surface temperatures from the Southern Ocean. *Climate of the Past*, 8: 215–226.

Jenkyns, H. C. & Winterer, E. L., 1982. Palaeoceanography of Mesozoic ribbon radiolarites. *Earth and Planetary Science Letters*, 60: 351–375.

Jo, A. J., Eberli, G. P. & Grasmueck, M., 2015. Margin collapse and slope failure along southwestern Great Bahama Bank. *Sedimentary Geology*, 317: 43–52.

Johns, H. D. & Moore, C. H., 1988. Reef to basin sediment transport using *Halimeda* as a sediment tracer, Grand Cayman Island, West Indies. *Coral Reefs*, 6: 187–193.

Kochman, A. & Matyszkiewicz, J., 2013. Experimental method for estimation of compaction in the Oxfordian bedded limestones of the southern Kraków-Częstochowa Upland, southern Poland. *Acta Geologica Polonica*, 63: 681–696.

Koša, E., 1998. Lithostratigraphy and depositional environment of Lower-Middle Jurassic crinoidal limestone formations of the Vysoká Nappe Unit (Malé Karpaty Mts., Western Carpathians). *Geologica Carpathica*, 49: 329–339.

Kozur, H., 1991. The evolution of the Meliata-Hallstatt Ocean and its significance for the early evolution of the Eastern Alps and Western Carpathians. *Palaeogeography, Palaeoclimatology, Palaeoecology*, 87: 109–135.

Kullberg, J. C., Olóriz, E., Marques, B., Caetano, P. S. & Rocha, R. B., 2001. Flat-pebble conglomerates: a local marker for Early Jurassic seismicity related to syn-rift tectonics in the Sesimbra area (Lusitanian Basin, Portugal). *Sedimentary Geology*, 139: 49–70.

Kwiatkowski, S., 1981. Sedimentation and diagenesis of the Niedzica Succession radiolarites in the Pieniny Klippen-Belt, Poland. *Annales Societatis Geologorum Poloniae*, 51: 45–61.

Larson, R. L. & Erba, E., 1999. Onset of the Mid-Cretaceous greenhouse in the Barremian-Aptian: Igneous events and the biological, sedimentary, and geochemical responses. *Paleogeography, Palaeoclimatology, Palaeoecology*, 14: 663–678.

Lee, G. H., Park, S. C. & Kim, D. C., 2000. Fluctuations of the calcite compensation depth (CCD) in the East Sea (Sea of Japan). *Geo-Marine Letters*, 20: 20–26.

Lefeld, J., 1969. Upper Jurassic carbo-silite sequence in the Sub-Tatric Succession of the Eastern Tatra Mts. *Bulletin of the Polish Academy of Sciences*, *Earth Sciences*, 17: 29–35.

Lefeld, J., 1974. Middle-Upper Jurassic and Lower Cretaceous biostratigraphy and sedimentology of the Sub-Tatric Succession in the Tatra Mts. (Western Carpathians). *Acta Geologica Polonica*, 24: 277–364.

Lefeld, J., 1981. Upper Jurassic radiolarite – nodular limestone vertical symmetry in the Polish Central Carpathians as reflection of regional depth changes in the ocean. *Studia Geologica Polonica*, 68: 89–96.

Lefeld, J., 1999. Tectonic of the Subtatric Units, Eastern Tatra Mts. *Studia Geologica Polnica*, 115: 139–166.

Lefeld, J., Gaździcki, A., Iwanow, A., Krajewski, K. & Wójcik, K., 1985. Jurassic and Cretaceous lithostratigraphic units in the Tatra Mts. *Studia Geologica Polonica*, 84: 7–93.

Leinfelder, R. R., Schmid, D. U., Nose, M. & Werner, W., 2002. Jurassic reef patterns: the expression of a changing globe. In:

Kiessling, W., Flügel, E. & Golonka, J. (eds), *Phanerozoic Reef Patterns. SEPM Special Publications*, 72: 465–520.

Lewandowski, M., Krobicki, M., Matyja, B. A. & Wierzbowski, A., 2005. Palaeogeographic evolution of the Pieniny Klippen Basin using stratigraphic and palaeomagnetic data from the Veliky Kamenets section (Carpathians, Ukraine). *Paleogeography, Palaeoclimatology, Palaeoecology*, 216: 53–72.

Łuczyński, P., 2001. Pressure-solution and chemical compaction of condensed Middle Jurassic deposits, High-Tatric series, Tatra Mountains. *Geologica Carpathica*, 52: 91–102.

Łuczyński, P., 2002. Depositional evolution of the Middle Jurassic carbonate sediments in the High-Tatric succession, Tatra Mountains, Western Carpathians, Poland. *Acta Geologica Polonica*, 52: 365–378.

Mallarino, G., Goldstein, R. H. & Di Stefano, P., 2002. New approach for quantifying water depth applied to the enigma of drowning of carbonate platforms. *Geology*, 30: 783–786.

Mamet, B. & Préat, A., 2006. Iron-bacterial mediation in Phanerozoic red limestones: State of the art. *Sedimentary Geology*, 185: 147–157.

Martire, L., 1992. Sequence stratigraphy and condensed pelagic sediments, an example from the Rosso Ammonitico Veronese, northeastern Italy. *Palaeogeography, Palaeoclimatology, Palaeoecology*, 94: 169–191.

Martire, L., 1996. Stratigraphy, facies and synsedimentary tectonics in the Jurassic Rosso Ammonitico Veronese (Altopiano di Asiago, NE Italy). *Facies*, 35: 209–236.

Martire, L. & Clari, P., 1994. Evaluation of sedimentation rates in Jurassic–Cretaceous pelagic facies of the Trento Plateau: relevance of discontinuities and compaction. *Giornale di Geologia*, 56: 193–209.

Martire, L., Clari, P., Lozar, F. & Pavia, G., 2006. The Rosso Ammonitico Veronese (Middle–Upper Jurassic of the Trento Plateau): A proposal of lithostratigraphic ordering and formalization. *Rivista Italiana di Paleontologia e Startigrafia*, 112: 227–250.

Martire, L. & Pavia, G., 2004. Jurassic sedimentary and tectonic processes at Montagna Grande (Trapanese Domain, Western Sicily, Italy). *Rivista Italiana di Paleontologia e Startigrafia*, 110: 23–33.

Márton, E., Grabowski, J., Tokarski, A. K. & Túnyi, I., 2016. Palaeomagnetic results from the fold and thrust belt of the Western Carpathians: An overview. *Geological Society Special Publication*, 425: 7–36.

Matyszkiewicz, J., 1996. The significance of *Saccocoma*-calciturbidites for the analysis of the Polish Epicontinental Late Jurassic Basin: an example from the Southern Cracow-Wieluń Upland (Poland). *Facies*, 34: 23–40.

Matyszkiewicz, J., 1999. Sea-bottom relief versus differential compaction in ancient platform carbonates: A critical reassessment of an example from Upper Jurassic of the Cracow-Wieluń Upland. *Annales Societatis Geologorum Poloniae*, 69: 63–79.

Matyszkiewicz, J. & Kochman, A., 2016. Pressure dissolution features in Oxfordian microbial-sponge buildups with pseudonodular texture, Kraków Upland, Poland. *Annales Societatis Geologorum Poloniae*, 86: 355–377.

McBride, E. F. & Folk, R. L., 1979. Features and origin of Italian Jurassic radiolarites deposited on continental crust. *Journal of Sedimentary Petrology*, 49: 837–868.

Michalk, J., 1994. Notes on the paleogeography and paleotectonics of the Western Carpathian area during the Mesozoic. *Mitteilungen der Österreichischen Geologischen Gesselschaft*, 86: 101–110.

Michalík, J., 2007. Sedimentary rock record and microfacies indicators of the latest Triassic to mid-Cretaceous tensional development of the Zliechov Basin (Central Western Carpathians). *Geologica Carpathica*, 58: 443–453.

Michalík, J., Bąk, M., Lintnerová, O. & Méres, Š., 2017. Biostratigraphy, geochemistry and sedimentology of Middle to Late Jurassic strata in the Strážovce section (Strážovské vrchy Mts), Krížna Nappe of the Central Carpathians, Slovakia. *Volumina Jurassica*, 15: 161–178.

Michalík, J., Lintnerová, O., Gaździcki, A. & Soták, J., 2007. Record of environmental changes in the Triassic–Jurassic boundary interval in the Zliechov Basin, Western Carpathians. Palaeogeography, Palaeoclimatology, *Palaeoecology*, 244: 71–88.

Michalík, J., Lintnerová, O., Wójcik-Tabol, P., Gaździcki, A., Grabowski, J., Golej, M., Šimo, V. & Zahradnikova, B., 2013. Paleoenvironments during the Rhetian transgression and the colonization history of marine biota in the Fatric Unit (Western Carpathians). *Geologica Carpathica*, 64: 39–62.

Michalík, J., Reháková, D., Halásová, E. & Lintnerová, O., 2009. The Brodno section – a potential regional stratotype of the Jurassic/Cretaceous boundary (Western Carpathians). *Geologica Carpathica*, 60: 213–232.

Michalík J., Reháková, D., Hladíková, J. & Lintnerová, O., 1995. Lithological and biological indicators of orbital changes in Tithonian and Lower Cretaceous sequences, Western Carpathians, Slovakia. *Geologica Carpathica*, 46: 161–174.

Michalík, J., Vašíček, Z. & Borza, V., 1990. Aptychi, tintinnids and stratigraphy of the Jurassic-Cretaceous (Zliechov unit of the Krížna Nappe, Strážovské Vrchy Mts., boundary beds in the Strážovce section Central Western Carpathians, Western Slovakia). *Knihovniča Zemního Plynu a Nafty*, 9a: 69–91. [In Slovak, with English summary.]

Mišík, M., 1959. Lithologisches Profil durch die Schichtenfolge des höheren Lias („Fleckenmergel") des Gebirges Belanské Tatry. *Geologický Sborník*, 10: 183–190. [In Slovak, with German summary.]

Missoni, S. & Gawlick, H.-J., 2011a. Jurassic mountain building and Mesozoic-Cenozoic geodynamic evolution of the Northern Calcareous Alps as proven in the Berchtesgaden Alps (Germany). *Facies*, 57: 137–186.

Missoni, S. & Gawlick, H.-J., 2011b. Evidence for Jurassic subduction from the Northern Calcareous Alps (Berchtesgaden Alps; Austroalpine, Germany). *International Journal of Earth Sciences*, 100: 1605–1631.

Mitchell, N. C., 1996. Creep in pelagic sediments and potential for morphologic dating of marine fault scarps. *Geophysical Research Letters*, 23: 483–486.

Molina, J. M., O'Dogherty, L., Sandoval, J. & Vera, J. A., 1999. Jurassic radiolarites in a Tethyan continental margin (Subbetic, southern Spain); palaeobathymetric and biostratigraphic considerations. *Palaeogeography, Palaeoclimatology, Palaeoecology*, 150: 309–330.

Molina, J. M., Reolid, M. & Mattioli, E., 2018. Thin-shelled bivalve buildup of the lower Bajocian, South Iberian paleomargin: development of opportunists after oceanic perturbations. *Facies*, 64: 19. [17 pp.]

Möller, N. K. & Kvingan, K., 1988. The genesis of nodular limestones in the Ordovician and Silurian of the Oslo Region (Norway). *Sedimentology*, 35: 405–420.

Monaco, P., 2016. Ichnocoenoses and taphocoenoses of posidoniid-bearing marl-limestone rhythmites and event beds, Toarcian-Aalenian, Northern Apennines, Italy. *Geobios*, 49: 365–379.

Morettini, E., Santantonio, M., Bartolini, A., Cecca, F., Baumgartner, P. O. & Hunziker, J. C., 2002. Carbon isotope stratigraphy and carbonate production during the Early-Middle Jurassic: example from the Umbria-Marche-Sabina Apennines (central Italy). *Palaeogeography, Palaeoclimatology, Palaeoecology,* 184: 251–273.

Mullins, H. T., Neumann, A. C., Wilber, R. J. & Bordman, M. R., 1980. Nodular carbonate sediment on Bahamian slope: Possible precursors to nodular limestones. *Journal of Sedimentary Petrology*, 50: 117–131.

Murray, R. W., Jones, D. L. & Buchholtz ten Brink, M. R., 1992. Diagentic formation of bedded chert: Evidence from chemistry of the chert-shale couplet. *Geology*, 20: 271–274.

Mutch, A. & Garrison, R. E., 1967. Determination of sedimentation rates by magnetic spherule abundances. *Journal of Sedimentary Petrology*, 37: 1139–1146.

Mutti, M. & Hallock, P., 2003. Carbonate systems along nutrient and temperature gradients: some sedimentological and geochemical constraints. *International Journal of Earth Sciences*, 92: 465–475.

Muttoni, G., Dallanave, E. & Channell, J. E. T., 2013. The drift history of Adria and Africa from 280 Ma to Present, Jurassic true polar wander, and zonal climate control on Tethyan sedimentary facies. *Palaeogeography, Palaeoclimatology, Palaeoecology,* 386: 415–435.

Muttoni, G., Erba, E., Kents, D. V. & Bachtadse, V., 2005. Mesozoic Alpine facies deposition as a result of past latitudinal plate motion. *Nature*, 434: 59–63.

Myczyński, R., 2004. Toarcian, Aalenian and Early Bajocian (Jurassic) ammonite faunas and biostratigraphy in the Pieniny Klippen Belt and the Tatra Mts, West Carpathians. *Studia Geologica Polonica*, 123: 7–131.

Myczyński, R. & Jach, R., 2009. Cephalopod fauna and stratigraphy of the Adnet type red deposits of the Krížna unit in the Western Tatra Mountains, Poland. *Annales Societatis Geologorum Poloniae*, 79: 27–39.

Navarro, V., Molina, J. M. & Ruiz-Ortiz, P. A., 2009. Filament lumachelle on top of Middle Jurassic oolite limestones: event deposits marking the drowning of a Tethysian carbonate platform (Subbetic, southern Spain). *Facies*, 55: 89–102.

Navarro, V., Ruiz-Ortiz, P. A. & Molina, J. M., 2012. Birth and demise of a Middle Jurassic isolated shallow-marine carbonate platform on a tilted fault block: Example from the Southern Iberian continental palaeomargin. *Sedimentary Geology*, 269–270: 37–57.

Nemčok, J., Bezák, Y., Biely, A., Gorek, A., Gross, P., Halouzka, R., Janák, M., Kahan, S., Kotański, Z., Lefeld, J., Mello, J., Reichwalder, P., Rączkowski, W., Roniewicz, P., Ryka, W., Wieczorek, J. & Zelman, J., 1994. *Geologická mapa Tatier, 1: 50 000*. Geologický Ústav Dionýza Štúra, Bratislava. [In Slovak.]

Neuweiler, F., Peckmann, J. & Ziems, A., 1999. Sinusoidally deformed veins ("Sigmoidal-klüftung") in the Lower Muschelkalk (Triassic, Anisian) of central Germany: sheet injection structures deformed within the shallow subsurface. *Neues Jahrbuch für Geologie und Paläontologie, Abhandlungen*, 214: 129–148.

Nieto, L. M., Reolid, M., Molina, J. M., Ruiz-Ortiz, P. A., Jiménez-Millán, J. & Rey, J., 2012. Evolution of pelagic swells from hardground analysis (Bathonian–Oxfordian, eastern External Subbetic, southern Spain). *Facies*, 58: 389–414.

Nisbet, E. G. & Price, I., 1974. Siliceous turbidites: bedded cherts as redeposited, ocean ridge derived sediments. In: Hsü, K. J. & Jenkyns, H. C. (eds), *Pelagic Sediments: On Land and Under the Sea*. *International Associations of Sedimentologists*, *Special Publications*, 1: 351–366.

O'Dogherty, L., Aguado, R., Baumgartner, P. O., Bill, M., Goričan, Š., Sandoval, J. & Sequeiros, L., 2018. Carbon-isotope stratigraphy and pelagic biofacies of the Middle–Upper Jurassic transition in the Tethys–Central Atlantic connection. *Palaeogeography, Palaeoclimatology, Palaeoecology*, 507: 129–144.

O'Dogherty, L, Martn-Algarra, A., Gursky, H.-J. & Aguado, R., 2001. The Middle Jurassic radiolarites and pelagic limestones of the Nieves unit (Rondaide Complex, Betic Cordillera): Basin starvation in a rifted marginal slope of the western Tethys. *International Journal of Earth Sciences*, 90: 831–846.

O'Dogherty, L., Sandoval, J., Bartolini, A., Bruchez, S., Bill, M. & Guex, J., 2006. Carbon-isotope stratigraphy and ammonite faunal turnover for the Middle Jurassic in the Southern Iberian palaeomargin. *Palaeogeography, Palaeoclimatology, Palaeoecology*, 239: 311–333.

Ogg, J. (database coordinator), 2019. TSCreator visualization of enhanced Geologic Time Scale 2016 database. Version 7.3; 2019. https://engineering.purdue.edu/Stratigraphy/tscreator [15.03.2019].

Ogg, J. G., Karl, S. M. & Behl, R. J., 1992. Jurassic through Early Cretaceous sedimentatiojn history of the central equatorial Pacific and of sites 800 and 801. *Proceedings of the Ocean Drilling Program, Scientific Results*, 129: 571–613.

Ogg, J. G., Ogg, G. M. & Gradstein, F. M., 2016. *A Concise Geological Time Scale 2016*. Elsevier, Amsterdam, 234 pp.

Ogg, J. G., Robertson, A. H. F. & Jansa, L. F., 1983. Jurassic sedimentation history of site 534 (western North Atlantic) and of the Atlantic-Tethys Seaway. In: Sheridan, R. E. & Gradstein, F. M. (eds), *Initial Reports of the Deep Sea Drilling Project*, 76: 829–884.

Ortner, H. & Kilian, S., 2016. Sediment creep on slopes in pelagic limestones: Upper Jurassic of Northern Calcareous Alps, Austria. *Sedimentary Geology*, 344: 350–363.

Pälike, H., Lyle, M. W., Nishi, H., Raffi, I., Ridgwell, A., Garnage, K., Klaus, A., Acton, G., Anderosn, L., Backman, J., Baldauf, J., Beltran, C., Bohaty, S. M., Bown, P., Busch, W., Channell, J. E. T., Chun, C. O. J., Delaney, M., Dewangan, P., Dunkley Jones, T., Edgar, K. M., Evans, H., Fitch, P., Foster, G. L., Gussone, N., Hasegawa, H., Hathorne, E. C., Hayashi, H., Herrle, J. G., Holbourn, A., Hovan, S., Hyeong, K., Ijima, K., Ito, T., Kamikuri, S., Kimoto, K., Kuroda, K., Leon-Rodriguez, L., Malinverno, A., Moor, T. C. Jr, Murphy, B. H., Murphy, D. P., Nakamura, H., Ogane, K., Ohneiser, Ch., Richter, C., Robinson, R., Rohling, E. J., Romero, O., Sawada, K., Scher, H., Schneider, L., Sluijs, A., Takata, H., Tian, J., Tsujimoto, A., Wade, B. S., Westerhold, T., Wilkens, R., Williams, T., Wilson, P. A., Yamamoto, Y., Yamamoto, S., Yamazaki, T.

& Zeebe, R. E., 2012. A Cenozoic record of the equatorial Pacific carbonate compensation depth. *Nature*, 488: 609–615.

Pellenard, P., Tramoy, R., Pucéat, E., Huret, E., Martinez, M., Bruneau, L. & Thierry, J., 2014. Carbon cycle and sea-water palaeotemperature evolution at the Middle–Late Jurassic transition, eastern Paris Basin (France). *Marine and Petroleum Geology*, 53: 30–43.

Picotti, V. & Cobianchi, M., 2017. Jurassic stratigraphy of the Belluno basin and Friuli Platform: a perspective on far-field compression in the Adria passive margin. *Swiss Journal of Geosciences*, 110: 833–850.

Plašienka, D., 2003. Dynamics of Mesozoic pre-orogenic rifting in the Western Carpathians. *Mitteilungen der Österreichischen Geologischen Gessellschaft*, 94: 79–98.

Plašienka, D., 2012. Jurassic syn-rift and Cretaceous syn-orogenic, coarse-grained deposits related to opening and closure of the Vahic (South Penninic) Ocean in the Western Carpathians – an overview. *Geological Quarterly*, 56: 601–628.

Plašienka, D., 2018. Continuity and episodicity in the early alpine tectonic evolution of the Western Carpathians: How large-scale processes are expressed by the orogenic architecture and rock record data. *Tectonics*, 37: 2029–2079.

Polák, M., Ondrejíčková, A. & Wieczorek, J., 1998. Lithostratigraphy of the Ždiar Formation of the Krížna nappe. *Slovak Geological Magazine*, 4: 35–52.

Pomar, L. & Hallock, P., 2008. Carbonate factories: A conundrum in sedimentary geology. *Earth-Science Reviews*, 87: 134–169.

Préat, A., Morano, S., Loreau, J.-P., Durlet, Ch. & Mamet, B., 2006. Petrography and biosedimentology of the Rosso Ammonitico Veronese (Middle-Upper Jurassic, north-eastern Italy). *Facies*, 52: 265–278.

Price, G. & Rogov, M., 2009. An isotopic appraisal of the Late Jurassic greenhouse phase in the Russian Platform. *Palaeogeography, Palaeoclimatology, Palaeoecology*, 273: 41–49.

Pszczółkowski, A., 1996. Calpionellid stratigraphy of the Tithonian-Berriasian pelagic limestones in the Tatra Mts (Western Carpathians). *Studia Geologica Polonica*, 109: 103–130.

Pszczółkowski, A., Grabowski, J. & Wilamowski, A., 2016. Integrated biostratigraphy and carbon isotope stratigraphy of the Upper Jurassic shallow water carbonates of the High-Tatric Unit (Mały Giewont area, Western Tatra Mountains, Poland). *Geological Quarterly*, 60: 893–918.

Racki, G. & Cordey, F., 2000. Radiolarian palaeoecology and radiolarites: is the present the key to the past? *Earth-Science Reviews*, 52: 83–120.

Railsback, L. B., 1993. Contrasting styles of chemical compaction in the Upper Pennsylvanian Dennis Limestone in the Midcontinent region, U.S.A. *Journal of Sedimentary Petrology*, 63: 61–72.

Rais, P., Louis-Schmid, B., Bernasconi, S. M. & Weissert, H., 2007. Palaeoceanographic and palaeoclimatic reorganization around the Middle–Late Jurassic transition. *Palaeogeography, Palaeoclimatology, Palaeoecology*, 251: 527–546.

Ramajo, J. & Aurell, M., 2008. Long-term Callovian–Oxfordian sea-level changes and sedimentation in the Iberian carbonate platform (Jurassic, Spain): possible eustatic implications. *Basin Research*, 20: 163–184.

Rameil, N., 2005. Carbonate sedimentology, sequence stratigraphy, and cyclostratigraphy of the Tithonian in the Swiss and French Jura Mountains. A high-resolution record of changes in sea level and climate. *GeoFocus*, 13: 1–246.

Raucsik, B., Demény, A., Borbély-Kiss, I. & Szabó, G., 2001. Monsoon-like climate during the Bajocian. Clay mineralogical and geochemical study on a limestone/marl alternation (Komló Calcareous Marl Formation, Mecsek Mountains, Southern Hungary). *Hantkeniana*, 3: 149–176.

Raucsik, B. & Varga, A., 2008. Climato-environmental controls on clay mineralogy of the Hettangian—Bajocian successions of the Mecsek Mountains, Hungary: An evidence for extreme continental weathering during the early Toarcian oceanic anoxic event. *Palaeogeography, Palaeoclimatology, Palaeoecology*, 265: 1–13.

Rea, D. K. & Lyle, M. W., 2005. Paleogene calcite compensation depth in the eastern subtropical Pacific: Answers and questions. *Paleoceanography*, 20: PA1012.

Reháková, D., 2000. Evolution and distribution of the Late Jurassic and Early Cretaceous calcareous dinoflagellates recorded in the Western Carpathian pelagic carbonate facies. *Mineralia Slovaca,* 32: 79–88.

Reháková, D., Matyja, B. A., Wierzbowski, A., Schlögl, J., Krobicki, M. & Barski, M., 2011. Stratigraphy and microfacies of the Jurassic and lowermost Cretaceous of the Veliky Kamenets section (Pieniny Klipen Belt, Carpathians, Western Ukraine). *Volumina Jurassica*, 9: 61–104.

Reijmer, J. J. G., Palmieri, P., Groen, R. & Floquet, M., 2015. Calciturbidites and calcidebrites: Sea-level variations or tectonic processes? *Sedimentary Geology*, 317: 53–70.

Reolid, M., Rivas, P. & Rodríguez-Tovar, F. J., 2015. Toarcian Ammonitico Rosso facies from South Iberian Paleomargin (Betic Cordillera, southern Spain): Paleoenvironmental reconstruction. *Facies*, 61, 22. [26 pp.]

Röhl, H.-J., Schmid-Röhl, A., Oschmann, W., Firmmel, A. & Schwark, L., 2001. The Posidonia Shale (Lower Toarcian) of SW-Germany: an oxygen-depleted ecosystem controlled by sea level and palaeoclimate. *Palaeogeography, Palaeoclimatology, Palaeoecology*, 165: 27–52.

Rychliński, T. & Jaglarz, P., 2017. An evidence of tectonic activity in the Triassic of the Western Tethys: a case study from the carbonate succession in the Tatra Mountains (S Poland). *Carbonates and Evaporites*, 32: 103–116.

Santantonio, M., 1993. Facies associations and evolution of pelagic carbonate platform/basin systems: examples from the Italian Jurassic. *Sedimentology*, 40: 1039–1067.

Santantonio, M., 1994. Pelagic carbonate platforms in the geologic record: Their classification, and sedimentary and Paleotectonic evolution. *American Association of Petroleum Geologists Bulletin*, 78: 122–141.

Santantonio, M., Galluzzo, F. & Gill, G., 1996. Anatomy and palaeobathymetry of a Jurassic pelagic carbonate platform/basin system. Rossa Mts, Central Apennines (Italy). Geological implications. *Palaeopelagos*, 6: 123–169.

Schieber, J. & Southard, J. B., 2009. Bedload transport of mud by floccule ripples – Direct observation of ripple migration processes and their implications. *Geology*, 37: 483–486.

Schmid, S. M., Bernoulli, D., Fügenschuh, B., Matenco, L., Scheffer, S., Schuster, R., Tischler, M. & Ustaszewski, K., 2008. The Alpine-Carpathian-Dinaridic orogenic system: correlation and evolution of tectonic units. *Swiss Journal of Geosciences*, 101: 139–183.

Silva, A. J. & Booth, J. S., 1984. Creep behavior of submarine sediments. *Geo-Marine Letters*, 4: 215–219.

Šimo, V. & Tomašových, A., 2013. Trace-fossil assemblages with a new ichnogenus in "spotted" (Fleckenmergel - Fleckenkalk) deposits: a signature of oxygen-limited benthic communities. *Geologica Carpathica*, 64: 355–374.

Snedden, J. W. & Liu, C., 2010. A compilation of Phanerozoic sea-level change, coastal onlaps and recommended sequence designations. *Search and Discovery Article, American Association of Petroleum Geologists,* 40594. [3 pp.]

Strasser, A., Védrine, S. & Stienne, N., 2012. Rate and synchronicity of environmental changes on a shallow carbonate platform (Late Oxfordian, Swiss Jura Mountains). *Sedimentology*, 59: 185–211.

Szulczewski, M., 1963. Stromatolites from the High-Tatric Bathonian of the Tatra Mountains. *Acta Geologica Polonica*, 13: 125–148. [In Polish, with English summary.]

Szulczewski, M., 1965. Observation sur la genèse des calcaires noduleux des Tatras. *Rocznik Polskiego Towarzystwa Geologicznego*, 35: 243–261. [In Polish, with French summary.]

Thierry, J. & Barrier, E., 2000. Map 8. Middle Toarcian (180–178 Ma). In: Dercourt, J., Gaetani, M., Vrielynck, B., Barrier, E., Biju-Duval, B., Brunet, M. F., Cadet, J. P., Crasquin, S. & Sandulescu, M. (eds), *Atlas Peri-Tethys. Palaeogeographical Maps*. Peri-Tethys Programme, Paris.

Tomás, S., Aurell, M., Bádenas, B., Bjorge, M., Duaso, M. & Mutti, M., 2019. Architecture and paleoenvironment of Mid-Jurassic microbial-siliceous sponge mounds, northeastern Spain. *Journal of Sedimentary Research*, 89: 110–134.

Tréguer, P., Nelson, D. M., van Bennekom, A. J., DeMaster, D. J., Leynaert, A. & Quéguiner, B., 1995. The balance of silica in the world ocean: a re-estimate. *Science*, 268: 375–379.

Tucker, M. E., 1974. Sedimentology of Palaeozoic pelagic limestones: the Devonian Griotte (southern France) and Cephalopodenkalk (Germany). In: Hsü, K. J. & Jenkyns, H. C. (eds), *Pelagic Sediments: On Land and Under the Sea*. *International Associations of Sedimentologists*, *Special Publications*, 1: 71–92.

Tyszka, J., 1994. Response of Middle Jurassic benthic foraminiferal morphogroups to dysoxic/anoxic conditions in the Pieniny Klippen Belt Basin, Polish Carpathians. *Palaeogeography, Palaeoclimatology, Palaeoecology*, 110: 55–81.

Tyszka, J., 2001. Microfossil assemblages as bathymetric indicators of the Toarcian/Aalenian "Fleckenmergel"-facies in the Carpathian Pieniny Klippen Belt. *Geologica Carpathica*, 52: 147–158.

Uchman, A. & Jach, R., 2017. Ichnological record in Jurassic sediments of the Fatricum Domain in the Tatra Mountains, southern Poland and northern Slovakia. In: Grabowski, J. (ed.), *Jurassica XIII, Jurassic Geology of Tatra Mts, Abstracts and Field Trip Guidebook, Poland, Kościelisko near Zakopane, June 19th–23rd, 2017*. Polish Geological Institute – National Research Institute, Warsaw, p. 60.

Uchman, A. & Myczyński, R., 2006. Stop B3.14 – Lejowa Valley: eastern of the Polana Huty Lejowe Alp – Upper Sinemurian – Lower Pliensbachian spotted limestones. In: Wierzbowski, A., Aubrecht, R., Golonka, J., Gutowski, J., Krobicki, M., Matyja, B. A., Pieńkowski, G. & Uchman, A. (eds), *Jurassic of Poland and Adjacent Slovakian Carpathians, Filed Trip Guidebook of 7th International Congress on the Jurassic System, Poland, Kraków, September 6–18, 2006*. Polish Geological Institute, Warsaw, pp. 114–116.

Vašíček, Z., Michalík, J. & Reháková, D., 1994. Early Cretaceous stratigraphy, palaeogeography and life in Western Carpathians. *Beringeria*, 10: 3–169.

Vecsei, A., Frisch, W., Pirzer, M. & Wetzel, A., 1989. Origin and tectonic significance of radiolarian chert in the Austroalpine rifted continental margin. In: Hein, J. R. & Obradovič, J. (eds), *Siliceous Deposits of the Tethys and Pacific Region*. Springer, New York, pp. 65–80.

Vera, J. A. & Martin-Algarra, A., 1994. Mesozoic stratigraphic breaks and pelagic stromatolites in the Betic Cordillera, southern Spain. In: Bertrand-Sarfati, J. & Monty, C. (eds), *Phanerozoic Stromatolites II*. Kluwer, Dordrecht, pp. 318–344.

Vörös, A., 2012. Episodic sedimentation on a peri-Tethyan ridge through the Middle–Late Jurassic transition (Villány Mountains, southern Hungary). *Facies*, 58: 415–443.

Wetzel, A. & Uchman, A., 2018. The former presence of organic matter caused its later absence: Burn-down of organic matter in oceanic red beds enhanced by bioturbation (Eocene Variegated Shale, Carpathians). *Sedimentology*, 65: 1504–1519.

Wieczorek, J., 1983. Uwagi o facji "ammonitico rosso". *Przegląd Geologiczny*, 31: 247–252. [In Polish.]

Wieczorek, J., 1988. Maiolica – a unique facies of the Western Tethys. *Annales Societatis Geologorum Poloniae*, 58: 225–276.

Wieczorek, J., 1995. Trace fossils from Fleckenmergel facies (Jurassic) of the Tatra Mts. *Geobios*, *Mémoir Spécial*, 18: 425–431.

Wieczorek, J., 2001. Condensed horizons as turning events in passive margin evolution: the Tatra Mts examples. *Zentralblatt für Geologie und Paläontologie*, *Teil 1*, 1/2: 199–209.

Wierzbowski, H., 2004. Carbon and oxygen isotope composition of Oxfordian–Early Kimmeridgian belemnite rostra: palaeoenvironmental implications for Late Jurassic seas. *Palaeogeography, Palaeoclimatology, Palaeoecology*, 203: 153–168.

Wierzbowski, H., 2015. Seawater temperatures and carbon isotope variations in central European basins at the Middle–Late Jurassic transition (Late Callovian – Early Kimmeridgian). *Palaeogeography, Palaeoclimatology, Palaeoecology*, 440: 506–523.

Wierzbowski, H., Anczkiewicz, R., Pawlak, J., Rogov, M. A. & Kuznetsov, A. B., 2017. Revised Middle–Upper Jurassic strontium isotope stratigraphy. *Chemical Geology*, 466: 239–255.

Wierzbowski, H., Rogov, M. A., Matyja, B. A., Kiselev, D. & Ippolitov, A., 2013. Middle–Upper Jurassic (Upper Callovian – Lower Kimmeridgian) stable isotope and elemental records of the Russian Platform: Indices pf oceanographic and climatic changes. *Global and Planetary Change*, 107: 196–212.

Wignall, P. B., 1993. Distinguishing between oxygen and substrate control in fossil benthic assemblages. *Journal of the Geological Society,* 150: 193–196.

Winterer, E. L. & Bosselini, A., 1981. Subsidence and sedimentation on Jurassic passive continental margin, Southern Alps, Italy. *American Association of Petroleum Geologists Bulletin*, 65: 394–421.

Wu, J. E., McClay, K., Whitehouse, P. & Dooley, T., 2009. 4D analogue modelling of transtensional pull-apart basins. *Marine and Petroleum Geology*, 26: 1608–1623.

Wynn, R. B. & Stow, D. A., 2002. Classification and characterisation of deep-water sediment waves. *Marine Geology*, 192: 7–22.

Zankl, H., 1969. Structural and textural evidence of early lithification in fine-grained carbonate rocks. *Sedimentology*, 12: 241–256.